Ozone-Climate Links in the Southern Hemisphere

A thesis submitted in partial fulfilment of the requirements for the Degree of Doctor of Philosophy in Physics at the University of Canterbury

by

Fraser Dennison

Supervisors: Dr. Adrian McDonald
Dr. Olaf Morgenstern

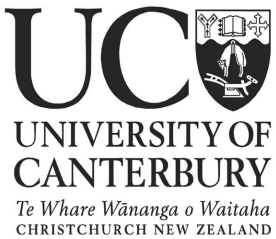

Department of Physics and Astronomy
University of Canterbury

September 2016

Abstract

This thesis details a number of the effects that changes in the abundance of stratospheric ozone over the period 1950-2100 are having on climate in the Southern Hemisphere. Beginning in the 1970s polar stratospheric ozone became increasingly depleted due to anthropogenic emissions of ozone depleting substances (ODSs), leading to the formation of what is known as the "ozone hole". The cessation of ODS emissions as a result of the Montreal Protocol and its amendments and adjustments is projected to lead to the recovery of polar stratospheric ozone over the course of the 21^{st} century. Ozone has a large effect on temperature in the stratosphere via its absorption of solar radiation and outgoing longwave radiation. Changes in ozone therefore will have an effect on stratospheric climate and also, as is demonstrated in this thesis, tropospheric climate.

This study utilizes the NIWA-UKCA coupled atmosphere-ocean-chemistry climate model (AOCCM). This model interactively simulates ozone chemistry, which is an advance on prior generations of general circulation models (GCMs) in which ozone is often prescribed. Comparison of model runs in which ODS concentrations vary according to historical and projected future values, to runs in which ODS concentrations are fixed at pre-ozone hole levels allows for the attribution of various changes in climate to changes in ozone.

Southern Hemisphere climate can be described, in large part, by the Southern Annular Mode (SAM). The SAM describes an oscillation of atmospheric mass between mid-latitudes and the pole. This results in a vacillation of the strength of the polar vortex in the stratosphere and a meridional meandering of the polar frontal jet in the troposphere. This thesis shows an increase in the frequency of extreme SAM events and an increase in persistence of the SAM in the stratosphere as a result of ozone depletion.

The SAM is also useful for examining coupling between the stratosphere and troposphere. Extreme SAM events in the stratosphere have been shown in previous studies to be followed by SAM anomalies in the troposphere that persist for around two months - much longer than the typical persistence in the troposphere. This thesis shows that the strength of this coupling

increases as a result of ozone depletion, with the tropospheric SAM showing an increased anomaly lagging the stratospheric anomaly by 40-60 days.

Another feature of tropospheric climate is atmospheric blocking. Blocking describes large, quasi-stationary, persistent anticyclonic anomalies that impede the mid-latitude zonal flow. It is shown that ozone depletion leads to a increase in the frequency of blocking during summer in the South Atlantic, followed by a decrease in frequency as ozone recovers over the 21^{st} century. In contrast, changes in ozone forcing show no influence on blocking in the South Pacific. The difference between the two regions is likely linked to the SAM as it is shown that blocking events in the Atlantic are preceded by positive SAM anomalies which is not the case for Pacific blocking events.

The distribution of ozone is also examined. It is known that ozone distribution is somewhat asymmetric, with the ozone hole displaced from the pole toward South America. This asymmetry is an important factor in the determining the temperature of the polar stratosphere. An eastward trend in the location of the ozone minimum over 1960-1999 is attributed to ozone depletion. An increase in greenhouse gas (GHG) forcing opposing the effect of ozone recovery during the 21^{st} century results in a relatively constant location of this minimum over this timespan.

The results presented in this thesis demonstrate the utility of accounting for changes in ozone and, in general, of accurately simulating the stratosphere when modelling the climate or producing long range weather forecasts.

Deputy Vice-Chancellor's Office
Postgraduate Office

UNIVERSITY OF CANTERBURY
Te Whare Wānanga o Waitaha
CHRISTCHURCH NEW ZEALAND

Co-Authorship Form

This form is to accompany the submission of any thesis that contains research reported in co-authored work that has been published, accepted for publication, or submitted for publication. A copy of this form should be included for each co-authored work that is included in the thesis. Completed forms should be included at the front (after the thesis abstract) of each copy of the thesis submitted for examination and library deposit.

Please indicate the chapter/section/pages of this thesis that are extracted from co-authored work and provide details of the publication or submission from the extract comes:
Chapter 3, with the exception of Section 3.4.4 and related material, was published in the Journal of Geophysical Research: Atmospheres (Dennison et al., 2015)

Please detail the nature and extent (%) of contribution by the candidate:
Fraser Dennison was the lead author; contribution 70%

Certification by Co-authors:
If there is more than one co-author then a single co-author can sign on behalf of all The undersigned certifies that:

- The above statement correctly reflects the nature and extent of the PhD candidate's contribution to this co-authored work
- In cases where the candidate was the lead author of the co-authored work he or she wrote the text

Name: Signature: Date:

Deputy Vice-Chancellor's Office
Postgraduate Office

UNIVERSITY OF CANTERBURY
Te Whare Wānanga o Waitaha
CHRISTCHURCH NEW ZEALAND

Co-Authorship Form

This form is to accompany the submission of any thesis that contains research reported in co-authored work that has been published, accepted for publication, or submitted for publication. A copy of this form should be included for each co-authored work that is included in the thesis. Completed forms should be included at the front (after the thesis abstract) of each copy of the thesis submitted for examination and library deposit.

Please indicate the chapter/section/pages of this thesis that are extracted from co-authored work and provide details of the publication or submission from the extract comes:
Chapter 4 was submitted to the Journal of Geophysical Research: Atmospheres

Please detail the nature and extent (%) of contribution by the candidate:
Fraser Dennison was the lead author; contribution 70%

Certification by Co-authors:
If there is more than one co-author then a single co-author can sign on behalf of all The undersigned certifys that:

- The above statement correctly reflects the nature and extent of the PhD candidate's contribution to this co-authored work
- In cases where the candidate was the lead author of the co-authored work he or she wrote the text

Name: Signature: Date:

Acknowledgements

I would like to thank my supervisors Dr. Adrian McDonald and Dr. Olaf Morgenstern for their encouragement, guidance and expertise.

This work relied on data from various climate model and reanalysis products. Thank you to the many people responsible for developing these models and providing the data. In particular, thank you to the developers of the NIWA-UKCA model, which was the primary tool used in this thesis.

Funding for this work was provided by the Department of Physics and Astronomy at the University of Canterbury, NIWA and the Marsden Fund, for which I am grateful.

Also, thank you to my colleagues in the Atmospheric Physics group whose collective wisdom surely improved the quality of my work and to the team at NIWA Lauder for their hospitality.

Contents

List of Figures

List of Tables

Chapter 1

Introduction

This thesis examines the effects of changes in ozone on the surface climate in the Southern Hemisphere. It is widely known that one function of the ozone layer is to block harmful UV radiation emitted by the Sun but it also plays a key role in climate. It is important to understand the effect ozone has on climate for a number of reasons: to improve our understanding of the mechanics of the atmosphere, to potentially improve seasonal forecasting ability, and also to separate these effects from climate change caused by greenhouse gas (GHG) related warming. It is particularly important to recognize the latter aspect at this point in time as the atmosphere transitions from a period of ozone depletion to a period of ozone recovery and thus, ozone effects that have previously reinforced GHG effects will possibly begin to oppose these GHG effects.

The geography of the Southern Hemisphere is such that ozone depletion has been more severe here than in the Northern Hemisphere. Severe ozone depletion over Antarctica motivated the phrase "ozone hole" which is used to describe an extended area in which the total column ozone has fallen below a threshold level; every spring since the early 1980s an ozone hole has been present in the Southern Hemisphere. In contrast an ozone hole only first occurred in the Northern Hemisphere in 2011. It is for this reason this thesis will focus on the Southern Hemisphere.

1.1 Thesis Outline

The remainder of this chapter covers the relevant background information, including the role of the ozone layer in the atmosphere and a brief description of the chemistry related to ozone depletion as well some important atmospheric features such as the Southern Annular Mode (SAM) which is the leading mode of climate variability in the Southern Hemisphere, atmospheric blocking and, stratosphere-troposphere coupling. It is intended that this section summarizes most of the relevant literature.

Chapter 2 details the NIWA-UKCA model, the primary model used throughout this study, as well as summarizing the CMIP5 set of models which are used in Chapter 3. This chapter also introduces the MERRA and ERA-Interim reanalysis data sets.

Chapter 3 examines the effect of ozone depletion on the SAM as well as coupling between the stratosphere and troposphere. This research was published in the Journal of Geophysical Research (Dennison et al., 2015). In addition to this, stratosphere - troposphere coupling is compared across a range of different climate models to determine what aspects of a model were important for simulating this atmospheric phenomenon (this portion is unpublished).

Chapter 4 examines the effect of ozone depletion on atmospheric blocking. This chapter has been submitted to the Journal of Geophysical Research.

The prior two chapters show ozone forcing acting on the climate via the SAM, a largely zonally symmetric mode. Chapter 5 complements these studies by focusing on the zonally asymmetric aspect of the ozone and examines what influence this has on the surface climate.

Finally, Chapter 6 provides some conclusions and possibilities for future work.

1.2 Background

1.2.1 Stratospheric Ozone

Ozone is primarily located in the stratosphere - the layer of the atmosphere beginning around 10 – 16 km above the Earth's surface and extending up to a height of around 50 km (see Figure 1.1). The stratosphere is characterized by increasing temperature with height and is bounded below by the tropopause and above by the stratopause which are the regions in which the vertical temperature gradient changes sign. The layer below the stratosphere is the troposphere which extends down to the surface. The troposphere contains only a small amount of ozone, some of this is transported from the stratosphere but it can also originate from industrial pollution and biomass burning (Lelieveld and Dentener, 2000; Sudo and Akimoto, 2007). Figure 1.2 shows a vertical ozone profile. The ozone mixing ratio begins to increase at the tropopause and reaches a maximum at around 25 km. The amount of ozone in the stratosphere is of the order of a few parts per million. The columnar density of ozone is measured in Dobson units (DU). One DU corresponds to a layer of gas 10 μm thick at standard temperature and pressure (STP). The ozone layer is of the order of a few hundred DU, the equivalent of a few millimetres thick at STP.

Ozone absorbs UV radiation from the Sun in the wavelength range of 200 - 315 nm (Molina and Molina, 1986; Matsumi and Kawasaki, 2003). This is important for life on Earth as radiation of this wavelength is a cause of skin cancer in humans and is also harmful to plant life (Rozema et al., 1997). This absorption is also responsible for the temperature distribution of the stratosphere. Although the majority of the ozone is located in the lower stratosphere, ozone absorption is sufficiently strong that most of the absorption occurs at higher altitudes resulting in increasing temperatures with height throughout the stratosphere (see Figure 1.1). Ozone has another absorption band between 9 and 10 μm which means that it also acts as a greenhouse gas.

Ozone is produced by the photolysis of O_2 by radiation with wavelengths smaller than 242 nm (hν in equation 1.1). The atomic oxygen produced in this reaction reacts rapidly with an O_2 molecule to form ozone.

$$O_2 + h\nu \rightarrow 2O \tag{1.1}$$

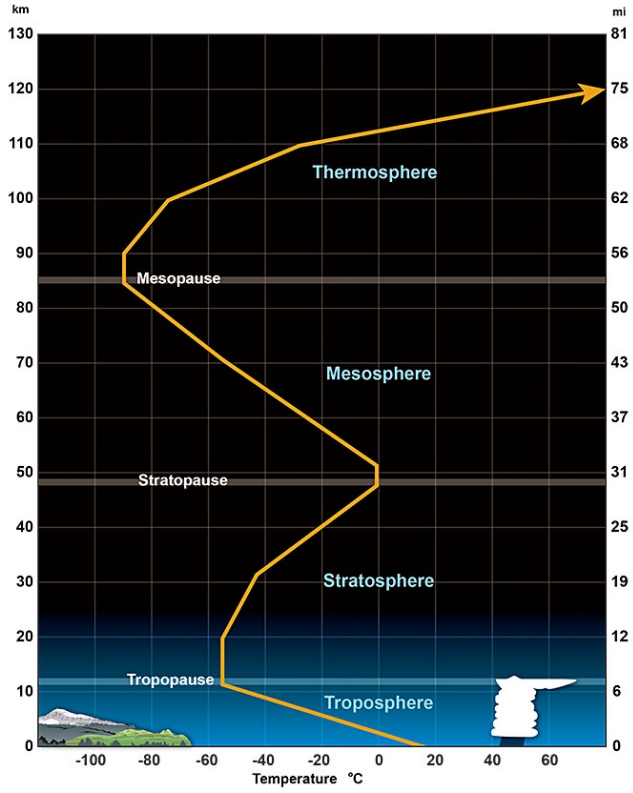

Figure 1.1: Temperature profile of the atmosphere (Source: http://www.srh.noaa.gov/jetstream/atmos/layers.html)

$$O_2 + O \rightarrow O_3 \tag{1.2}$$

Ozone is also destroyed by photolysis (equation 1.3, although in this case O_3 will mostly return promptly via equation 1.2, i.e. these two reactions define the O_3/O equilibrium) and by reaction with atomic oxygen (equation 1.4).

$$O_3 + h\nu \rightarrow O_2 + O \tag{1.3}$$

$$O_3 + O \rightarrow 2O_2 \tag{1.4}$$

Reactions 1.1-1.4 are known as the Chapman cycle (Chapman, 1930).

In addition to these reactions, ozone is also destroyed by reactions with free radical catalysts. Ozone destroying free radicals include OH, NO, Cl, and Br and are represented by X in the following reactions:

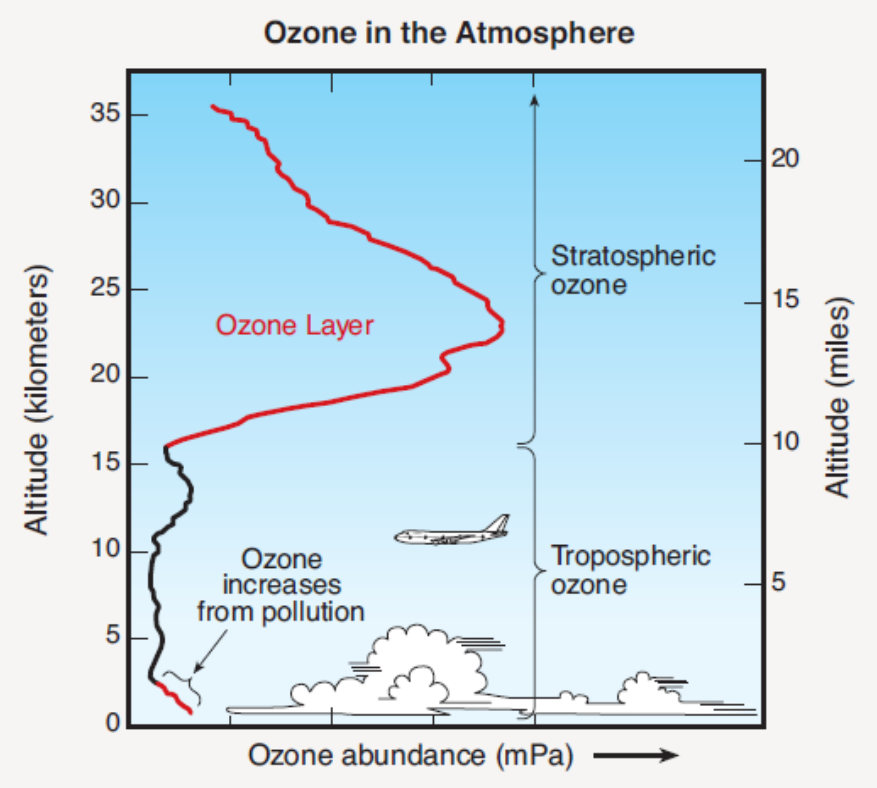

Figure 1.2: Illustration of the height profile of atmospheric ozone (Source: WMO (2011))

$$X + O_3 \rightarrow XO + O_2 \tag{1.5}$$

$$XO + O \rightarrow X + O_2 \tag{1.6}$$

The role of anthropogenic emissions in the destruction of ozone was first raised by Molina and Rowland (1974) and Crutzen (1974) which showed chlorofluoromethanes produced at the surface were able to reach the stratosphere where they would release ozone destroying chlorine upon photodissociation. This prompted significant monitoring efforts, one of which, detailed in Farman et al. (1985), detected thinning of the ozone layer over the Antarctic connected with the increased chlorine loading. Figure 1.3 shows this thinning of the ozone layer progressing to such a state that this feature would come to be commonly known as the "ozone hole". The area of the ozone hole is defined as the area in which column ozone is less than

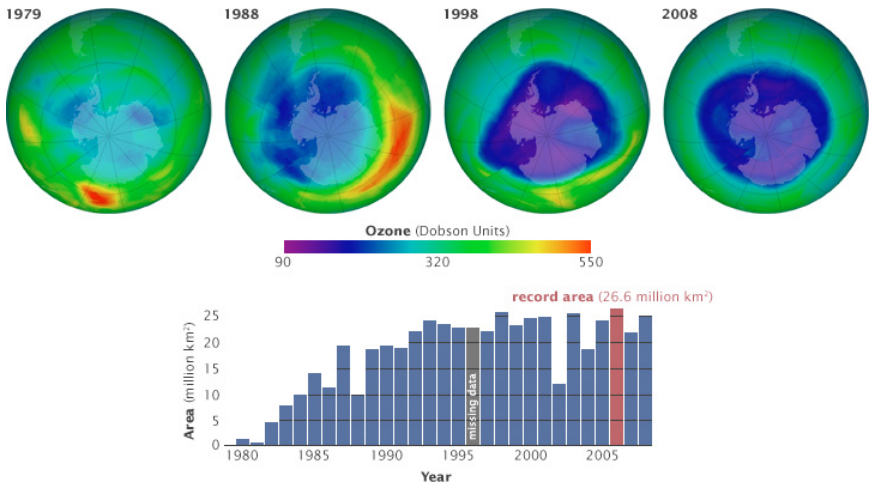

Figure 1.3: Evolution of the Antarctic ozone hole (Source: http://earthobservatory.nasa.gov/Features/EarthPerspectives/page3.php)

220 DU. This area peaked during 2006 at 26.6 million km^2 (an area roughly the size of North America). Solomon et al. (1986) showed that gas phase chemistry alone was insufficient to explain the observed ozone depletion at the pole and identified the role of polar stratospheric clouds (PSCs) in the heterogeneous chemistry responsible for ozone depletion. Man-made chlorofluorocarbons (CFCs) released into the troposphere will, when they reach the stratosphere, break down to form the reservoir species HCl and $ClONO_2$. Heterogeneous reactions on the surfaces of PSCs transform these reservoir species into species such as Cl_2, Cl_2O_2, HOCl, and $ClNO_2$ which can be photolysed into ozone destroying radicals when sunlight returns in the spring. The time evolution of these processes is illustrated in Figure 1.4.

In response to these observations, the United Nations implemented the Montreal Protocol in 1987, limiting the production of ozone depleting substances. Figure 1.5 shows the effect of the Montreal Protocol (and subsequent amendments and adjustments) on equivalent effective stratospheric chlorine (EESC, a measure of the total amount of ozone destroying gases in the stratosphere (Daniel et al., 1995; Newman et al., 2007)). As a result of the Montreal Protocol, EESC values have decreased by $\sim 10\%$ since the peak in stratospheric abundance around the year 2000. Observations have shown that springtime Antarctic total column ozone is now slowly, but significantly increasing (Solomon et al., 2016). Chemistry-Climate model simulations project that springtime ozone over the Antarctic region will

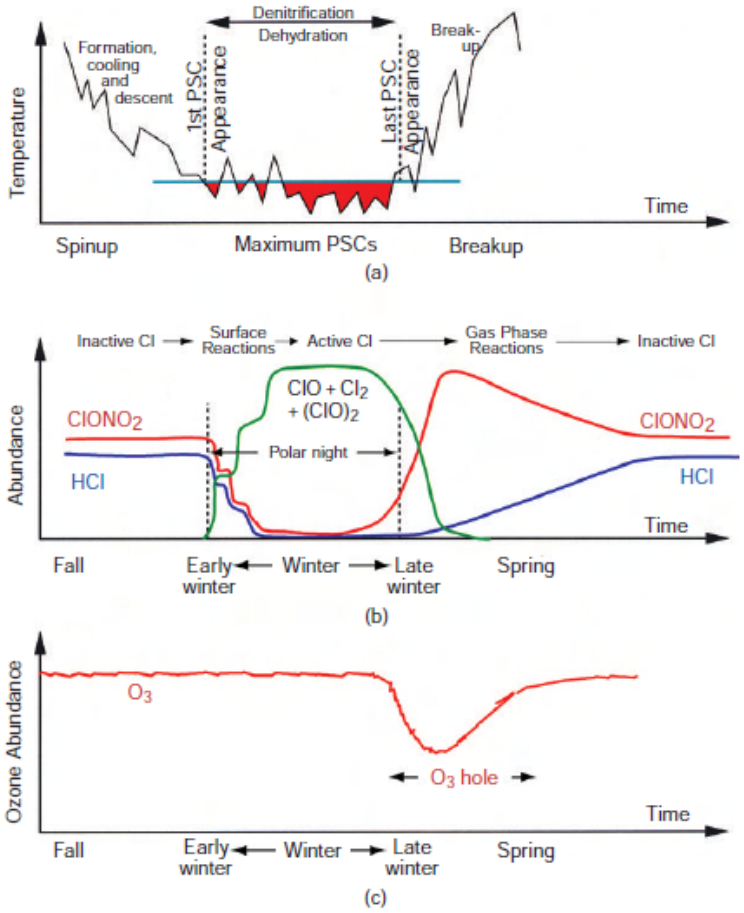

Figure 1.4: The processes associated with polar stratospheric ozone destruction (Wallace and Hobbs, 2006)

return to 1980 levels around 2050 (Eyring et al., 2010). The reason the decrease in EESC and resultant ozone recovery is slow (despite the relatively rapid halt to the emissions of CFCs) is that CFCs have long lifetimes in the stratosphere - ranging from approximately 50 to 100 years (Minschwaner et al., 2013; Hoffmann et al., 2014). Also, chlorine is neither consumed in the destruction of ozone nor is immediately "washed out" (as it can be in the troposphere when HCl is dissolved in water). Chlorine can be removed from the stratosphere via stratosphere-troposphere exchange (mostly as HCl). This process is also slow - governed by the stratospheric age-of-air which is of the order of 5 years.

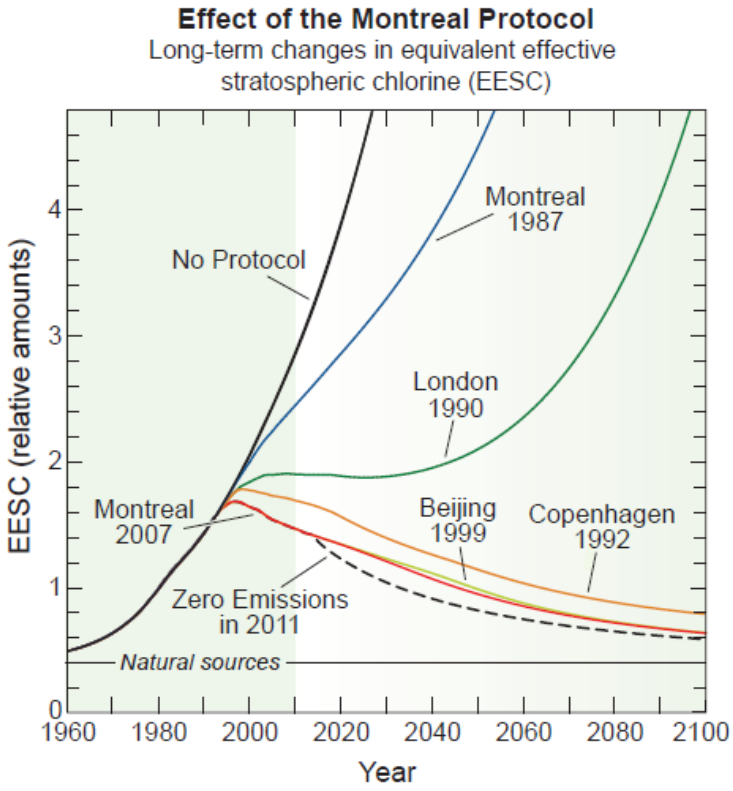

Figure 1.5: The effect of the Montreal Protocol on EESC (Source: WMO (2011))

1.2.2 The Southern Annular Mode

The Southern Annular Mode (SAM) is the leading mode of climate variability in the extra-tropical Southern Hemisphere. It describes the oscillation of atmospheric mass between the mid-latitudes and polar regions in a mostly zonally symmetric manner. The SAM is most commonly studied in the troposphere, where the oscillation manifests itself as latitudinal shift in the polar jet. In the stratosphere, it resembles more of a vacillation in the strength of the jet (Thompson and Wallace, 2000a). It was identified by examining the first empirical orthogonal function (EOF)[1] calculated over the southern extra-tropics (Kidson, 1988; Karoly, 1990; Gong and Wang, 1999;

[1]The EOFs are spatial patterns that are the result of decomposing the data set in terms of orthogonal basis functions. Each EOF has an associated index (or "Principal Component") that describes the variation over time concordant with the given spatial pattern.

Thompson and Wallace, 2000a). The first EOF by definition describes the spatial pattern that accounts for the largest amount of variability over the given region. Gong and Wang (1999) found by examining the first EOF of monthly mean sea level pressure (SLP) an approximately zonally symmetric structure that explained a sizeable proportion of the variance in that parameter (ranging from 17% in March to 33% in December). In the stratosphere, where synoptic scale variability is lower, the SAM explains a higher proportion of the variability; Thompson and Wallace (2000a) find the SAM at 50 hPa explains 56% of the variability during November.

As a index for this mode, Gong and Wang (1999) propose the difference in normalized zonal mean SLP between 40°S and 65°S, noting that these latitudes show a strong negative correlation (-0.59, significant at the 99% confidence level). The index is considered to be in its positive phase when pressure is anomalously low over the polar region. Based on this index, Marshall (2003) proposes an index calculated with SLP data collected from six stations located near 40°S and six stations near 65°S. While this index has the advantage of simplicity and remains popular, other studies of the SAM instead use an index based on the EOF technique. Various methods using this technique are examined by Baldwin and Thompson (2009). These other methods are particularly necessary when examining the vertical structure of the atmosphere because the Gong and Wang (1999) or Marshall (2003) indices are only defined at the surface. The method used in this thesis, which Baldwin and Thompson (2009) finds to be the simplest and most robust of the various methods they examine, uses an EOF of daily zonal-mean geopotential height (GPH)[2]. Further details on the calculation of the SAM index can be found in section 3.3.2.

The SAM exhibits a notable seasonality. The stratospheric SAM has a

[2]GPH is a measure of height above sea level adjusted for the variation of gravity; GPH measured across surfaces of constant pressure therefore provides information about the distribution of mass in the atmosphere. GPH (Z) as a function of elevation h is given by:

$$Z(h) = \frac{1}{g_0} \int_0^h g(\phi, z)\, \mathrm{d}z \tag{1.7}$$

where g is the local acceleration due to gravity, g_0 is the acceleration of gravity at the surface, ϕ is latitude, and z is elevation. The properties of GPH make it a useful atmospheric variable. For example, the average temperature of an atmospheric layer is proportional to the difference in GPH spanned by that layer. Also, the horizontal gradient of GPH is used to calculate the geostrophic wind (the theoretical wind that results from the balance between the Coriolis force and pressure gradient force).

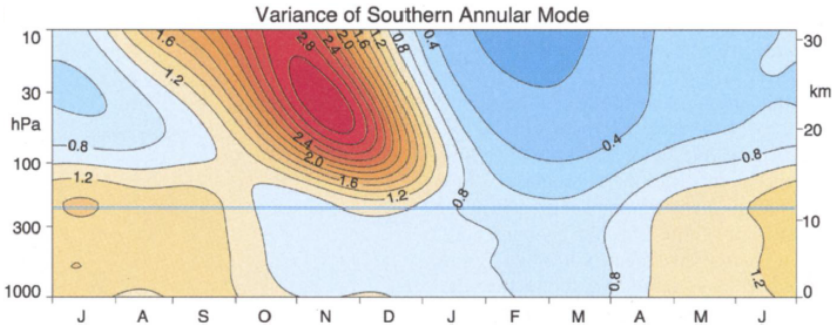

Figure 1.6: Variance of the SAM index for NCEP-NCAR reanalysis data 1979-2001. (Source: Baldwin et al. (2003))

maximum variance during September-December (Thompson and Wallace, 2000a; Baldwin et al., 2003). Noting this, Thompson et al. (2005) calculate the SAM EOF using only this season; this approach is also used in this thesis. Figure 1.6 shows a climatology of the variance in the SAM index. In the upper stratosphere the variance peaks in spring and at lower altitudes in the stratosphere the peak arrives progressively later (Baldwin et al., 2003). Thompson et al. (2005) show that this peak variance in the stratosphere coincides with the break-up of the Polar Vortex. In the troposphere the variability is somewhat larger during winter and early spring, Thompson et al. (2005) attribute this to increased tropospheric baroclinic activity during this season. In the troposphere, the variation in the SAM may be approximately modelled by Gaussian red noise with an auto-correlation of around 10 days (Hartmann and Lo, 1998). In the stratosphere, the persistence is longer, ranging from around 100 days during summer to 40 days during winter (Baldwin et al., 2003).

As the name implies, the SAM is largely a zonally symmetric feature. However, there are some deviations from zonal symmetry. Most notable is the zonal wavenumber 3 (Kidson, 1988). This is illustrated in Figure 1.7 which shows the 500 hPa SAM pattern (i.e. the 1^{st} EOF) and corresponding index calculated from the ERA-Interim reanalysis. The three centres of the wavenumber 3 pattern are approximately aligned with the Indian, Atlantic and Pacific Oceans. Also evident is some wavenumber 1 and 2 influence in the eastern Pacific. Kidston et al. (2009) calculates the variance attributable to each of the wave components using Fourier decomposition in both the

Table 1.1: Percentage of variance in the SAM pattern attributed to the first five Fourier components (Source: Kidston et al. (2009))

	Wavenumber				
	0	1	2	3	4
Summer	61.3	11.2	8.4	5.4	6.9
Winter	49.7	12.9	11.1	14.7	6.3

summer and winter seasons (see Table 1.2.2). They find that the SAM is more zonally symmetric in the summer, in which wavenumber 0 accounts for 61.3% of the variance, than the winter in which it accounts for just 49.7%. Another notable finding is that wavenumber 3 is more prominent in winter than summer.

The SAM is the Southern Hemisphere equivalent of the Northern Annular Mode (NAM). The differences in geography between the hemispheres - the south featuring a large continent at the pole surrounded by mostly ocean in the mid latitudes, the North featuring an ocean at the pole surrounded by two continents separated by two oceans - leads to some differences in the characteristics of the modes. Most notably the NAM is less zonally symmetric than the SAM in the troposphere (Thompson and Wallace, 2000a; Cohen and Saito, 2002), where the mid-latitude variability in the NAM is focused in the Atlantic Ocean sector. For this reason the NAM is often interpreted instead as the North Atlantic Oscillation (NAO). Wallace (2000) argues that the NAM and NAO are just different metrics describing the same phenomenon. The SAM explains more near-surface variance (27% compared to 20% on the monthly time scale (Thompson and Wallace, 2000a)). The seasonality of the modes also differs been the hemispheres. As noted previously, the variance of the SAM in the stratosphere is largest during September-December i.e. spring and early summer, coinciding with the break-up of the polar vortex. The NAM differs in that the variance is largest during December-March - the winter season, when the vortex is strongest (Thompson and Wallace, 2000a). Variability in the annular modes is caused by wave-mean flow interaction (wherein wave-breaking deposits momentum into the mean flow causing a deceleration). The reason the stratospheric SAM variance is relatively low during winter is due to the lack of upward propagating planetary waves (Thompson and Wallace, 2000a). The strength of the Southern Hemisphere polar jet at its peak is such that waves cannot

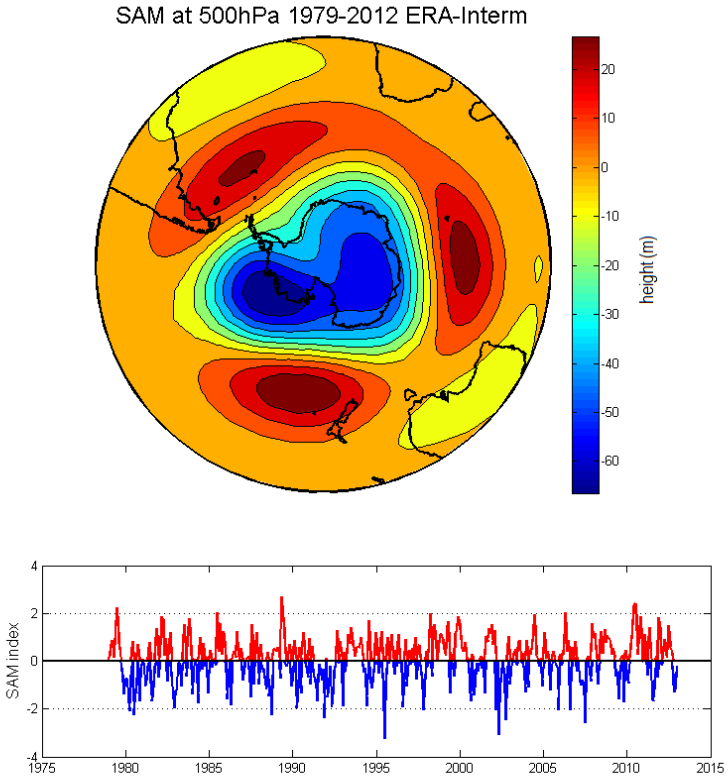

Figure 1.7: 500 hPa SAM pattern (above) and index (below)

propagate (Charney and Drazin, 1961) and are instead reflected back towards the troposphere. The Northern Hemisphere jet is not as strong and hence allows propagation of waves into the stratosphere more often, which accounts for the increased variability.

The SAM is an "internal" mode of variability, meaning it is a naturally occurring process in the climate system and not the result of external forcing. When considering the mechanisms responsible for the SAM it is convenient to consider the SAM in terms of shifting of the mid-latitude (eddy-driven) jet. A positive SAM, occurring when pressure is anomalously low over the pole, features a strong jet that is shifted poleward of its mean position. The meandering of the jet from its mean position is the result of a positive feedback between transient synoptic scale eddies and the jet (Hartmann and Lo, 1998; Limpasuvan and Hartmann, 1999, 2000; Lorenz and Hartmann,

2001). When the jet is displaced poleward there is enhanced equatorward eddy propagation (Hartmann and Lo, 1998). The propagation of wave activity away from the jet generates poleward momentum fluxes into the jet (Lorenz and Hartmann, 2001). Barnes and Hartmann (2010) find that this feedback is stronger during summer, explaining the greater persistence of the SAM during this season. During winter, they find the eddy feedback is weak over the Pacific region which results in a pulsing of the mid-latitude jet rather than a shifting of the jet in this region.

The SAM has numerous effects on climate on a regional scale (the following describes the effect of the positive SAM; an opposite effect is implied for the negative SAM). The large scale shifting of atmospheric mass that constitutes the SAM affects the meridional pressure gradient and therefore the zonal wind speed; a positive SAM is associated with anomalously strong westerlies over the Southern Ocean and anomalously weak westerlies around 30 to 45°S. This change affects temperatures in the Antarctic (Thompson and Solomon, 2002; Marshall et al., 2006; Marshall, 2007; van den Broeke and van Lipzig, 2004; Gillett et al., 2006). Over most of Antarctica, and especially over East Antarctica, the positive SAM is linked to lower surface temperatures. However, over the Antarctic Peninsula and southern Patagonia, the positive SAM is associated with warming due to the stronger westerlies increasing advection of warm air from the Southern Ocean (Thompson and Solomon, 2002). Marshall (2007) finds these correlations between the SAM and Antarctic temperatures to be strongest during summer and autumn. Focusing on the Antarctic Peninsula, Marshall et al. (2006) finds the SAM to have a greater effect on temperatures on the eastern side of the Peninsula compared to the west. This is likely due to the stronger westerlies resulting in a greater probability of the winds passing over the orographic barrier (Orr et al., 2004), thus advecting more of the climatologically warmer air from the west, as well as warming due to the Föhn effect as air descends over the barrier. This warming contributed to the collapse of the Larsen B ice shelf in 2002 (van den Broeke, 2005).

Over the Southern Ocean, Yin (2005) associates a poleward shift in the Southern Ocean storm track with a positive SAM, which leads to changes in precipitation patterns in the mid-latitudes (Gillett et al., 2006; Renwick and Thompson, 2006; Ummenhofer and England, 2007; Ummenhofer et al., 2009; Kidston et al., 2009; Meneghini et al., 2007; Hendon et al., 2007). The

positive SAM is associated with generally dry conditions in South America, New Zealand, and Tasmania and anomalously wet conditions over much of Australia and South Africa (Gillett et al., 2006). Kidston et al. (2009) focus on the New Zealand region. Here a positive SAM results in less summer rainfall over most of the country, especially the west coast of the South Island; the exception to this is the far north and east coast of the North Island and north east of the South Island. In winter, a positive SAM is instead related to increased rainfall on the west coast of the South Island. Ummenhofer et al. (2009) notes that in large areas of the North Island, the SAM has contributed as much as 80% to the decline in summer precipitation over recent decades. Hendon et al. (2007) focuses on Australia in which a positive SAM is associated with increased spring and summer rainfall on the southern east coast of Australia and decreased rainfall in western Tasmania. During winter, the positive SAM is instead associated with decreased rainfall over the south-east and south-west of Australia. Hendon et al. (2007) find that the SAM explains around 10-15% of the variance in the weekly rainfall in these regions. Meneghini et al. (2007) also find the positive SAM to be associated with increased rainfall over Northern Australia. The positive SAM is also associated with cooling over much of Australia and warming over Argentina, Tasmania, and New Zealand (Gillett et al., 2006).

The SAM also affects precipitation in the subtropics. Kang et al. (2011) find an increase in summer precipitation in the latitude band between 15°S and 35°S, particularly over the western Pacific, associated with a poleward shift in the extra-tropical jet. This is found to be the result of a poleward shift in the subtropical edge of the Hadley Cell linked to ozone depletion (Son et al., 2009; Polvani et al., 2011).

The change in the westerly wind associated with the SAM also affects the ocean by modifying the Ekman drift (Ekman, 1905). Stronger circumpolar westerlies at the surface produce enhanced northward Ekman drift at latitudes around 60°S, while weaker westerlies further to the north enhance southward Ekman drift around 30°S (Hall and Visbeck, 2002; Lefebvre et al., 2004). This in turn results in increased upwelling along the Antarctic coast and downwelling at around 45°S. This increases the density gradient and hence, increases the strength of the circumpolar current (Hall and Visbeck, 2002). Also, the positive SAM is associated with increased Southern Ocean Eddy activity (Meredith and Hogg, 2006), cooler sea surface temper-

ature (SST) over the Southern Ocean and warmer SSTs over mid-latitudes (Sen Gupta and England, 2006) and decreased Southern Ocean CO_2 uptake (Lenton and Matear, 2007).

The SAM also affects sea-ice in a number of ways. Hall and Visbeck (2002) find that the enhanced northward Ekman drift causes greater equatorward advection of sea ice and hence, a larger sea ice extent over the June to November period. Sen Gupta and England (2006) find a similar result for the January to April period but note that the Bellingshausen Sea and Antarctic Peninsula regions instead show a decrease in sea ice associated with the positive SAM due to the absence of enhanced Ekman drift in these regions. In the June to September period, however, Sen Gupta and England (2006) show large decreases in the sea ice concentration over the South Atlantic associated with SAM-driven warm SST anomalies. Lefebvre et al. (2004) points to meridional winds resulting from the non-annular component of the SAM advecting warmer air toward the Weddell Sea and the Antarctic peninsula and cooler air toward the Amundsen and Ross Seas which have the effect of decreasing and increasing the sea ice concentration in the respective regions. Considering all the impacts, the small overall trend toward greater Antarctic sea ice extent does not however, appear to be related to the trend toward a positive SAM (Lefebvre et al., 2004; Sigmond and Fyfe, 2010, 2014).

The SAM is influenced by various external forcings such as: ozone depletion, GHGs, volcanic eruptions and solar variance. In the stratosphere there has been a trend towards a positive SAM over recent decades. Thompson and Wallace (2000b) shows that the trend is strongest in November and December, meaning it is consistent with a delayed break-up of the polar vortex[3]. Haigh and Roscoe (2009) find the date of final warming to be increasingly delayed over the latter decades of the twentieth century, which they attribute primarily to ozone depletion. McLandress et al. (2010), using a climate model forced with changing ODSs while holding GHG concentrations fixed, have replicated this increase in stratospheric zonal wind speed / delay in final warming, thus demonstrating the influence of ozone depletion on the SAM. Similarly, they also predict a reversal in this trend, associated

[3]The break-up of the polar vortex may be quantified as the date of "final warming". This refers to the warming of the polar stratosphere due to mixing of warmer air from the mid-latitudes made possible by the weakened vortex. Usually this date is defined as the point at which the zonal mean wind changes from westerly to easterly.

with ozone recovery over the 21^{st} century. However, these future trends will be partially offset by the increasing influence of GHG forcing which acts to cool the polar stratosphere.

The impact of ozone depletion on the SAM in the stratosphere can, in part, be explained by the reduction in absorption of incoming shortwave radiation by stratospheric polar ozone, increasing the meridional temperature gradient (Randel and Wu, 1999) and hence the zonal wind speed via geostrophic balance. However, the effect on the SAM occurs is strongest during summer - after peak ozone depletion during the spring - which suggests the effect of ozone on atmospheric dynamics is also important (Orr et al., 2012, 2013; Ivy et al., 2016). The radiative cooling of the polar stratosphere and resultant increase in vortex strength begins a positive feedback wherein the stronger vortex results in fewer upward propagating planetary waves and hence, less planetary wave drag, further strengthening the vortex (Orr et al., 2012).

Similarly, in the troposphere, the SAM has also displayed a trend towards its positive polarity (Thompson and Wallace, 2000b; Marshall, 2003). Arblaster and Meehl (2006) investigate the influence of various external forcings on this trend by examining climate model runs in which each of the forcings exists in isolation; their findings are summarized in Table 1.2.2. The annual SAM trend is shown to be driven primarily by changes in GHG and ozone concentrations. The positive trend driven by GHGs is evident across all seasons. On the other hand, ozone forcing is much more important in summer. This ozone driven decadal trend may be explained in large part by cooling of the polar troposphere resulting from a reduction in downwelling radiation (Grise et al., 2009). However, the stratosphere (and hence ozone depletion) also influences the troposphere on shorter timescales; this is discussed more in section 1.2.3.

The recovery of ozone over the 21^{st} century has been simulated by climate models to exert the reverse influence on the SAM (Karpechko et al., 2010b; McLandress et al., 2011). McLandress et al. (2011) find that the influence of ozone on the SAM is opposed by GHG forcing over the 21^{st} century; this is illustrated in Figure 1.8. This figure shows the effect of ozone and GHG to be almost equally balanced such that the mean summer SAM remains relatively constant over the 21^{st} century. Morgenstern et al. (2014) produce a similar finding.

Table 1.2: Trend in SAM index over the period 1958-99 in the observations and model with various forcings (normalized units: 30 yr^{-1}). Bold font indicates significance at the 90% level (Source: Arblaster and Meehl (2006))

	Annual	DJF	MAM	JJA	SON
Obs. (Marshall 2003)	**1.51**	**1.56**	1.33	0.52	0.04
Volcanic	-0.16	-0.18	-0.56	0.26	-0.02
Solar	0.34	0.46	0.32	0.21	-0.09
GHG	**0.80**	0.37	0.60	0.59	0.49
Sulfate	-0.25	-0.44	-0.08	-0.25	0.22
Ozone	0.71	**1.27**	0.33	0.07	0.10
All forcings	**1.80**	**1.77**	**1.67**	0.42	0.58

While McLandress et al. (2011) find the ozone and GHG effects on the SAM to be additive, i.e. the sum of the trends is statistically indistinguishable from the trend in the simulation with the forcings combined, Morgenstern et al. (2014) do, however, find some interaction between the two forcings. Comparing simulations run with fixed ODSs and fixed ozone, they find that the regression of the SAM on the GHG-induced radiative forcing in the fixed ozone simulations is approximately twice as strong as the fixed ODS simulations. This suggests that the influence of ozone offsets around half of the effect of increasing GHGs (although it is noted that this value is subject to a considerable amount of uncertainty).

Amongst the other external forcings, volcanic and sulphate aerosol forcing generally produces negative trends and solar forcing produces generally positive trends; these forcings are weaker and are not considered statistically significant overall or for individual seasons. Although volcanic eruptions are shown not to have a significant influence on the recent SAM trend, there is some mixed evidence of shorter term effects. Roscoe and Haigh (2007) and Gillett and Fyfe (2013) find a negative correlation with volcanic aerosol. However, Karpechko et al. (2010a) and Barnes et al. (2016) find a positive SAM response to volcanic eruptions and Robock et al. (2007) find no significant effect. There is likely some cancellation between direct and indirect aerosol effects. The direct effect is likely a warming of the stratosphere, whereas the indirect effect is increased ozone depletion, causing cooling. Similarly, solar forcing (which varies on an 11 year cycle), while not contributing significantly to the overall positive trend in the SAM, has been shown to have a positive correlation with the SAM (Gillett and Fyfe, 2013).

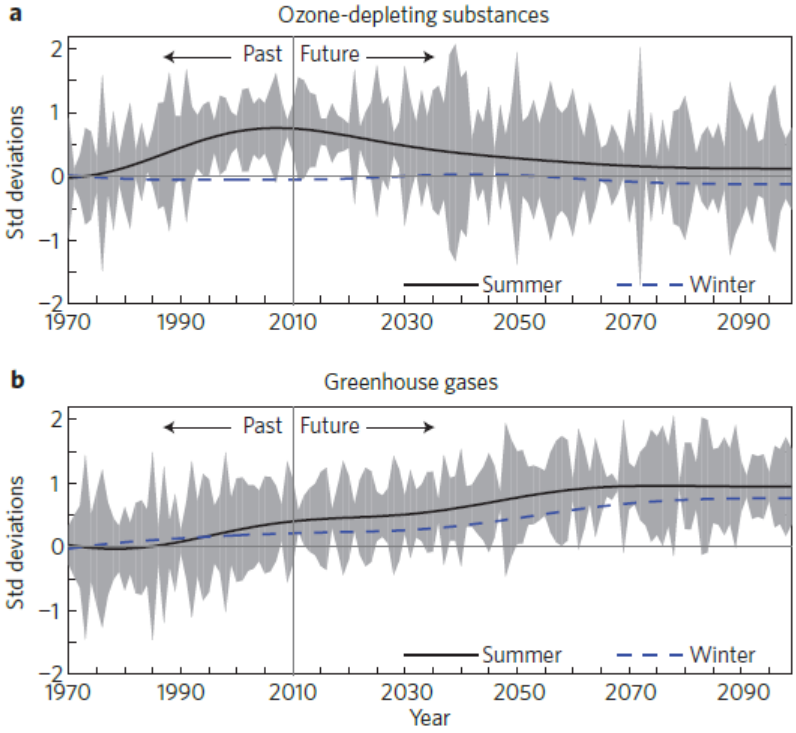

Figure 1.8: SAM index forced by changes in ODSs (top) and GHGs (bottom)(Source: Thompson et al. (2011))

In addition to the external forcings discussed above, the SAM also interacts with other modes of internal variability. The other major mode of internal variability in the Southern Hemisphere is the El Niño - Southern Oscillation (ENSO). ENSO is primarily a tropical phenomenon related to variation in Pacific Ocean sea surface temperature but has been found to have some interaction with the SAM. Fogt et al. (2011) find a slight preference for combinations of positive SAM/La Niña and negative SAM/El Niño during summer. Lim et al. (2013) report a similar finding where the correlation between SAM and El Niño is found to be around -0.45 ($p < 0.05$) during late spring and early summer. The relationship between the two modes is due to the conditions associated with El Niño(La Niña) being suited to produce weak(strong) anti-cyclonic wave breaking on the equatorward side of the polar jet which drives negative(positive) tendency in the SAM (Gong et al., 2010).

1.2.3 Stratosphere-Troposphere Coupling

It is unsurprising that ozone affects the stratosphere as that is where ozone is most abundant and ozone depletion is occurring. However, the primary focus of this thesis is tropospheric climate. There exist numerous studies demonstrating that the stratosphere is coupled to the troposphere. The annular modes have proven to be a useful diagnostic for examining this phenomenon. Stratosphere-troposphere coupling was first examined in the Northern Hemisphere; Baldwin and Dunkerton (2001) showed that large NAM anomalies in the stratosphere of either sign are often followed by anomalies of the same sign in the troposphere that last for around 60 days. The equivalent was later demonstrated for the SAM by Thompson et al. (2005). This is illustrated in Figure 1.9 which shows a composite of the SAM index over the depth of the stratosphere and troposphere for occasions linked to an extreme SAM at 10 hPa. The large SAM anomaly in the stratosphere persists for 2-3 months, slowly propagating downward. Beginning at around 20 days after the peak in the stratosphere, anomalies are observed in the troposphere and occur for around two months. Thompson et al. (2005) present the composite as the difference between the positive and negative extreme events, making the implicit assumption that the coupling behaviour is symmetrical for positive and negative SAM events. Baldwin and Dunkerton (2001) find that such a symmetry of coupling behaviour holds for the NAM. Coupling has also been demonstrated in analyses that do not utilize the annular modes. For example, Graversen (2003) show that the annual cycle in zonal mean zonal wind propagates downward from 10 hPa to the surface on a timescale of about two months.

The coupling between the stratosphere and troposphere has been identified to be important for extended range weather forecasts (Kuroda, 2008). For example, Baldwin et al. (2003) show that the NAM in the lower stratosphere is a better predictor of the 30 day mean NAM (beginning at a 10 day lag) at 1000 hPa than the 1000 hPa NAM itself. Similarly Christiansen (2005) found that the prediction of near surface zonal mean zonal wind at 60°N is greatly improved when the lower stratosphere zonal wind is used as a predictor, and that restricting the prediction to periods in which this predictor was more anomalous improved the prediction.

Stratosphere-troposphere coupling is observed in many climate and chemistry-climate models. Gerber et al. (2010) illustrates the Northern Hemisphere

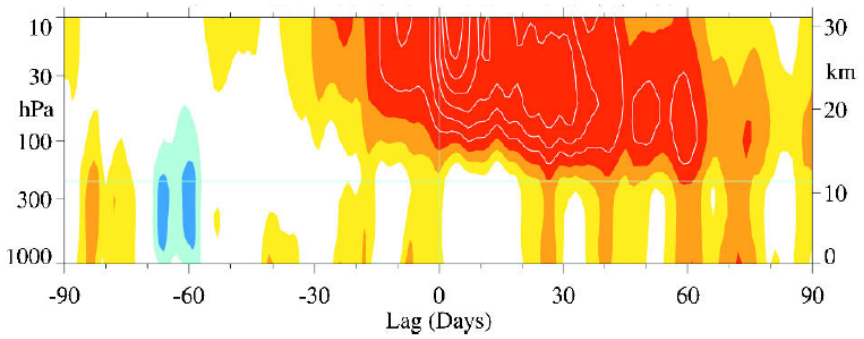

Figure 1.9: Composite difference of SAM index between seven extreme positive events and seven extreme negative events. Zero lag corresponds to the time at which the SAM index crosses +/-2. Contours and shading are increments of 0.5, reds denote positive values of the SAM index. Source: Thompson et al. (2005)

coupling in a number of models from the Coupled Model Intercomparison Project phase 3 (CMIP3) and the Chemistry-Climate Model Validation Activity phase 2 (CCMVal-2), using the composite technique described above. Most models exhibited some degree of coupling, with many overestimating the strength of the coupling. This is likely due to the annular mode in the stratosphere being too persistent in models. Gerber et al. (2010) also examine the fraction of variance of the 850 hPa annular mode index explained by the mode at other levels (see Figure 1.10). The coupling is shown to be stronger in the Southern Hemisphere than in the North in both the reanalysis and models. For the models, the strong coupling occurs later in the year in both hemispheres and, particularly in the south, is active over a longer time period compared to the reanalysis. It is also notable that the variance explained peaks around the middle of the stratosphere in the reanalysis, but near the tropopause in the models. Morgenstern et al. (2010a) also examines coupling in a number of CCMVal-2 models, using the technique of calculating the correlation between the NAM at different heights with the 50 hPa NAM. They find the majority of models to underestimate the correlation in winter but, as an ensemble, perform better in spring - albeit with a large spread among the models.

While the evidence of coupling behaviour is robust in both observations and models, the mechanisms involved are not well understood. One mechanism in which the stratosphere affects the troposphere is via "downward

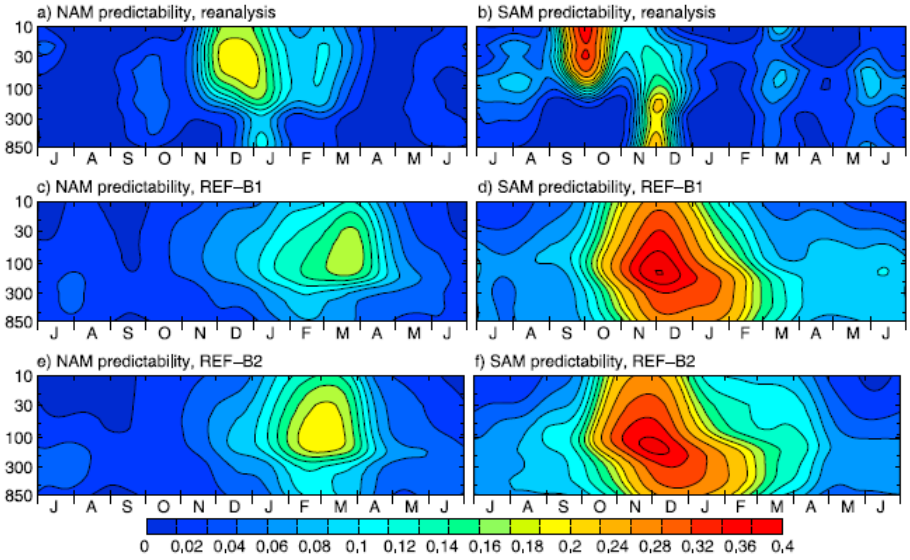

Figure 1.10: Climatology of the fraction of variance of the 30 day mean 850 hPa NAM (left) or SAM (right) explained by the mode at other levels. ERA-40 reanalysis (top) and REF-C1 (middle) and REF-C2 (bottom) experiments from an ensemble of CCMVal-2 models. Source: Gerber et al. (2010)

control" (Haynes et al., 1991; Kidston et al., 2015). This mechanism works as follows: an increase in the zonal wind speed in the stratosphere is accompanied by an anomalous meridional circulation (Andrews et al., 1987) due to the conservation of angular momentum. This circulation constitutes ascending flow (inducing adiabatic cooling) over the pole and descending flow (adiabatic heating) in mid/low latitudes. This flow induces changes in the troposphere in order to retain hydrostatic/geostrophic/thermal wind balance - in particular low pressure anomalies over the pole and high pressure anomalies over mid-latitudes, i.e a positive SAM anomaly. However, it is thought that this mechanism alone is not sufficient to account for the observed coupling (Thompson et al., 2006; Kunz and Greatbatch, 2013).

Studies in simplified climate models have been able to reproduce the phenomenon (e.g. Polvani and Kushner, 2002), showing a poleward shift of the tropospheric jet in response to an imposed cooling of the polar stratosphere, while not satisfactorily revealing the mechanism in full (Kushner and Polvani, 2004). These studies do, however, reveal some aspects of the mechanism such as: the role of eddies (Kushner and Polvani, 2004), the

importance of stratospheric variability (Gerber and Polvani, 2009), planetary waves (Song and Robinson, 2004) and the position of tropospheric jet (Garfinkel et al., 2013). These factors are important in the mechanism demonstrated by Orr et al. (2012) in which a stronger polar vortex (resulting from the radiative impact of ozone depletion or variation in the upward planetary wave flux) reduces the upward propagation of planetary waves, further strengthening the vortex. This positive feedback has the effect of drawing the wind anomalies downward as the height to which the vertical waves can propagate is successively lowered (Kuroda and Kodera, 1999; Baldwin and Dunkerton, 2001; Christiansen, 2001). Upon reaching the tropopause these wind anomalies have the effect of trapping planetary waves in the troposphere (Song and Robinson, 2004) and increasing the equatorward propagation of synoptic eddies in the upper troposphere which is important in maintaining a poleward shift of the jet (Hartmann and Lo, 1998). Chen and Held (2007) also find that an increase in the lower stratospheric westerlies has the effect of increasing the eastward phase speed of the synoptic eddies and hence the latitude of subtropical wave breaking, shifting the pattern of eddy momentum flux convergence poleward.

Coupling also appears to occur due to wave reflection. Shaw et al. (2010) find that, in addition to a reflective layer in the stratosphere, there must also be a high latitude meridional waveguide required for coupling to occur. They find that in the Southern Hemisphere, this type of coupling occurs during September to December. In contrast to the wave - mean flow interaction mechanism, this type of coupling occurs on time scales of less than 10 days rather than months (Perlwitz and Harnik, 2004). Shaw et al. (2011) show that this type of coupling is affected by ozone depletion, in that the delayed break-up of the vortex increases the season in which this coupling is active.

While the mechanisms described above are well established ways in with the stratosphere may interact with the troposphere, their relative importance in the coupling events of the type identified by Baldwin and Dunkerton (2001) remains a subject of much debate.

1.2.4 Blocking

Atmospheric blocking refers to large, quasi-stationary, high pressure (anticyclonic) features that persist beyond the synoptic timescale (around 5 days) and inhibit the mid-latitude zonal flow. Most of the blocking in the Southern Hemisphere occurs in the South Pacific region and, to a lesser extent, the south-western Atlantic and exhibits a strong seasonal cycle with blocking being more common during winter and autumn (see Figure 1.11) (Trenberth and Mo, 1985; Sinclair, 1996; Renwick, 2005; Parsons et al., 2016). In contrast, blocking in the Northern Hemisphere is more common in winter and spring (Wiedenmann et al., 2002; Barriopedro et al., 2006). The physical mechanisms that lead to a blocking event are not well understood (Barnes et al., 2012; Cowan et al., 2013; Christensen et al., 2013), but the absorption of synoptic scale eddies has been identified as an important feature in the maintenance of existing events (Shutts, 1983, 1986; Yamazaki and Itoh, 2009).

There is no universally accepted metric with which to diagnose blocking; generally, the methods used are variations on two approaches. One is based on the work of Rex (1950) which takes reversals in the meridional GPH or potential temperature gradient as indications of blocking (Lejenäs and Ø kland, 1983; Tibaldi and Molteni, 1990; Pelly and Hoskins, 2003). The other looks for persistent positive anomalies (PPAs) in either surface pressure or GPH fields (Dole and Gordon, 1983; Renwick, 2005; Parsons et al., 2016). In comparing the two approaches, Liu (1994) found that PPAs centred around 60°N correspond well with the Rex (1950) definition of blocking, but not as well for PPAs centred around 45°N. In this study we use the PPA approach.

Climate models tend to underestimate the frequency of blocking (Palmer et al., 2008). The simulation of blocking is found to be sensitive to the horizontal resolution of the model; Matsueda et al. (2009) demonstrate an increase in blocking frequency by increasing the resolution of their model. Anstey et al. (2013) shows a similar result by comparing blocking frequency across a range of different models. Errors in blocking frequency have also been shown to be linked to errors in simulation of the climatological mean state (Scaife et al., 2010).

Blocking has been shown to have significant effects on weather over mid-latitude continental regions. For example, South Atlantic blocking events

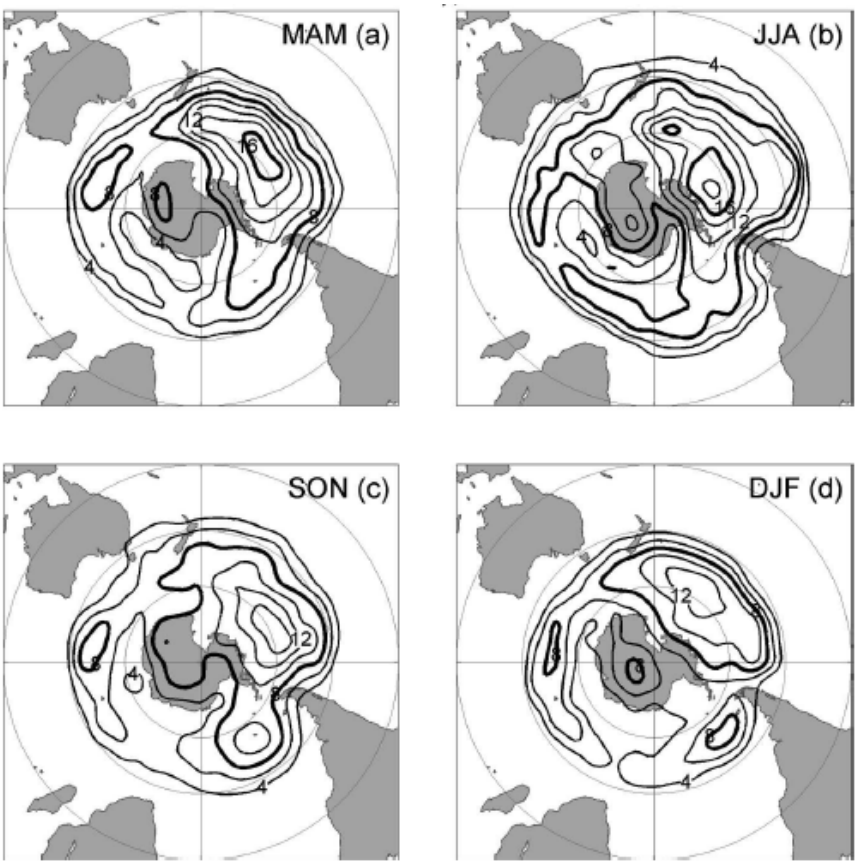

Figure 1.11: Climatology of the blocking frequency (%) for (a) autumn, (b) winter, (c) spring and (d) summer. Source: Renwick (2005)

result in colder conditions over much of Argentina and warmer conditions on the southern tip of the South American continent and the Antarctic Peninsula (Mendes et al., 2008). Kayano (1999) find that blocking over the East Pacific during summer results in colder, drier conditions in South America south of 40°S. Blocking in the Oceania region is found to produce significantly colder conditions in Southern Australia (Mendes et al., 2008). The amount of rainfall in Southern Australia is also influenced by blocking with the direction of influence determined by the location of the blocking event (Risbey et al., 2009; Cowan et al., 2013; Pook et al., 2013). Generally, blocking events to the south of Australia cause a decrease in rainfall in Northern Australia during summer and an increase in rainfall over south-eastern regions in the other seasons, especially spring (Risbey et al., 2009; Pook et al., 2013). Cowan et al. (2013) find that blocking events occurring

further to the east instead have the effect of decreasing rainfall in Eastern Australia. Blocking also plays a role in Australian heat waves (Pezza et al., 2012).

Large scale modes of variability such as the SAM and ENSO are known to have an effect on blocking in the Southern Hemisphere. Oliveira et al. (2014) show that El Niño conditions are related to an increase in the number of blocked days over the Central and Eastern Pacific, while La Niña conditions are linked to a decrease in the number of blocked days over the Western and Central Pacific. Mendes and Cavalcanti (2014) find that blocking in the West Pacific and Atlantic regions is more frequent when the SAM is positive and more frequent in the South East Pacific when the SAM is negative. Berrisford et al. (2007) and Parsons et al. (2016) also find a positive correlation between SAM and blocking frequency in the Western Pacific. The interplay between the ENSO and SAM is also significant (Oliveira et al., 2014), for example: negative SAM combined with El Niño enhances the blocking frequency over the eastern Pacific, while the positive SAM combined with La Niña is unfavourable for the formation of blocking events in the western Pacific.

Oliveira et al. (2014) find no significant trend in Southern Hemisphere winter blocking frequency over the period 1958-2010. Parsons et al. (2016) find a decrease in South Pacific blocking over the 21^{st} century in simulations forced by increasing GHG concentrations. Similar results have been found in the Northern Hemisphere (Matsueda et al., 2009; Barnes et al., 2012). The 5^{th} Assessment Report (AR5) of the Intergovernmental Panel on Climate Change (IPCC) also states, with medium confidence, that blocking will not increase in either hemisphere in the future (Christensen et al., 2013). The link between blocking and the SAM suggests that ozone depletion (in its driving of a positive SAM trend) may have an effect on blocking, although there is no research that explicitly links the two. Woollings et al. (2010) show some downward influence from the stratosphere (via annular mode anomalies) on blocking events in the Northern Hemisphere but no equivalent study exists for the Southern Hemisphere.

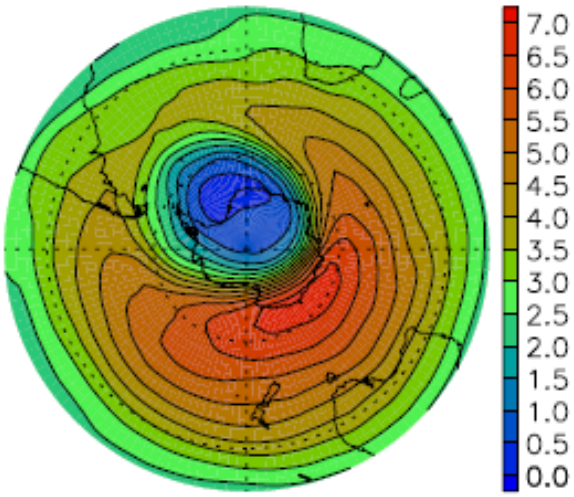

Figure 1.12: ERA-40 Ozone mass mixing ratio(mg/kg) at 50 hPa during October 2000. Source: Crook et al. (2008)

1.2.5 Zonally Asymmetric Ozone

While the distribution of ozone, and the ways in which it affects the climate are largely zonally symmetric, it is also important to account for effects of zonal asymmetries in the ozone distribution. The asymmetry in ozone in winter and spring is caused by planetary wave driven displacement or distortions of the polar vortex (Wirth, 1993; Quintanar and Mechoso, 1995; Waugh, 1997). The polar vortex and ozone hole are closely linked as the degree of ozone depletion affects the temperature gradient and thus the strength of the vortex, while the strength of the vortex affects the degree to which ozone depleted air is isolated from the relatively ozone rich air in the mid-latitudes (Beron-Vera et al., 2012; Smith and McDonald, 2014). The spatial distribution of ozone varies with low wavenumber patterns, primarily wavenumber 1. Ialongo et al. (2012) show that wavenumbers 1 and 3 explain more than 95% of the ozone longitudinal variation which can exhibit perturbations of up to 50% of the zonal mean value. They also show that this asymmetry extends over the depth of the stratosphere. The asymmetry is typically such that ozone depleted air extends further equatorward in the Atlantic region (see Figure 1.12).

Until recently, most GCMs have prescribed zonally averaged ozone distributions (Randall et al., 2007; Hegerl, 2007), but a number of studies

have since emphasized the importance of modelling the zonal asymmetry of ozone. These studies take the approach of comparing model simulations run with zonally average ozone to those with either prescribed three dimensionally varying ozone (Crook et al., 2008) or interactively modelled ozone (Gillett et al., 2009; Waugh et al., 2009). Crook et al. (2008) find a larger stratospheric cooling associated with the asymmetric ozone. This cooling was located at around 150°E - the region with above average ozone - which showed that this effect is not due directly to radiative heating but instead to dynamical heating. The amount of cooling from the asymmetric ozone effect is found to be approximately as large as the magnitude of the radiative effect of ozone depletion itself over the last 30 years. However, Crook et al. (2008) note that the year studied (2000) exhibited a particularly large ozone asymmetry so this perhaps represents an upper bound of this zonal asymmetric effect. Gillett et al. (2009) and Waugh et al. (2009) expand on the work of Crook et al. (2008) by instead interactively modelling ozone, thus ensuring the ozone is consistent with the atmospheric dynamics. The findings of these studies are consistent with those of Crook et al. (2008). Additionally, Waugh et al. (2009) notes that the zonally asymmetric cooling effect is larger when the ozone hole itself is larger, meaning that Antarctic temperature trends are underestimated as a result of zonally averaged ozone being used in climate models.

In addition to the effect on stratospheric temperature, zonally asymmetric ozone also affects tropopause height. Evtushevsky et al. (2008) find that the tropopause height and sharpness are influenced by zonally-asymmetric ozone during the spring, the below average ozone regions being associated with a higher tropopause and a thicker transition layer. Thickening of the transition layer between the stratosphere and the troposphere increases troposphere - stratosphere exchange and mixing activity (Pan et al., 2004). This is important as exchange of ODSs and GHGs across the tropopause lead to various chemical and radiative impacts on climate (Holton et al., 1995, and references therein).

Ozone has been shown to be an important factor modulating the refractive index and thus the propagation of planetary waves (Nathan and Cordero, 2007; Gabriel et al., 2007; McCormack et al., 2011). Gabriel et al. (2007) find the introduction of zonally asymmetric ozone results in a change in the upward and eastward directed wave flux. Compared to the case of

zonally symmetric ozone, these wave fluxes are increased in the western Northern Hemisphere stratosphere and reduced in the east. Albers and Nathan (2012) explore the ways in which zonally asymmetric ozone, via its influence on wave propagation, affects the polar vortex. They identify two pathways in which the polar vortex is influenced. The first describes the effect of zonally asymmetric ozone on vertical energy flux and planetary wave drag, the second describes the effect on zonal-mean temperature (and hence thermal wind balance) of wave-ozone flux convergence. Both pathways are found to be important in influencing the polar vortex.

Over the period 1979-2003, Grytsai et al. (2005) found the position of the ozone minimum at 65°S drifted eastward at a rate of 23.6±7.2° per decade, with the position of the maximum remaining constant. Grytsai et al. (2007) extended this study showing eastward trends in the ozone minimum for all latitudes between 50 and 80°S. However, the cause of this trend was not identified.

1.2.6 Statistical Methods

Student's t Test

Student's t test is a statistical hypothesis test. It tests the hypothesis that the mean of a distribution is not equal to zero (one sample t test) or that two distributions have different means (two sample t test). In this thesis the two sample version is used. The assumptions required for the test are that the distributions are normally distributed and have equal variances. The test uses the t statistic which is calculated using the following formula:

$$t = \frac{\bar{X_1} - \bar{X_2}}{\sigma\sqrt{\frac{1}{n_1} + \frac{1}{n_2}}} \tag{1.8}$$

where

$$\sigma = \sqrt{\frac{(n_1 - 1)\sigma_1^2 + (n_2 - 1)\sigma_2^2}{n_1 + n_2 - 2}} \tag{1.9}$$

In which X_1 and X_2 are the means, σ_1 and σ_2 the standard deviations and, n_1 and n_2 the sizes of the two samples. A p value for the test may then be obtained from the resulting t statistic by using Student's t distribution. For a chosen significance level the null hypothesis (i.e. the two distributions have equal mean) may be rejected if the p value is below a certain level.

For example, if a 95% significance level is chosen the null hypothesis is rejected for $p < 0.05$. Rejection of the null hypothesis indicates that the difference found between the means of the two distributions is unlikely to have occurred by chance (where the degree of unlikelihood is given by the significance level).

Wilcoxons Rank Sum Test

Wilcoxon's rank sum test (Wilcoxon, 1945) is a statistical hypothesis test that determines the likelihood that two samples come from populations with the same distributions. Unlike Student's t test it does not require the assumption of normal distributions. While the Student's t focuses on the means of the two samples, Wilcoxon's rank sum test examines the "shape" of the distribution. Specifically, the null hypothesis of the test is that the probability of an observation from population 1 being greater than an observation from population 2 is equal to the probability of an observation from population 1 being less than an observation from population 2. The test statistic U is calculated using the following procedure:

- Assign a numeric rank to each observation of the combined and ordered set of observations i.e. the lowest value will be assigned a rank of 1 and the highest value will be assigned the rank of $n_1 + n_2$.
- Sum the ranks assigned to observations from population 1.
- Calculate U_1 using the following equation:

$$U_1 = R_1 - \frac{n_1(n_1 + 1)}{2} \tag{1.10}$$

  where R_1 is the sum of ranks from sample 1.

As in the case of the t, a p value can be obtained based on the known distribution of U. For small sample sizes this is tabulated; for large sample sizes the distribution U is approximately normally distributed. Note that the above calculates U based on sample 1, but one could also use sample 2. They are related by the following equation:

$$U_1 + U_2 = n_1 n_2 \tag{1.11}$$

Tables for U are typically formulated in terms of the smaller of the two values.

1.2.7 Summary and Outlook

- The SAM is a major mode of climate variability in the Southern Hemisphere. It is linked to variations in temperature and precipitation over Antarctica and mid-latitude land masses. The mean state of the SAM has been shown to be influenced by changes in stratospheric ozone. This thesis will examine the influence of ozone on other properties of the SAM, namely: the frequency of extremes and the persistence.

- The stratosphere is known to be coupled to the troposphere. Large SAM anomalies in the stratosphere are followed by similarly signed anomalies in the troposphere persisting well beyond typical tropospheric timescales. This thesis investigates the effect of changes in ozone on the strength of this coupling. The mechanisms underlying the coupling are not well understood. This thesis aims to add to the understanding by examining the coupling simulated by different climate models.

- Atmospheric blocking occurs in the Southern Hemisphere primarily in the Pacific and Western Atlantic regions. These blocking events have an impact on temperature and precipitation in nearby continental regions. Blocking frequency has been shown to decrease in response to increasing GHG forcing, but the effect of changing ozone is not known; this is investigated in this thesis.

- The distribution of ozone in the stratosphere is somewhat zonally asymmetric, with the ozone hole displaced from the pole in the direction of South America. This is an important consideration in climate models as this asymmetry has been shown to influence polar stratospheric temperatures via dynamical heating. The minima in ozone have been shown to trend toward the east over recent decades, although the cause of this trend is unidentified. The relationship been ozone depletion and this trend and other changes in the ozone distribution is investigated in this thesis.

Chapter 2

Models and Data

2.1 NIWA-UKCA Model

The primary model used in this study is the National Institute of Water and Atmospheric Research-United Kingdom Chemistry and Aerosols (NIWA-UKCA) coupled atmosphere-ocean chemistry-climate model (AOCCM). The model combines an early, low-resolution version of the Hadley Centre Global Environment Model version 3 atmosphere ocean (HadGEM3-AO) model (Hewitt et al., 2011), which includes the Met Office Unified Model (UM) atmosphere model (Davies et al., 2005), the Nucleus for European Modelling of the Ocean (NEMO) ocean model (Madec, 2011), and the Los Alamos sea ice model (CICE) (Hunke et al., 2015), with the NIWA-UKCA chemistry module (Morgenstern et al., 2009, 2017). The UM atmosphere model is non-hydrostatic and fully compressible and uses a semi-Lagrangian advection scheme, it also includes an interactive land surface scheme. The version of the UM used here features a number of improvements over the version described by Davies et al. (2005). These are detailed by Hewitt et al. (2011) and include: a change from a diagnostic to a prognostic cloud scheme which increased the cloud persistence and thus improved the simulation of cloud cover, an improved simulation of detrainment in the convection scheme which provides a better representation of convective clouds, an improved resolution of the orography, and a new method for calculating soil hydraulic conductivity. The version used in this study has a horizontal resolution of 3.75° by 2.5°, a model top of 84 km and 60 model levels. The version of the NEMO ocean model used has a horizontal resolution of $\sim$2°

by 1° and 31 model levels.

The NIWA-UKCA model is particularly well suited for analysis of the interaction between ozone and climate due to its representation of the stratosphere and largely explicit stratospheric chemistry module. The model has a top near the mesopause and a relatively large number of model levels. This is an improvement over previous generations of models, many of which had a model top below the stratopause. The chemistry module includes more than 60 chemical species and around 250 different reactions (Morgenstern et al., 2009, 2013, 2017). Importantly the simulation of ozone is fully interactive, meaning that it responds to atmospheric dynamics as well as chemistry. This is an improvement on previous generations of models in which ozone was prescribed or calculated "semi-offline" (Eyring et al., 2013a). The high vertical resolution, and the interactive chemistry, impose a high computational cost; for this reason the model has lower horizontal resolution than the standard HadGEM3 model.

Analysis of NIWA-UKCA output has been published in Morgenstern et al. (2014) and Oberländer-Hayn et al. (2016) in addition to the two papers included this in thesis. Oberländer-Hayn et al. (2016) examine the tropical upward mass flux as part of an investigation of the Brewer-Dobson circulation. They show that the model climatology agrees with reanalysis output within the uncertainty bounds and that the model trend over the 21^{st} century is consistent with the other models examined. Morgenstern et al. (2014) investigate the ozone and GHG-related forcing of the mean state of the SAM. Comparisons with reanalysis output show that the model correctly identifies a positive historical trend in the tropospheric SAM index. The trend is somewhat underestimated in the model, although the variability in the trend amongst the model ensemble is such that this is not necessarily a failing of the model representation of the SAM. The modelled SAM index over the 21^{st} century shows no trend which is consistent with other model studies (e.g., Karpechko et al., 2010b; McLandress et al., 2011; Gillett and Fyfe, 2013). It is also shown by Morgenstern et al. (2014) that the annual cycle total column ozone agrees well with observations.

2.2 Model Simulations

Three simulation ensembles, with differing combinations of forcings, are used in this thesis. The reference simulation ensemble, which consists of five simulations, has GHGs following the Representative Concentration Pathway 6.0 (RCP6.0) scenario (Meinshausen et al., 2011; van Vuuren et al., 2011; Masui et al., 2011) and chlorinated or brominated ozone-depleting substances (ODSs) following the A1 scenario (WMO, 2011). This experiment is referred to as "REF-C2" and covers 1950-2100. To isolate the effect of ozone depletion, this ensemble will be compared to a second ensemble of two SEN-C2-fODS simulations; these runs differ from REF-C2 only in that ODSs are held fixed at their 1960 levels. Similarly, the effect of GHGs may be isolated by comparing the REF-C2 ensemble to an ensemble of three SEN-C2-fGHG simulations in which GHGs are held fixed at 1960 levels. It is important to note here the overlap between radiative and chemical effects of ODSs and GHGs. In the case of the SEN-C2-fODS simulations, holding the ODS fixed means that, in addition to fixing their chemical effect on ozone, the radiative impact of the ODSs is also fixed. Likewise, for the SEN-C2-fGHG simulations, holding GHG gases fixed means fixing their radiative impact, but also some of these GHGs also have a impact on ozone chemistry (such as NO_x and HO_x). Overall, these effects are small and do not figure into the results presented in this thesis.

Both SEN-C2-fODS and SEN-C2-fGHG are initialized from two REF-C2 simulations and cover 1960-2100. These experiments are defined in Eyring et al. (2013b) as part of the Chemistry-Climate Model Initiative (CCMI). The RCP6.0 is one of four scenarios used by climate models to describe future GHG concentrations; the others being RCP2.6, RCP4.5 and RCP8.5 (see Figure 2.1). The number corresponds to the increase in radiative forcing in the year 2100 relative to pre-industrial values, i.e. RCP6.0 has an increase in radiative forcing of 6.0Wm^{-2}. In RCP6.0, GHG emissions peak around 2060 (Masui et al., 2011), although concentrations, and hence the radiative forcing, rise throughout the 21^{st} century and stabilize after 2100 at around 850 ppm of CO_2 equivalent (van Vuuren et al., 2011). RCP6.0 should be thought of as a "medium" baseline scenario (van Vuuren et al., 2011); the fifth assessment report (AR5) of the Intergovernmental Panel on Climate Change (IPCC) states that the likely increase in global mean temperature

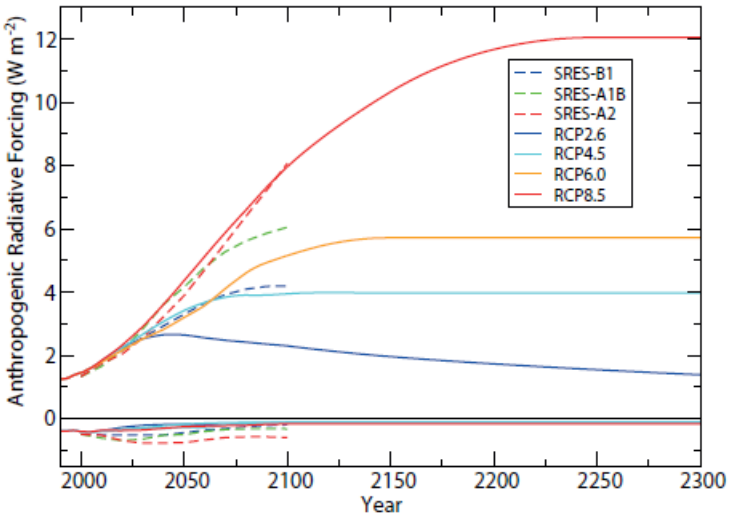

Figure 2.1: Time evolution of anthropogenic radiative forcing for the RCP scenarios (used in CMIP5) and SRES scenarios (used in CMIP3). Negative values represent the forcing of anthropogenic aerosols. Source: Collins et al. (2013)

by the end of the century under RCP6.0 is 1.4-3.1°C (Collins et al., 2013).

The A1 scenario assumes future ODS emissions consistent with the Montreal Protocol and subsequent amendments and adjustments (see Figure 1.5), such that equivalent effective stratospheric chlorine (EESC) continues a steady decline from its peak in the late 1980s. Under this scenario, most chemistry climate models predict a recovery to 1980 levels of global annual mean ozone around 2030 and springtime southern polar ozone around 2050 (Eyring et al., 2010). Using 1960s levels as the baseline global mean annual mean, recovery occurs around 2060, while springtime southern polar ozone does not fully recover by the end of the 21^{st} century (recovering only 95% of the deficit from the peak of ozone depletion by the year 2100). Södergren et al. (2016), using an ensemble of simple climate models (SCMs), estimates the uncertainty in return date arising from variations in model tunings and the choice of carbon cycle model. At 85°S, the ensemble forced by the A1 and RCP6.0 scenarios, returned to 1960 ozone levels during 2071 with a standard deviation of approximately 3 years. The recovery of ozone is also shown to be sensitive to GHG forcing. Increased GHG forcing, via cooling of the stratosphere and resultant suppression of some temperature depen-

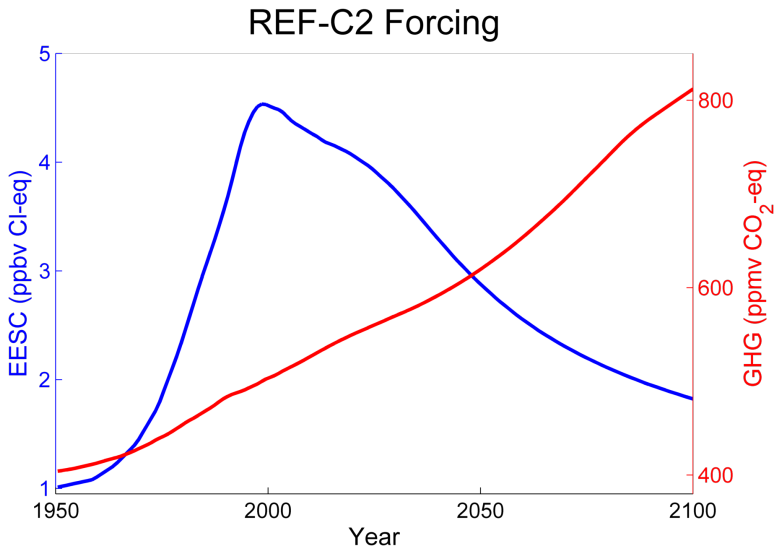

Figure 2.2: Evolution of EESC (blue) and GHG (red) forcing for the REF-C2 simulations

dant reactions, increases the speed of ozone recovery and lowers the return date uncertainty (Södergren et al., 2016). The evolution of EESC and GHG (CO_2 radiative forcing equivalent) concentrations in the REF-C2 experiment is illustrated in Figure 2.2.

2.3 CMIP 5 Models

An ensemble of 29 Atmosphere-Ocean General Circulation Models (AOGCMs) from the Coupled Model Intercomparison Project phase 5 (CMIP5) (Taylor et al., 2012) are also used in Chapter 3. This generation of models produced output for use in the 5th Assessment Report (AR5) of the IPCC (Flato et al., 2013). The models used were those for which geopotential height output is available at daily resolution; this amounts to 29 unique models although some of these are not totally independent as they share the same model core. One run from each model is used. In terms of ozone chemistry, this ensemble is generally not as advanced as the NIWA-UKCA model. Only three of the models used have explicit stratospheric ozone chemistry, the rest use prescribed or "semi-offline" calculated stratospheric ozone (Eyring et al., 2013a). In terms of atmospheric dynamics, the CMIP5 models and the NIWA-UKCA model are of roughly equal sophistication.

The models are listed in Table 2.3 along with various properties. These properties are used to group the models for the analysis presented in Section 3.4.4. "Levels" is the total number of model atmosphere levels, the "H" (high) and "L" (low) notation refers to the number of these levels concentrated in the upper troposphere and lower stratosphere (UTLS, see Section 3.4.4 for definition). "Top" is the pressure level of the model top. "Lat. Res." is the latitudinal resolution. "Chem." refers to the models treatment of stratospheric ozone chemistry, the classifications P (prescribed), SO (semi-offline) and I (interactive) are taken from Eyring et al. (2013a).

Simulations from the "historical" experiment are used in this thesis. This experiment covered the period 1850-2005, but only the period 1979-2005 is used in this study so as to be comparable to the reanalysis (see 2.4). These simulations are forced by observed GHG concentrations, and either ODSs following the A1 scenario (WMO, 2011) or prescribed ozone concentrations. In most cases the prescribed ozone is from the International Global Atmospheric Chemistry (IGAC)/Stratospheric Processes and their Role in Climate (SPARC) ozone database (Cionni et al., 2011) which is zonally averaged in the stratosphere. Further details on the models and the ozone radiative forcing each uses is covered by Eyring et al. (2013a).

2.4 Reanalyses

A reanalysis is a dataset produced by running either a general circulation model (GCM) or numerical weather prediction (NWP) model that is nudged/constrained by the assimilation of observations. The assimilated data are drawn from a wide variety of sources including satellites, weather stations, radiosondes, ship and buoy observations (Rienecker et al., 2011; Dee et al., 2011). Hence, the product combines the benefits of a model: a global, smooth, gridded dataset, yet mitigates model biases due to the assimilation of observations. Reanalyses are therefore well suited for the purpose of validating climate models.

Data from both the Modern-Era Retrospective Analysis for Research and Applications (MERRA) (Rienecker et al., 2011) and the ERA-Interim (Dee et al., 2011) reanalyses are used in this work. The MERRA reanalysis is used in Chapter 3 and ERA-interim in Chapters 4 and 5. This difference is simply due to data availability and not influenced by the properties of

Model	Levels	Top (hPa)	Lat. Res. (°)	Chem.
ACCESS1.0	38	2.9	1.25	P
ACCESS1.3	38	2.9	1.25	P
BCC-CSM-1.1	26^L	2.9	1.25	P
BCC-CSM-1.1m	26^L	2.9	1.00	P
BNU-ESM	26^L	2.9	2.8	SO
CanESM2	35^L	1.0	2.8	P
CCSM4	26^L	3.54	0.95	SO
CMCC-CESM	39^L	0.01	3.7	P
CMCC-CM	31	10	0.75	P
CMCC-CMS	95^H	0.01	1.9	P
CNRM-CM5	31	10	1.4	I
FGOALS-g2	26^L	2.2	2.8	P
GDFL-CM3	48^L	0.017	2	I
GDFL-ESM2g	24^L	3	2	P
GDFL-ESM2m	24^L	3	2	P
HadGEM-CC	60	0.026	1.25	P
HadGEM-ES	38	2.9	1.25	P
IPSL-CM5A-LR	39^L	0.04	1.9	SO
IPSL-CM5B-MR	39^L	0.04	1.3	SO
IPSL-CM5B-LR	39^L	0.17	1.9	SO
MIROC-ESM-CHEM	80^H	0.026	2.8	I
MIROC-ESM	80^H	0.0036	2.8	P
MIROC5	80^H	0.0036	2.8	P
MPI-ESM-LR	47	0.01	1.9	P
MPI-ESM-MR	95^H	0.01	1.8	P
MPI-ESM-P	47	0.01	1.9	P
MRI-CGCM3	48	0.01	1.1	P
MRI-ESM1	48	0.01	1.1	P
NorESM1-m	26^L	3.54	1.9	SO

Table 2.1: List of CMIP5 models used in this work along with various model properties.

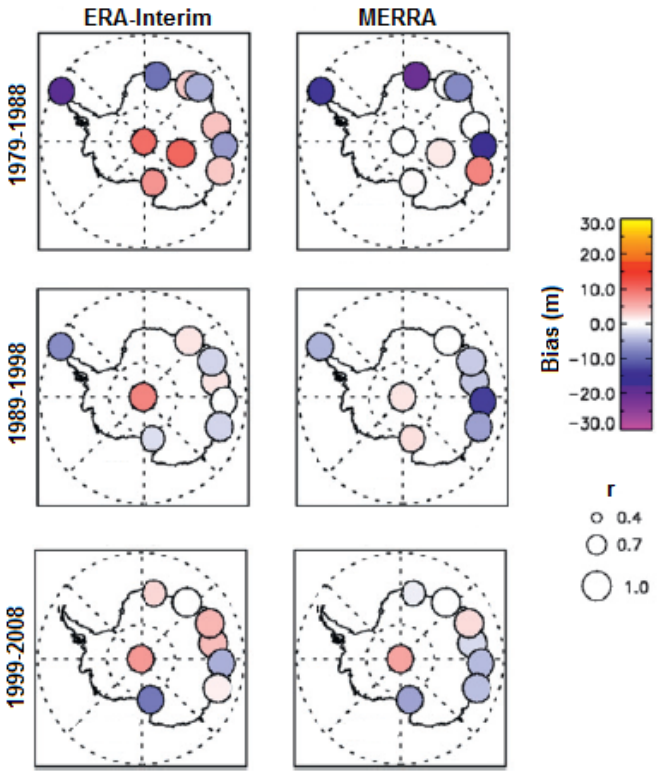

Figure 2.3: Annual mean difference between ERA-Interim (left), MERRA (right) and observations over the period 1979-1988 (top), 1989-1998 (middle) and 1999-2008 (bottom). Bias is indicated by colour and correlation coefficient by marker size. (Source: Bracegirdle and Marshall (2012))

the reanalyses. Indeed, many of the same observations are assimilated into both reanalyses and so they produce similar output. Rienecker et al. (2011) compares the output of the two reanalysis and finds that variables such as temperature and wind speed compare well, especially in the extra-tropics. Bracegirdle and Marshall (2012) also compare both reanalyses to Antarctic station data. The 500 hPa temperature and GPH trends in both reanalysis were found to be consistent with the observations. Figure 2.3 shows the difference in 500 hPa GPH between reanalysis and observation from Bracegirdle and Marshall (2012). In cases where there is a bias with respect to the observations it was generally similar for both reanalyses. Note that the mean 500 hPa GPH over the Antarctic is of the order of 5000 m, so these biases represents an error of less than 0.5%.

Both of these reanalyses begin in 1979 when satellite observations first

became available. Prior to this date, ground-based observations were sparse, particularly at high latitudes in the Southern Hemisphere. Hence, reanalysis products with output before 1979 are of lower quality (Hines et al., 2000). For the purpose of model validation, the NIWA-UKCA model is compared to the reanalysis over this 1979–present historical period.

Chapter 3

The SAM and Stratosphere-Troposphere Coupling

3.1 Abstract

The aim of this study is to investigate the influence of ozone depletion and recovery on the Southern Annular Mode (SAM) and stratosphere-troposphere coupling. Using the NIWA-UKCA chemistry-climate model, we compare reference runs that include forcing due to greenhouse gases and ozone depleting substances to sensitivity simulations in which ozone depleting substances are fixed at their 1960 levels. We find that ozone depletion leads to an increased frequency of extreme anomalies and increased persistence of the SAM in the stratosphere as well as stronger, more persistent stratosphere-troposphere coupling. Currently, the stratosphere provides an appreciable amount of predictability to the troposphere on time scales of one or two months. However, we find that this effect reduces over time as stratospheric ozone recovers to pre-ozone hole levels towards the latter part of this century.

3.2 Introduction

The Southern Annular Mode (SAM) is the dominant mode of climate variability in the extra-tropical Southern Hemisphere, impacting the atmosphere, ocean, and sea ice (Hall and Visbeck, 2002; Thompson and Wallace, 2000a). A recent summertime trend towards the positive polarity SAM has been associated with polar stratospheric ozone depletion (Thompson and Solomon, 2002; Arblaster and Meehl, 2006). In models, projected ozone recovery will reverse this trend although this may be offset by forcing associated with increasing concentrations of long-lived greenhouse gases (GHGs) (McLandress et al., 2011; Karpechko et al., 2010b; Thompson et al., 2011). Analysis of long term trends in the SAM associated with changes in the concentrations of ozone and GHGs in the same model as used in this study can be found in Morgenstern et al. (2014).

The impact of ozone depletion on the SAM in the stratosphere is readily explained by the reduction in absorption of incoming shortwave radiation by stratospheric polar ozone, increasing the meridional temperature gradient (Randel and Wu, 1999). The stratosphere can, in turn, have an impact on the troposphere. For the Northern Annular Mode (NAM; the Northern-Hemisphere equivalent of the SAM); Baldwin and Dunkerton (2001) show that anomalies in the stratosphere of either sign are often followed by anomalies of the same sign in the troposphere that last for around 60 days; the equivalent also holds for the SAM (Thompson et al., 2005). Graversen (2003) showed that the annual cycle in zonal mean zonal wind propagates downward from 10 hPa to the surface on a timescale of about two months. Haigh and Roscoe (2009) examine the date of final warming of the Antarctic polar vortex; this process takes between 10 and 40 days to progress down through the lower stratosphere. This date is increasingly delayed over the latter decades of the twentieth century, which can be attributed to ozone depletion.

Stratosphere-troposphere coupling is captured by many climate and chemistry-climate models (Gerber et al., 2010). This coupling between the stratosphere and troposphere is important for extended range weather forecasts (Kuroda, 2008). For example, Baldwin et al. (2003) show that the NAM in the lower stratosphere is a better predictor of the 30 day mean NAM (beginning at a 10 day lag) at 1000 hPa than the 1000 hPa NAM itself. Similarly Chris-

tiansen (2005) found that prediction of near surface zonal mean zonal wind at 60°N is greatly improved by using the value in the lower stratosphere as a predictor, and that restricting the prediction to periods in which the predictor was more anomalous improved the prediction. No such findings have been reported for the Southern Hemisphere.

In this study we use a chemistry-climate model to assess changes in the deep coupling characterizing the SAM that are caused by anthropogenic ozone depletion. The advantages of using a chemistry-climate model include: several realizations can be produced leading to more robust statistics, alternative scenarios without changes in climate drivers such as ozone depletion can be explored, and we can straightforwardly extend the study to the future. The inclusion of interactive ozone chemistry in climate models has also been shown to have significant effects on climate sensitivity (Nowack et al., 2015).

3.3 Data and Methods

3.3.1 Model

The model used in this study is the National Institute of Water and Atmospheric Research-United Kingdom Chemistry and Aerosols (NIWA-UKCA) coupled atmosphere-ocean chemistry-climate model (AOCCM). We investigate the influence of ozone depleting substances (ODSs) by comparing REF-C2 runs to SEN-C2-fODS runs. An ensemble of models from CMIP5 was also used to investigate the variation in the simulation of stratosphere-troposphere coupling between different models. See Chapter 2 for further details.

To evaluate the performance of the model we compare the model output to the MERRA reanalyses (Rienecker et al., 2011) . We limit the comparison to the period 1979-2011 as the satellite observations assimilated into the reanalyses over this period provide a more accurate simulation of the stratosphere. The stratospheric sudden warming (SSW) event during 2002 is not included in the comparison as it is substantially larger than typical SAM anomalies. This provides a fairer comparison to the model which does not simulate SSWs.

3.3.2 SAM Calculation

The SAM index is calculated using daily zonal-mean geopotential height (GPH) data and an empirical orthogonal function (EOF) method; Baldwin and Thompson (2009) argue that this method is simpler and more robust than other methods. GPH anomalies are calculated by first removing global mean GPH for each day (this partially accounts for an expansion of the atmosphere due to global warming (Morgenstern et al., 2010b)), then at each latitude removing a slowly varying climatology to account for shifts in the mean state associated with changing climate and ozone. This climatology is calculated by applying a 15-year running-mean low-pass filter and averaging across the model runs (separate climatologies are produced for the REF-C2 and the SEN-C2-fODS experiments). This procedure for calculating anomalies produces a SAM that has no long term trend and reflects only internal variability (Gerber et al., 2010). The resultant GPH anomalies are then weighted by the square root of the cosine of the latitude to account for the convergence of meridians towards the poles (North et al., 1982). The first EOF is calculated using the weighted anomalies of all runs (REF-C2 and SEN-C2-fODS combined) in the region south of 20°S and for September to December (this period is chosen as it has the largest variance (Thompson et al., 2005)). The SAM index is the projection of the zonal mean GPH anomalies on this EOF, normalized such that it has zero mean and unit standard deviation. This procedure is repeated on each pressure level.

3.3.3 Extreme SAM Composite

The response to extreme SAM anomalies in the stratosphere is examined using SAM composites similar to those used by Baldwin and Dunkerton (2001). Extreme SAM events are identified by selecting all events in which the SAM index crosses the 2.8 or -3.6 thresholds at 50 hPa. Events must also be separated by at least 60 days to ensure they are independent of one another. The thresholds are chosen to select events that are sufficiently extreme that they influence the troposphere, and to have approximately equal numbers of positive and negative events. The asymmetry reflects the fact that the distribution of the SAM indices has a longer tail on the negative side. The thresholds are discussed further in section 3.5. The composite shows the average of all these events (negative events are multiplied by -1

and are combined with the positive events). The reference time (i.e. lag = 0) in Figure 3.1 and 3.5 corresponds to the time at which the extreme at 50 hPa occurred (note this differs from the definition used by Baldwin and Dunkerton (2001) where it corresponds to the time at which the threshold was crossed, this results in a timing difference on the order of a few days but otherwise has little impact).

An estimate of the uncertainty in the composite is found by performing a Monte Carlo simulation of event selection. The method is as follows: a SAM composite is produced from n randomly selected times (where n is equal to the number of events in the extreme composite being considered). As in the case of the extreme composite, instances in which the SAM at 50 hPa and 0 lag is negative are multiplied by -1. Then for each pressure level and lag in the composite the SAM index is averaged over a range of timespans (up to 40 days). This is then repeated for 10000 different random composites, thus giving a distribution of the expected SAM index anomaly at each pressure level, lag, and, timespan. Finding the 95^{th} percentile of these distributions gives a significance threshold which is a function of pressure level, lag and, timespan. It is important we account for each of these factors as we intuitively expect the mean SAM anomaly to be smaller at lower levels (as the persistence time is shorter), at greater lags (as the SAM index becomes less correlated with the 50 hPa, 0 lag SAM) and, when averaged over longer timespans. The composite composed of extreme events is assessed by averaging the SAM index at each pressure level and lag over the range of timespans. If the mean SAM index exceeds the significance threshold (at the corresponding pressure level and lag) for any timespan, then the SAM index is judged to be significantly anomalous at that point. In order to judge the significance of the difference between two composites the distribution is instead built from the difference between 10000 pairs of random composites and, additionally, the 5^{th} percentile used as a threshold for negative differences.

3.4 Results

3.4.1 NIWA-UKCA Model Evaluation

To confirm that the NIWA-UKCA model is able to realistically reproduce stratosphere-troposphere coupling, we compare it to the MERRA reanaly-

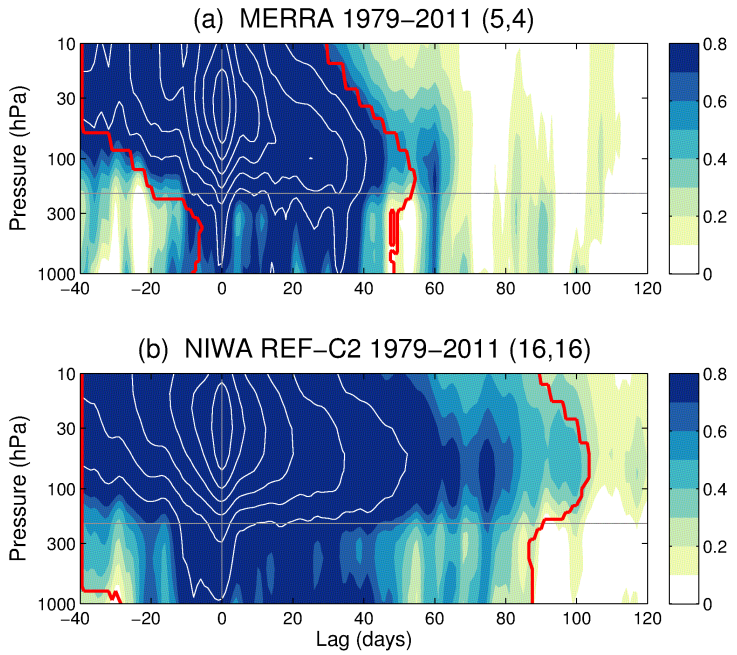

Figure 3.1: Composite SAM index of extreme events for (a) MERRA and (b) NIWA-UKCA REF-C2 over the period 1979-2011. White contours show increments of 0.5 beginning at +1. The number of positive and negative events in each composite is shown in parentheses. The red contour indicates regions exceeding the 95% significance level

sis. Figures 3.1(a) and (b) show extreme SAM composites for the MERRA reanalysis and the 5 REF-C2 runs, respectively, over the period 1979-2011. In general, the model reproduces the observed coupling, i.e. anomalies in the stratosphere are followed by anomalies in the troposphere; however, the coupling is somewhat too persistent. This has been found to be the case in other models, e.g. various CCMVal-2 models (Gerber et al., 2010) (for the NAM).

3.4.2 SAM variability in the NIWA-UKCA model

This study examines changes to the SAM due to ozone depletion and recovery. To illustrate the evolution of polar ozone, Figure 3.3(a) shows the October total column ozone south of 70°S as simulated in REF-C2 runs. October is the month in which this measure is climatologically at a minimum. The period 1987-2036 in which the ensemble mean ozone falls below 220 Dobson Units is chosen to represent the period of enhanced ozone depletion

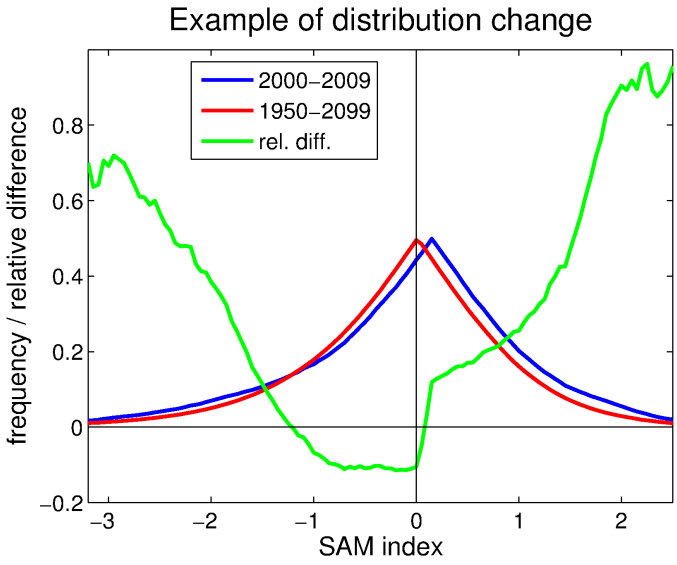

Figure 3.2: Distributions of the 2000-2009 REF-C2 (blue), 1950-2099 REF-C2 baseline (red) and the relative difference between the two (green)

utilized later in the analysis.

We examine the changing frequency distribution of the SAM index in order to investigate the effect of ozone on the SAM variability. The distribution of the 50 hPa September to February SAM over a 10 year window is calculated and compared to a baseline distribution of the REF-C2 ensemble over the 1950-2099 period. The distribution that we use is a modification of the cumulative distribution function in which the right hand side (i.e. $f(x) > 0.5$) becomes $1 - f(x)$ such that the interpretation of the distribution changes from "fraction less than x" to "fraction more extreme than x". The September-February period was chosen because this is where the influence of ozone changes would be expected to occur. An example distribution is shown in Figure 3.2 which compares the distribution for 2000-2009 (blue) to the baseline distribution (red). The relative difference between the two is shown in green. For example, occurrences of SAM events of 1.5 or greater are 47% more frequent in the 2000-2009 period relative to the 1950-2099 period.

Figure 3.3 shows this relative difference for the REF-C2 runs (b) and the SEN-C2-fODS runs (c) over the course of the simulation using a 10-year sliding window. The difference between each 10-year distribution and the base-

line distribution is tested with the Kolmogorov-Smirnov test (Feller, 1948). Instances for which the test shows no significant difference ($p < 0.01$) are indicated by cross-hatching. Figure 3.3(b) shows that over the period 1990 to 2020 there is a large increase in the occurrence of SAM extrema (shown in red). This period corresponds closely to the period with enhanced anthropogenic ozone depletion shown in Figure 3.3(a). Hence we hypothesize that polar ozone depletion is responsible for this change in the SAM variability. There appears to be more variability shown in Figure 3.3(c), but this is likely due to there only being two SEN-C2-fODS runs as opposed to the five runs used in Figure 3.3(b). Figure 3.3(c) shows a less coherent pattern than the REF-C2 simulation which gives credence to the hypothesis that the large coherent feature indicating an increase in occurrence of extrema during the 1990 to 2020 period observed in the REF-C2 simulations is associated with ozone depletion. Overall there is more area of negative anomaly (blue) in Figure 3.3(c) indicating a general tendency for less frequent occurrences of extreme SAM events in the SEN-C2-fODS simulation. It must be noted that the uncertainty in frequency change necessarily increases towards the tail ends of the SAM distribution. For this reason the SAM range in Figure 3.3 only covers -3.25 to 2.5 (the 1^{st} and 99^{th} percentiles of the baseline SAM distribution).

As with the frequency of extreme SAM events, the persistence timescale of the SAM varies due to changing ozone forcing. The persistence timescale is taken as the e-folding time of the SAM index autocorrelation function. Figure 3.4(a) shows the climatology of the persistence timescale, smoothed using a Gaussian filter with $\sigma = 10$ days, over the period 1987-2036 in the REF-C2 runs. The equivalent result for the SEN-C2-fODS simulations (Figure 3.4(b)) indicates a considerable decrease of persistence of the SAM in the summer stratosphere. There is also a shift in the timing of the maximum persistence toward early summer in the SEN-C2-fODS ensemble relative to REF-C2, as indicated by the coloured contours. It is possible this shift is associated with the delayed vortex break-up identified by Haigh and Roscoe (2009). As there are only two SEN-C2-fODS simulations, it is necessary to check that these differences from REF-C2 are significant. We compared climatologies produced using every combination of two REF-C2 runs to Figure 3.4(b) and found that none of the 10 combinations produced a similar result to the SEN-C2-fODS climatology, suggesting that the difference is

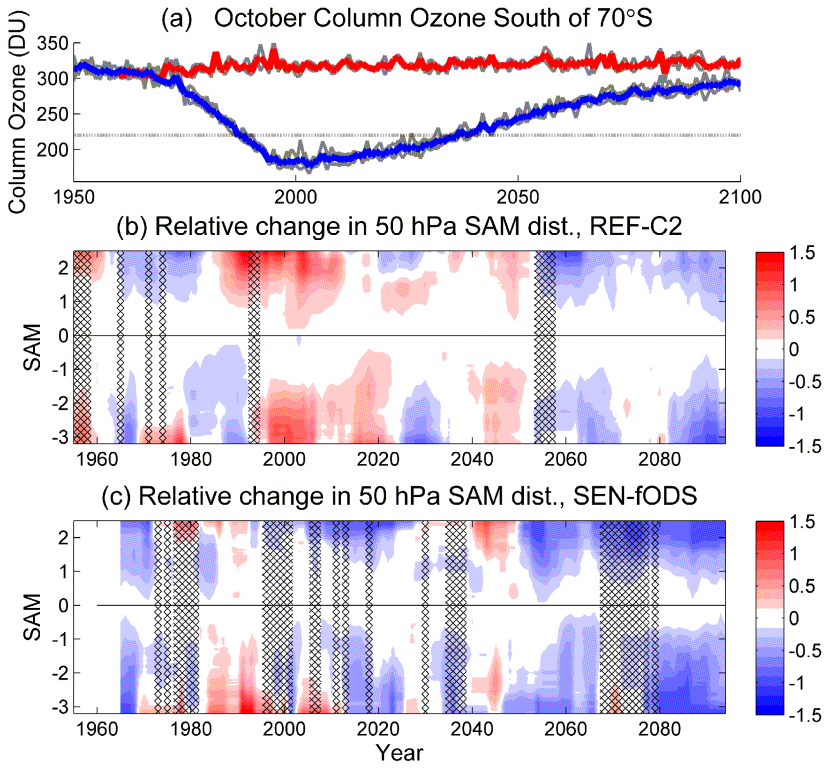

Figure 3.3: (a) The October Column Ozone South of 70°S as simulated in the REF-C2 (ensemble mean is blue) and SEN-C2-fODS (ensemble mean is red) runs and the change in the decadal distribution of the September-February SAM in the (b) REF-C2, and (c) SEN-C2-fODS simulations. Hatching indicates distributions which were not deemed to be significantly different using the Kolmogorov-Smirnov test ($p < 0.01$)

statistically robust.

Figure 3.4(c) shows the equivalent for the 2050-2099 period (characterized by ozone recovery) in the REF-C2 simulation. Relative to this later period, the persistence in REF-C2 for 1987-2036 is substantially longer in the stratosphere during summer and into autumn. Although this lends some support to the hypothesis that ozone depletion causes an increase in persistence, it is possible that a difference in GHG forcing or an interaction between ozone recovery and GHG forcing drives some of the difference in this comparison. Indeed, Figure 3.4(d) shows that the SEN-C2-fODS simulation over the period 2050-2099 also produces a pronounced decrease in persistence relative to the earlier period, suggesting that this may be a prod-

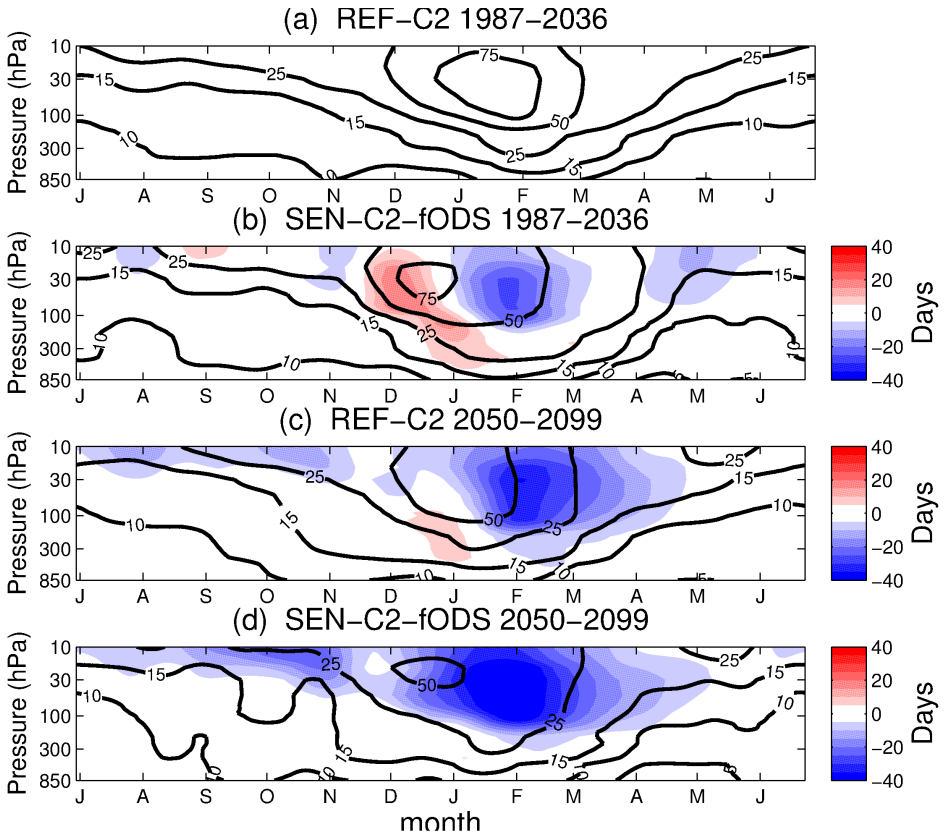

Figure 3.4: Climatological persistence of the SAM for the (a) REF-C2 runs over the period 1987-2036, (b) the SEN-C2-fODS runs over the same period, (c) the REF-C2 over the 2050-2099 period, and (d) the SEN-C2-fODS over the 2050-2099 period. In panels (b), (c), and (d) the coloured contours display the difference with respect to (a).

uct of increased GHG concentrations.

3.4.3 Coupling in the NIWA-UKCA model

We have shown that changes in stratospheric ozone produce changes in the frequency of SAM extrema and the persistence of the SAM in the stratosphere. One might expect that these properties influence the coupling of the stratosphere to the troposphere, given that this coupling is observed to occur on occasions when the stratospheric SAM is most extreme.

Figure 3.5(a) and (b) show SAM composites for the REF-C2 and SEN-C2-fODS runs, respectively, over the period 1987-2036; Figure 3.5(c) shows the difference between the two. Over the 30 to 90 day lag period the SAM

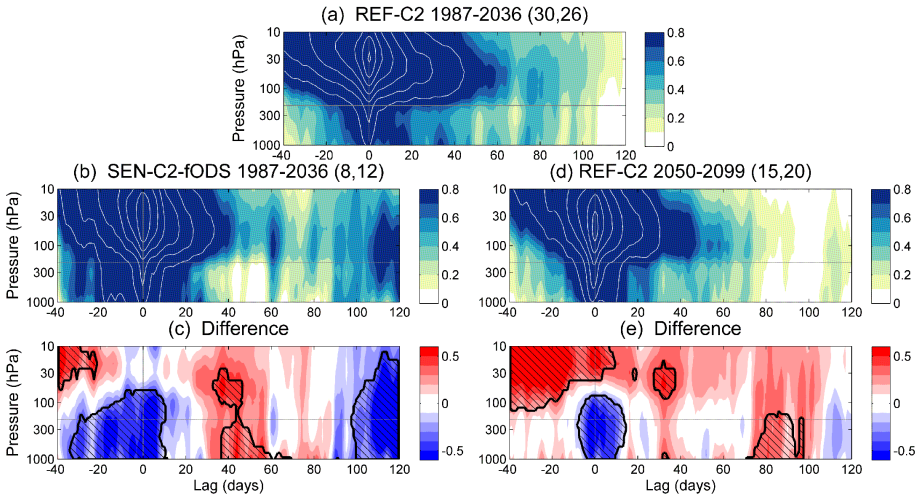

Figure 3.5: Extreme SAM composites for (a) REF-C2 over the period 1987-2036, (b) SEN-C2-fODS 1987-2036, (c) the difference between (a) and (b), (d) REF-C2 over the period 2050-2099, and (e) the difference between (a) and (d). White contours in (a), (b) and (d) show increments of 0.5 beginning at +1. The number of positive and negative events in each composite is shown in parentheses, significant differences ($p < .05$) are marked with hatching

.

signal in the troposphere is stronger in the case of the REF-C2 runs than the SEN-C2-fODS runs. The difference for the 35 to 70 day lag period is shown to be significant at the 95% level using the method described in section 3.3.3.

The longer persistence in the stratosphere due to ozone depletion is also apparent in Figure 3.5(a) in that the stratospheric signal is stronger for the REF-C2 runs than for the SEN-C2-fODS for positive lags, which is as expected based on Figure 3.4. Note also the differing frequency of extrema: the REF-C2 composite includes 56 events which correspond to, on average, approximately 11 per simulation (REF-C2 is comprised of 5 simulations), whereas the SEN-C2-fODS composite includes only 10 per simulation (total of 20 split over 2 simulations). However, despite this imbalance, the mean SAM index at 50 hPa and lag = 0 (i.e. the point at which the selection criteria was applied) shows no significant difference. This may suggest that it is the increased persistence, rather than the increased frequency of extrema that leads to the stronger stratosphere-troposphere coupling observed during the period of highest ozone depletion.

Furthermore, the difference between the 1987-2036 REF-C2 composite (Figure 3.5(a)) and the 2050-2099 REF-C2 composite (Figure 3.5(d)) as shown in Figure 3.5(e) displays a similar pattern to Figure 3.5(c). As in the case of Figure 3.4(c), this corroborates our finding that there is an influence of ozone depletion although, the comparison is less straightforward due to the different GHG abundances.

3.4.4 Simulation of Coupling Across Different Climate Models

The chapter, to this point, has been published in the Journal of Geophysical Research (Dennison et al., 2015); this section further examines the topic of stratosphere-troposphere coupling but has not been published. This section uses a collection of CMIP5 models (see Section 2.3) to investigate the differences in coupling between different models.

As an ensemble, the CMIP5 models simulate the observed coupling reasonably well. Figure 3.6 shows the composite SAM for the extreme events in the MERRA reanalysis (top) and CMIP5 (bottom). The composite is produced in the manner described in Section 3.3.3 with one exception. Rather than selecting all events in which the 50 hPa SAM exceeds a threshold, here only the n most positive and n most negative events for each model were selected (this method was used by Thompson et al. (2005)). This ensures the composite, which is made up from different models, weights each model equally. The choice of $n = 6$ was made as to be approximately consistent with the composites in Section 3.4 and the results presented here hold for different values of n. Similar to the NIWA-UKCA model in Section 3.4, the coupling simulated by the CMIP5 ensemble is too persistent. However, the SAM anomaly in the troposphere for the month following the stratospheric extreme is of approximately the correct magnitude.

Studies such as Morgenstern et al. (2010a) and Gerber et al. (2010) have shown considerable variance amongst climate models in their simulation of the coupling in the Northern Hemisphere. We find this is also true for the Southern Hemisphere. Figure 3.7 illustrates this by showing the strength of coupling in each of the individual CMIP5 models. The strength of the coupling here is quantified as the correlation between the 50 hPa SAM and 10-day lagged 500 hPa SAM over the November-February season, 1979-2005. The 500 hPa SAM is averaged over a 30 day span which begins at a 10 day

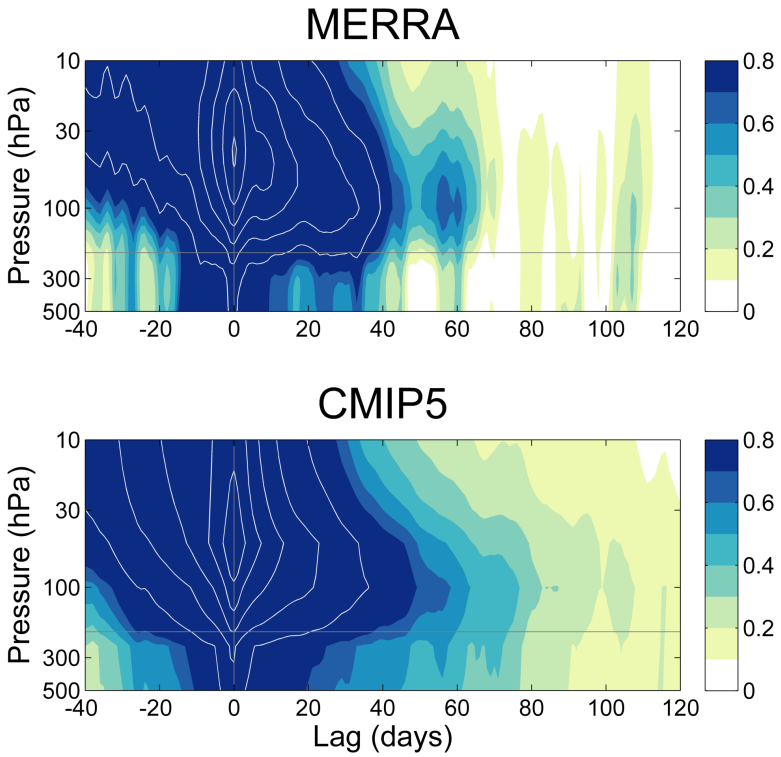

Figure 3.6: Composite SAM for extreme events in the MERRA reanalysis (top) and CMIP5 ensemble (bottom) of the period 1979-2005

lag relative to the 50 hPa value. The coupling in the MERRA reanalysis ($r = 0.28$) is replicated by a number of the models, but as was shown by Figure 3.6, the models generally overestimate the strength of coupling. Amongst the set of models, correlation ranges from 0.26 to 0.68.

To investigate possible sources of this variance, composites were produced by grouping CMIP5 models according to the following properties:

a Vertical resolution in the upper troposphere/lower stratosphere (UTLS); models with 10 or more levels between 7 and 14 km in altitude are classified "High" and those with six or fewer are classified "Low".

b Height of model top; models with the top level at 1 hPa or above are classified as "High Top" and below 1 hPa are "Low Top".

c Ozone chemistry; models with either interactive or semi-offline chemistry are classified "Chem" and those in which ozone is prescribed are "No Chem".

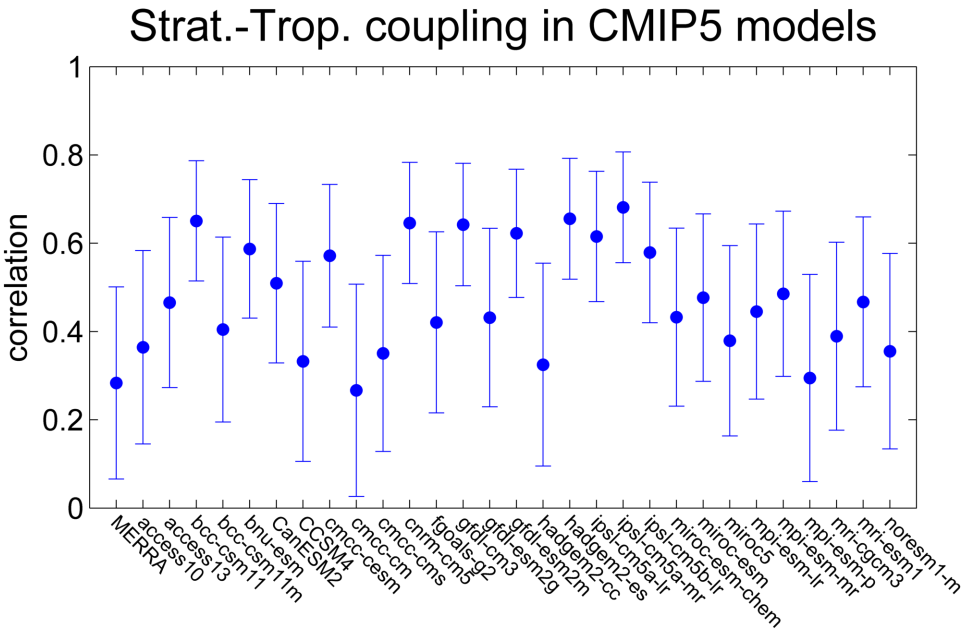

Figure 3.7: Correlation between the 50 hPa SAM and 30 day mean 500 hPa SAM lagged 10 days for November-February 1979-2005. Error bars show the 95% confidence interval.

d Horizontal resolution; models with latitudinal resolution $< 1.5°$ are classified as "High" and $> 1.5°$ are classified as "Low".

Figure 3.8 shows the differences between the two subsets for each of four categories listed above. Significant differences were identified using Wilcoxon's ranked sum test (Wilcoxon, 1945) and are indicated by hatching. Figure 3.8(a) reveals that the subset of models with a high vertical resolution in the UTLS display a weaker (and therefore more realistic) coupling than the low subset. The difference is particularly notable shortly after the SAM extreme in the mid-stratosphere and at larger lags in the troposphere. In contrast, Figure 3.8(b) shows the difference between the high and low top models is mostly limited to the upper stratosphere. It is not surprising that low top models would have trouble producing realistic simulations in the stratosphere as in some models the model top is as low as 10 hPa. However, the finding that the height of the model top has little influence in the response of the troposphere emphasizes that it is the region around the tropopause that is critical for coupling.

Figure 3.8(c) shows that the ensemble of models that simulate ozone

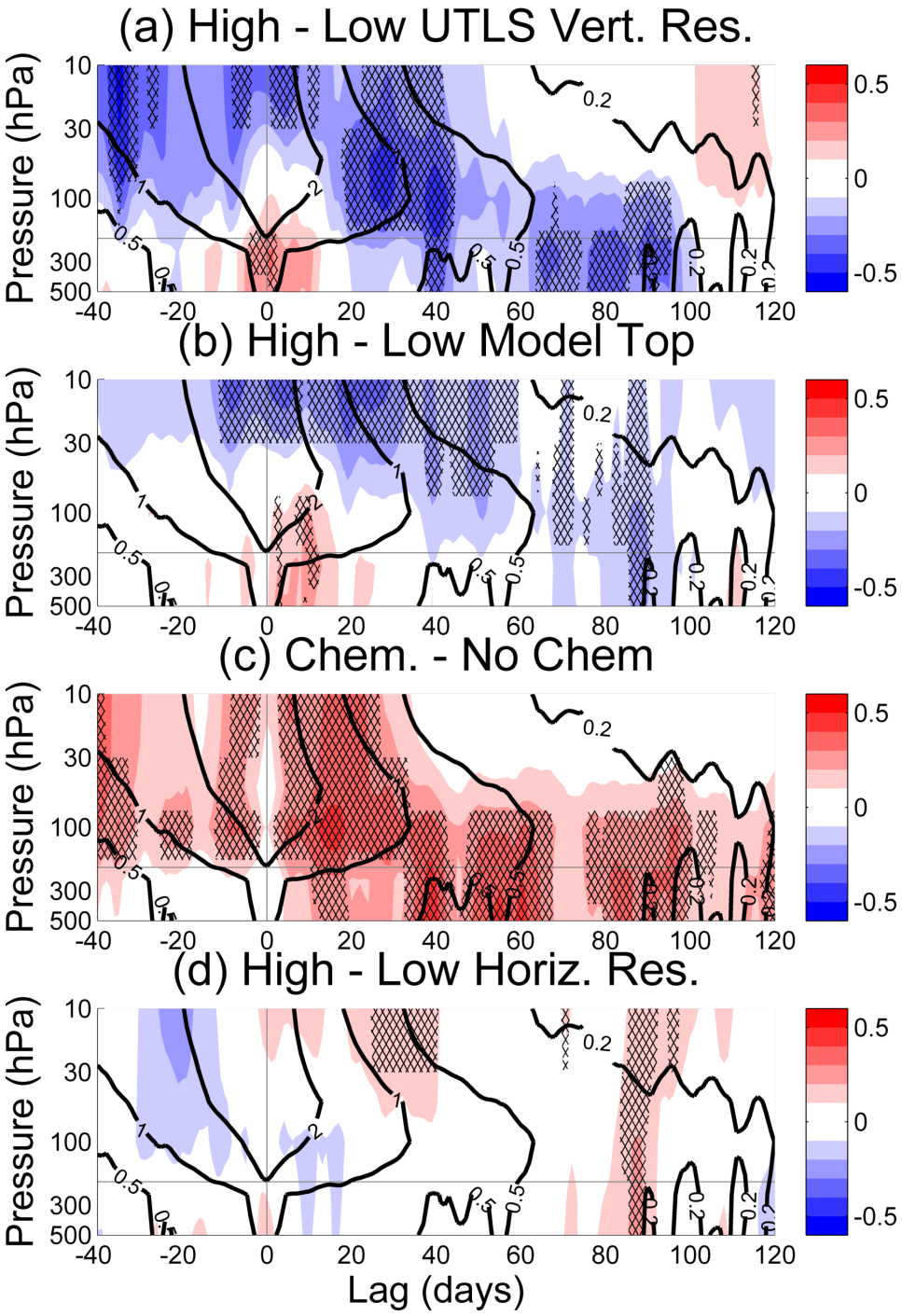

Figure 3.8: Difference in the composite SAM between various subsets of the CMIP5 model ensemble. Hatching indicates significant differences ($p < 0.05$), contours indicate the all-model ensemble

chemistry display stronger coupling than those with prescribed ozone. This is somewhat surprising as one might assume the simulation of chemistry would aid the accuracy of the simulation. Adding chemistry increases the complexity of the system, so it may be that altering the dynamics of the stratosphere-troposphere coupling may be an unintended consequence of the chemistry module which may improve the model in other ways. The "Chem" subset in this example includes both interactive and semi-offline ozone. The models with interactive ozone alone produce results similar to the semi-offline ozone subset in the troposphere. However, the interactive ozone subset only includes three models (CNRM-CM5, GFDL-CM3 and MIROC-ESM-CHEM), of these only MIROC-ESM-CHEM is also in the high vertical resolution subset. By the metric used in Figure 3.7, this model is the closest of the three to the MERRA reanalysis. Indeed, of the whole "Chem" subset, MIROC-ESM-CHEM is the only model also in the high vertical resolution subset. This perhaps indicates that any advantage the simulation of ozone chemistry may bring is not realized due to the lack of vertical resolution in the UTLS.

Figure 3.8(d) shows that there is very little difference between the high and low horizontal resolution models. As horizontal resolution is important for simulating small scale eddies, this result perhaps indicates that these do not play a crucial role in stratosphere-troposphere coupling.

3.5 Discussion and Summary

A notable issue with producing SAM composites is the selection of events. In this study events were chosen based on the SAM index at 50 hPa; other studies have used 10 hPa (Baldwin and Dunkerton, 2001; Thompson et al., 2005; Gerber et al., 2010). Baldwin et al. (2003) and Christiansen (2005) find that the stratosphere becomes a better predictor of the troposphere at lower levels (in the case of the NAM); similarly we find that extrema at 50 hPa elicited a larger response in the troposphere than those at 10 hPa. This, combined with the fact that 50 hPa is close to the height of the ozone layer maximum, validates the reason for choosing this lower level. Another consideration is the number of events to include in the composite. The approach taken here was to select extrema of the SAM index which fell outside the interval of -3.6 to 2.8. These thresholds were chosen such that the ex-

trema were large enough to produce a noticeable effect on the troposphere, yet ensuring enough events were composited to be representative (given that the variance amongst individual events was considerable). The distribution of the SAM index is skewed with a longer negative tail so asymmetric thresholds were necessary to obtain a sample that included an approximately equal number of positive and negative SAM events. Another approach would be to select the n most extreme events (Thompson et al., 2005). However, as this study uses comparisons of composites, and given that the composites are selected from records with differing distributions (Figure 3.3 (b) shows that the distribution of the SAM at 50 hPa over the 1987-2036 period will differ from the 2050-2099 period), it was decided that this approach would not provide the fairest comparison. For example, if the 56 most extreme events (to match the number selected for Figure 3.5(a)) were instead chosen for the composite shown in Figure 3.5(d), the additional 21 events selected would mean the events would be, on average, less anomalous. In this case the difference is significant enough that it would produce a noticeable difference in the tropospheric response.

In this study positive and negative events were combined together into a single composite. This was the approach taken by Thompson et al. (2005) and Gerber et al. (2010), while Baldwin and Dunkerton (2001) produced separate composites. There are only slight differences between the composite of the positive events and the composite of the negative events in the stratosphere, but the extent to which the troposphere is impacted by the stratospheric anomaly (at a lag of > 20 days) is similar in both composites. It was therefore decided that, for the purposes of this study, a combined composite was sufficient to illustrate stratosphere-troposphere coupling behavior. However, a difference between the positive and negative composites in the troposphere does arise around lag $= 0$ where the negative composite shows a larger anomaly.

In Figures 3.5(c) and (e) it can be seen that in the troposphere and lower stratosphere around lag $= 0$ the SAM is more anomalous in the SEN-C2-fODS and REF-C2 2050-2099 composites relative to the REF-C2 1987-2036 composite. This is partly due to the previously noted difference in negative SAM events: as these composites feature a larger proportion of negative events, the SAM anomaly around lag $= 0$ will be larger. However, this effect alone is not enough to account for the difference shown in Figures 3.5(c) and

(e). It is possible that differences in the mean state of the atmosphere in the various composites may have an important effect in this area. Polvani and Waugh (2004) show that large stratospheric anomalies are caused by vertically propagating planetary waves, with anomalously weak (strong) stratospheric vortex anomalies preceded by anomalously strong (weak) eddy heat flux in the troposphere. As the initial state of the stratosphere differs due to the presence/absence of an ozone hole this requires a difference in the upward propagating planetary waves needed to produce an extreme event. This difference could be due to a different state of the troposphere/tropopause, either in terms of wave production (for example due to a difference in temperature differential between land and ocean), or wave propagation (due to changes in the effective refractive index of the atmosphere (Orr et al., 2012)), which is perhaps manifested in terms of a difference in SAM index in Figures 3.5(c) and (e).

The results show that ozone depletion has the effect of increasing the frequency of SAM extrema and the persistence time of the SAM in the stratosphere as well as the strength of the coupling between the stratosphere and troposphere. As polar stratospheric ozone recovers from the effects of ODSs over the course of the century, we expect to observe a decrease in the strength of this coupling; this will have the effect of reducing the efficacy of extended range weather forecasts. Although, as Figure 3.5(d) shows, the changing GHG forcing may also have some effect on the strength of the coupling.

Examining an ensemble of CMIP5 models showed a wide variation in the simulation of stratosphere-troposphere coupling and a tendency of the model ensemble to overestimate the strength of the coupling. It was notable that, as a group, the models with higher vertical resolution in the UTLS produced a more accurate simulation of the coupling strength. Future work would be useful to confirm this result by testing the sensitivity of coupling strength to vertical resolution in a single model (thus eliminating the other inter-model differences that may be playing a role in this study).

Chapter 4

Blocking

4.1 Abstract

We investigate the influence of ozone depletion and recovery on tropospheric blocking in the Southern Hemisphere. Blocking events are identified using a persistent positive anomaly method applied to 500hPa geopotential height. Using the NIWA-UKCA chemistry-climate model, we compare reference runs that include forcing due to greenhouse gases and ozone depleting substances to sensitivity simulations in which ozone depleting substances are fixed at their 1960 abundances and other sensitivity simulations with greenhouse gases (GHGs) fixed at their 1960 abundances. Blocking events in the South Atlantic are shown to follow stratospheric positive anomalies in the Southern Annular Mode (SAM) index; this is not the case for South Pacific blocking events. This relationship means that summer ozone depletion, and corresponding positive SAM anomalies, leads to an increased frequency of blocking in the South Atlantic while having little effect in the South Pacific. Similarly, ozone recovery, having the opposite effect on the SAM, leads to a decline in blocking frequency in the South Atlantic, although this may be somewhat counteracted by the effect of increasing GHG concentrations.

4.2 Introduction

Atmospheric blocking refers to large, quasi-stationary, high pressure features that persist beyond the synoptic time scale and inhibit the mid-latitude zonal flow. Most of the blocking in the Southern Hemisphere occurs in the South Pacific region and, to a lesser extent, the Southwestern Atlantic and exhibits a strong seasonal cycle with blocking being more common during winter and autumn (Trenberth and Mo, 1985; Sinclair, 1996; Renwick, 2005). Blocking has been shown to have significant effects on the weather over mid-latitude continental regions. South Atlantic blocking events result in colder conditions over much of Argentina and warmer conditions on the southern tip of the South American continent and the Antarctic Peninsula (Mendes et al., 2008). Kayano (1999) found that blocking over the East Pacific during summer results in colder, drier conditions in South America south of 40°S. Blocking in the Oceania region was found to produce significantly colder conditions in Southern Australia (Mendes et al., 2008). The amount of rainfall in Southern Australia is also influenced by blocking with the direction of influence determined by the location of the blocking event (Risbey et al., 2009; Cowan et al., 2013; Pook et al., 2013). Blocking also plays a role in the Australian heat waves (Pezza et al., 2012).

There is no universally accepted metric with which to diagnose blocking; generally, the methods used are variations on two approaches. One is based on the work of Rex (1950) which takes reversals in the meridional geopotential height (GPH) or potential temperature gradient as indications of blocking (Lejenäs and Ø kland, 1983; Tibaldi and Molteni, 1990; Pelly and Hoskins, 2003). The other looks for persistent positive anomalies (PPAs) in either surface pressure or GPH fields (Dole and Gordon, 1983; Renwick, 2005; Parsons et al., 2016). In comparing the two approaches, Liu (1994) found that PPAs centered around 60°N correspond well with the Rex (1950) definition of blocking, but not as well for PPAs centered around 45°N. In this study we use the PPA approach.

Large scale modes of variability such as the El Niño - Southern Oscillation (ENSO) and Southern Annular Mode (SAM) are known to have an effect on blocking in the Southern Hemisphere. Oliveira et al. (2014) showed that the El Niño conditions had the effect of increasing the number of blocked days over the Central and Eastern Pacific, while La Niña conditions decrease

the number of blocked days over the Western and Central Pacific. Mendes and Cavalcanti (2014) found that blocking in the West Pacific and Atlantic regions is more frequent when the SAM is positive and more frequent in the South East Pacific when the SAM is negative. The interplay between the ENSO and SAM is also significant (Oliveira et al., 2014).

In this paper we investigate the influence of ozone depletion and recovery on blocking in the Southern Hemisphere. To reveal the effect of ozone forcing, we use a coupled atmosphere-ocean chemistry-climate model (AOCCM) which produces simulations in which ozone depleting substances (ODSs) are either prescribed according to historical and projected concentrations or held fixed. Further information on the model and data analysis procedures is contained in section 4.3. In section 4.4 we assess the model simulation of atmospheric blocking by comparison with reanalysis data and also illustrate the effect of ozone forcing on blocking, with particular regard to how this varies by region. Section 4.5 includes a discussion of the mechanisms behind the relationship between ozone forcing and blocking as well as a summary of the results. The appendix provides some additional evaluation of the model

4.3 Data and Methods

4.3.1 Model

The model used in this study is the National Institute of Water and Atmospheric Research-United Kingdom Chemistry and Aerosols (NIWA-UKCA) coupled atmosphere-ocean chemistry-climate model (AOCCM). We investigate the influence of ODSs and GHGs by comparing REF-C2 runs to SEN-C2-fODS and SEN-C2-fGHG runs, respectively (see Chapter 2 for further details).

We compare the model output to the European Centre for Medium-Range Weather Forecasts (ECMWF) Interim Reanalysis (ERA-Interim) (Dee et al., 2011). ERA-Interim assimilates meteorological and ozone measurements from a variety of sources; the ozone product has been shown to be consistent with independent satellite measurements (Dragani, 2011).

4.3.2 Blocking Metric

Blocking is examined using the persistent positive anomaly (PPA) approach (Renwick, 2005). A grid point is defined as blocked if an anomaly of greater than 100 m in the 500 hPa GPH persists for five or more days. The blocking frequency is the percentage of days for which this criterion is met over a given time frame. This technique allows blocking to be examined on a regional basis. In this paper we consider two regions, namely the Pacific (120°W to 180°W and 42.5°S to 60°S) and Atlantic (45°W to 15°E and 42.5°S to 60°S). We define these regions as "blocked" if the number of grid points within the geographic limits described above exceeds a threshold, and "not blocked" if none of the grid points fit the definition. The threshold for model data is 20 (of 102) grid points, for the reanalysis (which has a higher longitudinal resolution relative to the model) the threshold is 30 (of 150) grid points.

4.3.3 SAM calculation

The Southern Annular Mode (SAM) index is calculated from zonal mean GPH anomalies using an empirical orthogonal function (EOF) method. GPH anomalies are calculated relative to a slowly varying mean such that ozone depletion and recovery have no effect on the mean state of the SAM. Full details of the calculation can be found in Dennison et al. (2015).

4.4 Results

In order to evaluate the model we examine the annual mean blocking frequency for the period 1979-2014, shown in Figure 4.1 for both the ERA-Interim reanalysis (top) and the REF-C2 ensemble (bottom). The model does well in simulating the spatial pattern, correctly positioning the maxima in blocking frequency in the Eastern Pacific sector and the minima in the Indian Ocean sector. The spatial correlation between these patterns is 0.88. However, the model underestimates the magnitude of the blocking frequency by around a third. Underestimation of the blocking frequency is a common problem amongst climate models (D'Andrea et al., 1998; Scaife et al., 2010); this is discussed further in section 4.5.

We now examine the seasonal cycle of blocking and the effect on blocking of ozone depletion. To highlight the effect of ozone depletion, we initially

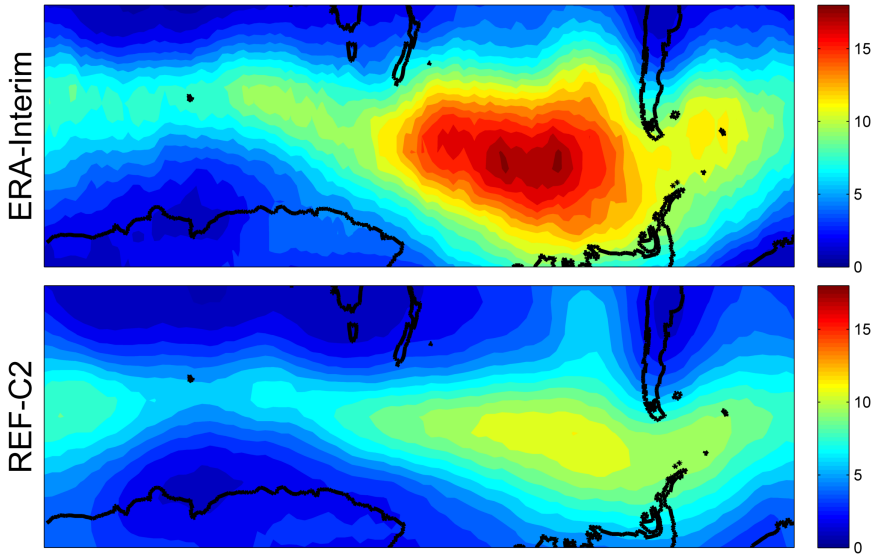

Figure 4.1: Annual mean blocking frequency in ERA-Interim (top) and REF-C2 (bottom) over the period 1979-2014

examine the period 1987-2036 which corresponds to the period of maximum ozone depletion as simulated by the model. During this period the October- and areal-mean total column ozone south of 70°S is less than 220 Dobson Units (see Figure 4.10 in appendix). The top row of Figure 4.2 shows the seasonal blocking frequencies in the REF-C2 runs. There is a large seasonal cycle with blocking more frequent during the winter season. This seasonal cycle is consistent with other studies (e.g., Renwick, 2005; Mendes et al., 2008; Parsons et al., 2016). The second row of Figure 4.2 illustrates the effect of ozone depletion by showing the differences between the REF-C2 and SEN-C2-fODS ensembles in each season. The differences are presented as percentage changes relative to the REF-C2 blocking frequency. For example, if the blocking frequency in the REF-C2 ensemble is 6% and in SEN-C2-fODS it is 4%, then the difference is +33%. Significant differences are marked with cross-hatching. Differences are considered significant if the difference in the ensemble means exceeds twice the REF-C2 intra-ensemble standard deviation. This analysis shows two instances where ozone depletion appears to have affected the blocking frequency: (1) In the South Atlantic in summer blocking appears to have increased as a result of ozone depletion. (2) In the Southern Indian Ocean in winter (and to a lesser extent in spring) blocking has decreased. The South Atlantic effect is the larger of the two

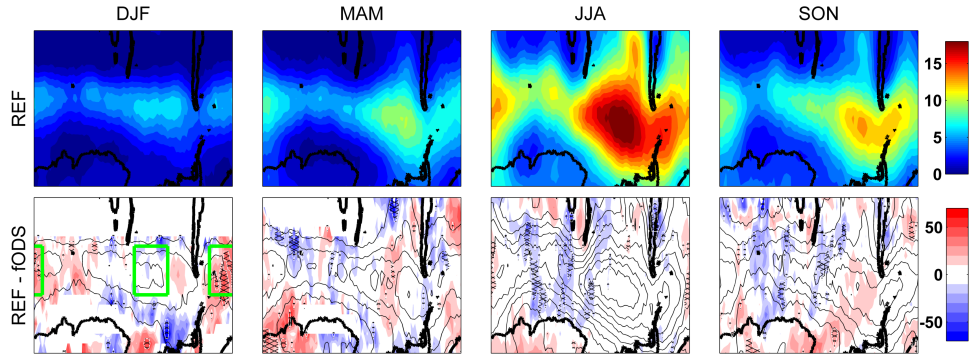

Figure 4.2: Seasonal mean blocking frequencies for REF-C2 (top row) and the percentage difference between REF-C2 and SEN-C2-fODS (bottom, shading) over the period 1987-2036. The mean blocking frequency of SEN-C2-fODS is also illustrated on the bottom row in contours (increments of 2% beginning at 2%). The green boxes indicate the Pacific and Atlantic regions referenced throughout this paper

and our *a priori* expectation is that ozone depletion generally effects the summer season (Thompson et al., 2011). For these reasons we will focus on the Atlantic region during summer. In contrast to the South Atlantic, modelled blocking in the South Pacific is not affected by ozone depletion. By contrasting these two regions we will investigate the reasons behind the change in the Atlantic region. The regions are highlighted in Figure 4.2.

Figure 4.3 shows the time series of the summer blocking frequency over the Atlantic and Pacific regions for the three scenarios and the ERA-Interim reanalysis. The shaded region around the REF-C2 ensemble illustrates the 95% confidence interval, this was estimated based the deviations of individual runs with respect to the ensemble mean and assumes the variance is proportional to the magnitude of the blocking frequency and does not otherwise vary as a function of time. The time series of the REF-C2 and SEN-C2-fODS ensembles confirm that the difference between the two in the Atlantic that was shown in Figure 4.2 is confined to the ozone depletion period. The ensemble means begin to diverge during the late 1990's and converge around 2050, while closely tracking each other at the beginning and end of the simulation. The SEN-C2-fODS ensemble lies outside the bounds of the REF-C2 confidence interval over the period 2010-2025.

As was indicated by Figure 4.1, the blocking frequency calculated for the ERA-Interim dataset is larger than the model. To aid comparison, we

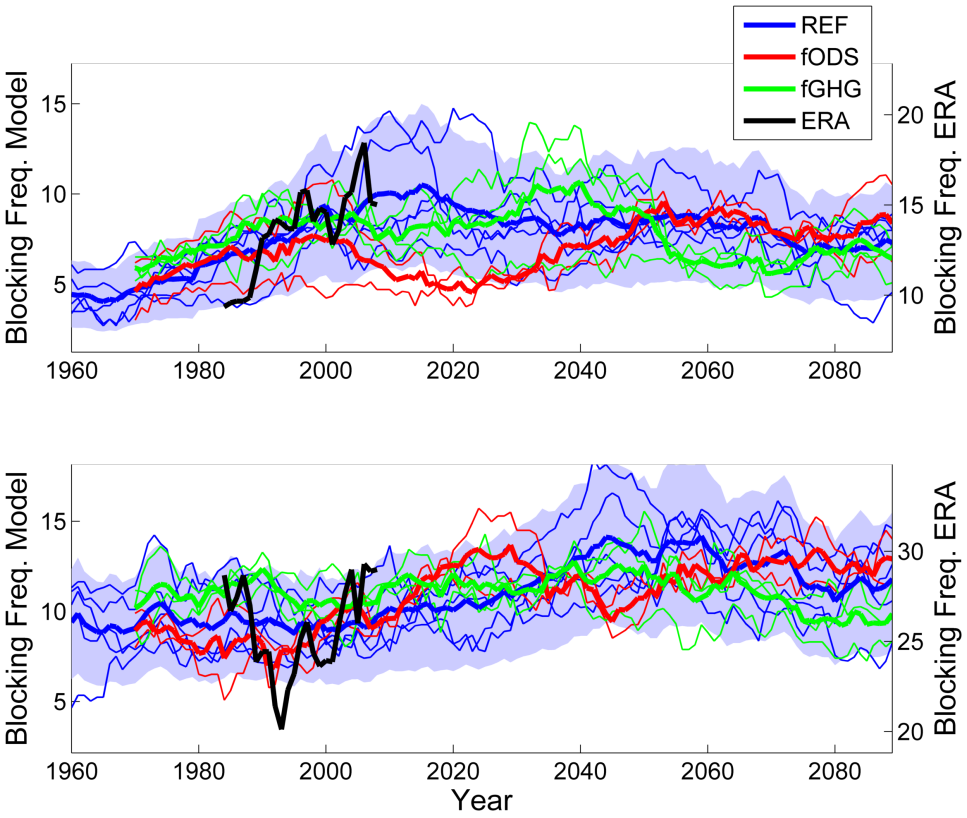

Figure 4.3: Time series of the summer blocking frequency in the Atlantic (top) and Pacific (bottom) in each of the model simulations REF-C2 (blue), SEN-C2-fODS (red), SEN-C2-fGHG (green) and the ERA-Interim reanalysis (black). Thin lines show the individual model runs, thick lines show the ensemble mean, and the shading indicates the 95% confidence interval around the REF-C2 ensemble mean. Note that the model and ERA–Interim reanalysis use different scales on the vertical axis to aid comparison.

therefore use different vertical scales for the model and ERA–Interim output in Figure 4.3. The ERA-Interim trends in blocking frequency in each of the regions match the modelled trends, namely a positive trend in the South Atlantic and no significant trend in the South Pacific. For the South Atlantic region, the trend in ERA-Interim is larger than the mean REF-C2 one, although Figure 4.3 indicates that there is substantial variability amongst the ensemble members with two of the five REF-C2 runs exhibiting trends of magnitudes similar to the ERA-Interim trend. Also, if the trends are expressed relative to the mean blocking frequency, then there is no significant disagreement with a 16.5%/decade trend (relative to the 1979-2014 mean blocking frequency) for the REF-C2 ensemble ($p = 0.076$) and 18.9%/decade trend for ERA-Interim ($p = 0.137$).

The REF-C2 time series for the Atlantic blocking has two clear trends, increasing up until about 2010 with a slower decrease thereafter. The timing of this change might be expected from an ozone driven effect as ozone depletion peaks at around that time before slowly recovering over the remainder of the 21st century. A similar pattern is also observed for the fGHG time series although the turning point is less clear due to substantial variability and the smaller ensemble size. In contrast to the Atlantic, the Pacific region shows no significant differences between the REF-C2 and fODS simulations over the entire course of the simulations. While the fGHG ensemble shows no trend in either region, both the REF-C2 and fODS ensembles have small positive trends over the duration of the simulation and exhibit a larger blocking frequency at the end of the 21st century than the fGHG runs. This suggests that increasing GHGs have the effect of increasing blocking frequency across the hemisphere. Thus, the response of blocking to ozone forcing appears to be more regional than is the case for GHG forcing.

We now investigate the characteristics of the stratospheric planetary waves for the two blocking regions, as wave breaking has been shown to be a contributor to blocking (Berrisford et al., 2007). Figure 4.4 shows the probability density functions (PDFs) of the amplitude and phase of planetary waves with zonal wavenumbers 1 to 4 during periods where the Atlantic region is concurrently blocked (red) or not blocked (blue), based on the criterion as defined above. The waves components are calculated by performing a fast Fourier transform (FFT) on the 55°S GPH anomaly at 10 hPa over the entire duration of the REF-C2 simulations. It is clear that summer blocking

is associated with waves of a certain phase, particularly for waves with zonal wavenumber 1 to 3. Futhermore, blocking is associated with increased wave amplitude for each of the four wave components. Similarly, in the case of Pacific blocking, Figure 4.5 shows that zonal wavenumbers 1 to 3 have a clear phase preference, but there is little to no preference for an enhanced wave amplitude in this situation. The difference in median amplitude for each wavenumber is noted in the corner of the plot, bold font indicates whether the difference in distributions is significant ($p < 0.05$) according to the Wilcoxon rank sum test (Wilcoxon, 1945).

Figures 4.4 and 4.5 reveal that the state of the stratosphere is perturbed during the presence of tropospheric blocking. However, it is possible that the stratosphere is playing a role in initiating the blocking event and/or that the stratosphere becomes perturbed as a result of the blocking event. Previous studies have suggested that the stratospheric state can impact tropospheric blocking (Woollings et al., 2010)and also that blocking can impact the stratospheric state (Martius et al., 2009). Figure 4.6 shows GPH anomalies associated with summer blocking events in the Atlantic on the 10, 100 and 500 hPa pressure levels. Composites are produced for two successive ten day periods leading up to the tropospheric blocking event, the blocking event itself, and two ten day periods following the blocking event. The GPH is calculated relative to a slowly varying climatology in order to remove the effect of both ozone depletion and GHG forcing on the mean state. All shaded anomalies are significant ($p < 0.05$) according to Wilcoxon's signed rank test (Wilcoxon, 1945). Prior to the blocking event, at 10 hPa, the main feature is the negative anomaly over the polar region i.e. a positive SAM-type pattern, which is consistent across the entire 20 day lead up. In addition to the SAM-type pattern, there are also some small-amplitude wave 1 and 2 patterns. During the blocking event, the amplitude of the wave 1 pattern increases to become the dominant feature. The wave 1 pattern persists for the ten days following the blocking event, then dissipates over days 11-20. Similarly, at 100 hPa, the SAM type pattern occurs prior to the blocking event. Again the anomaly pattern characteristic of the blocking event persists in the composite of the following ten days, but it dissipates faster than at 10 hPa. The 500 hPa level does not show the same SAM feature and, in contrast to the 10 hPa level where waves 1 and 2 are more prominent, this level is dominated by waves with higher wavenumbers, particularly in the

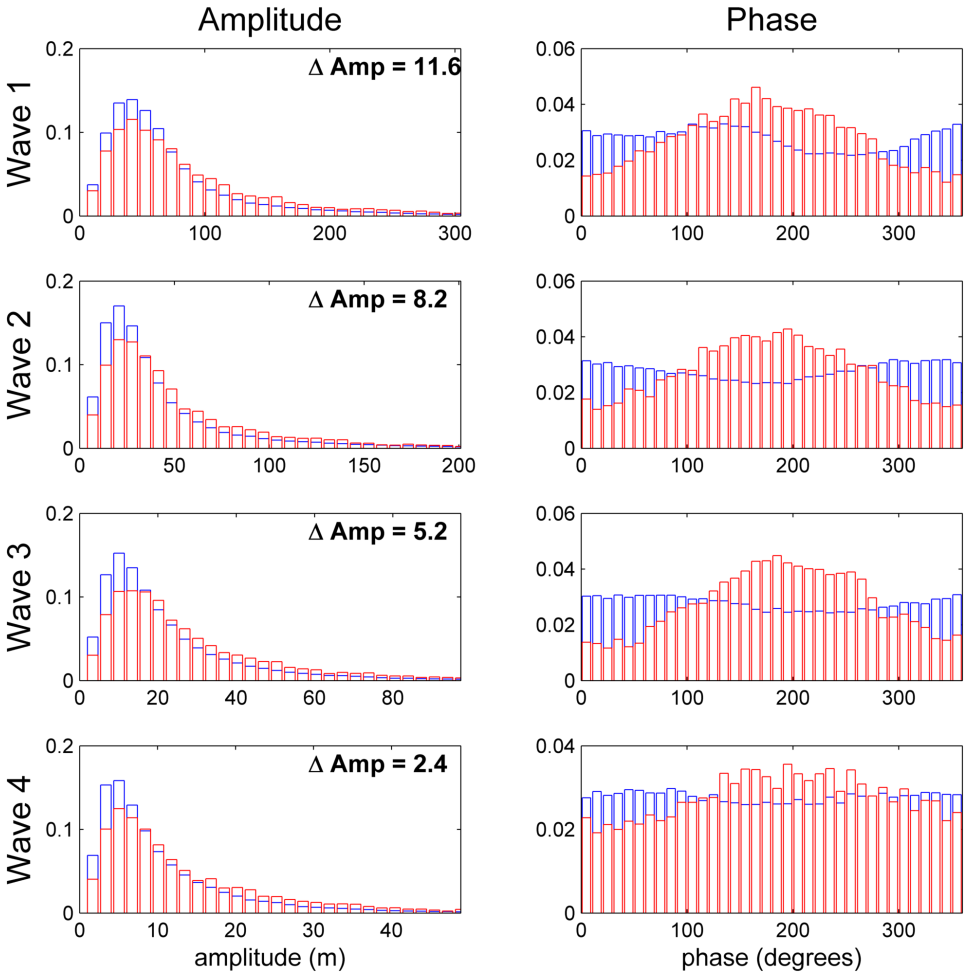

Figure 4.4: PDFs of the amplitude (left) and phase (right) of the first four wave components at 10 hPa during summer blocking events (red) and without blocking (blue) in the Atlantic over the period 1950-2099. ΔAmp notes the difference in medians and is bold if the difference is significant ($p < 0.05$)

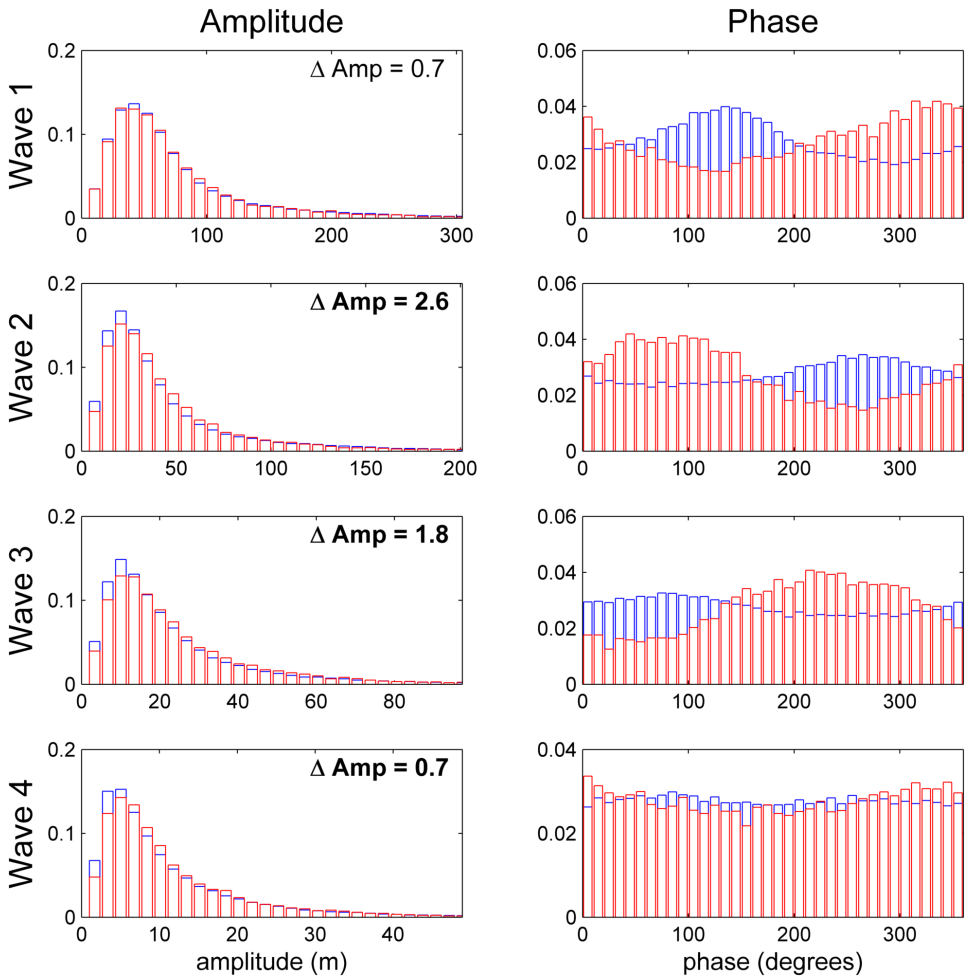

Figure 4.5: As for Figure 4.4 with Pacific blocking

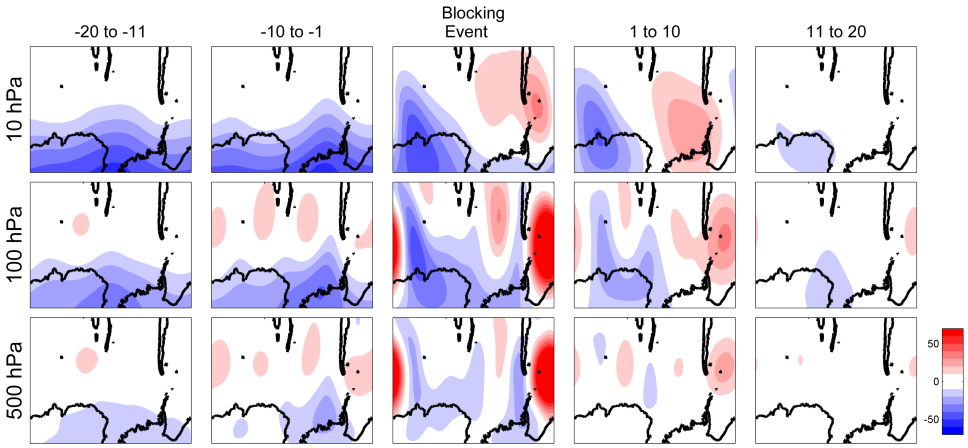

Figure 4.6: GPH anomalies prior to, during and following (left to right) summer blocking events in the Atlantic at pressure levels 10 (top), 100 (middle) and 500 hPa (bottom) for the REF-C2 runs over the period 1950-2099. All colored anomalies are significant ($p < 0.05$) according to Wilcoxon's signed rank test

periods immediately prior to and following the blocking event. Figure 4.7 shows the equivalent for blocking events in the Pacific. In contrast to the Atlantic, there is no sign of any SAM type patterns, but rather just the wave 1 pattern dominating the 10 hPa level and higher wavenumbers at the lower levels.

To further investigate the preference for positive SAM anomalies prior to blocking, we present SAM composites showing a more detailed picture over the depth of the stratosphere and troposphere before and after the blocking event. The upper panel of Figure 4.8 shows the SAM composite corresponding to blocking events in the Atlantic. Lag is relative to the onset of the blocking event; lag 0 corresponds to the first day of the blocking event. Significant SAM anomalies ($p < 0.05$) are identified by Wilcoxon's signed rank test (Wilcoxon, 1945) and are indicated by hatching. As Figure 4.6 suggested, there is a positive SAM anomaly prior to the blocking event. This anomaly lasts for 40-50 days and peaks around 30-50 hPa but extends through much of the lower stratosphere and upper troposphere. It comes to an end abruptly at the onset of the blocking event. The contrast is clear when comparing this behavior to the equivalent structure for the Pacific region shown in the lower panel of Figure 4.8. In this case, the SAM anomaly is much smaller and confined to the troposphere. Figure 4.9 shows

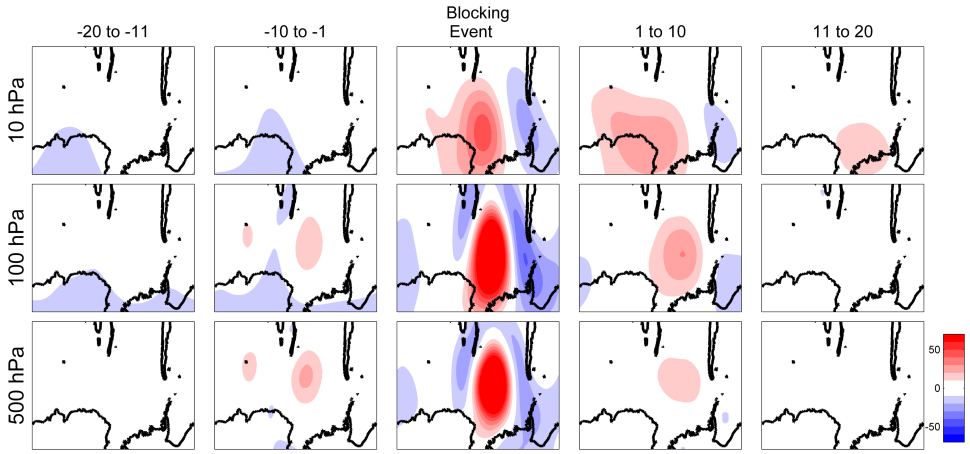

Figure 4.7: As for Figure 4.6 with Pacific blocking

the same analysis applied to the ERA-Interim reanalysis. As was the case for the model, this shows a strong positive SAM anomaly in the stratosphere preceding blocking events in the Atlantic and very little anomalous behavior associated with Pacific blocking. Note that although the stratospheric anomalies are larger for the reanalysis, they are not shown to be significant. This might be expected because the Figure 4.8 composite is drawn from five 150 year runs while Figure 4.9 is from just 36 years of data, making statistical significance more difficult to obtain. A notable difference for the reanalysis is the presence of a positive SAM anomaly in the troposphere after the onset of the blocking event.

4.5 Discussion and Summary

The NIWA-UKCA model, when compared to the ERA-Interim reanalysis, generally simulates well many of the aspects of blocking such as the spatial distribution, seasonal cycle and associations with the SAM. However, it underestimates the blocking frequency by around a third. This is a common problem among climate models (D'Andrea et al., 1998; Scaife et al., 2010), especially those with low horizontal resolution (Anstey et al., 2013) (as is the case for the NIWA-UKCA model). Such models cannot simulate small-scale eddies which are important for maintaining blocking events (Matsueda et al., 2009). Scaife et al. (2010) also find that biases in the mean state of the model cause errors in the simulation of blocking. This may also be

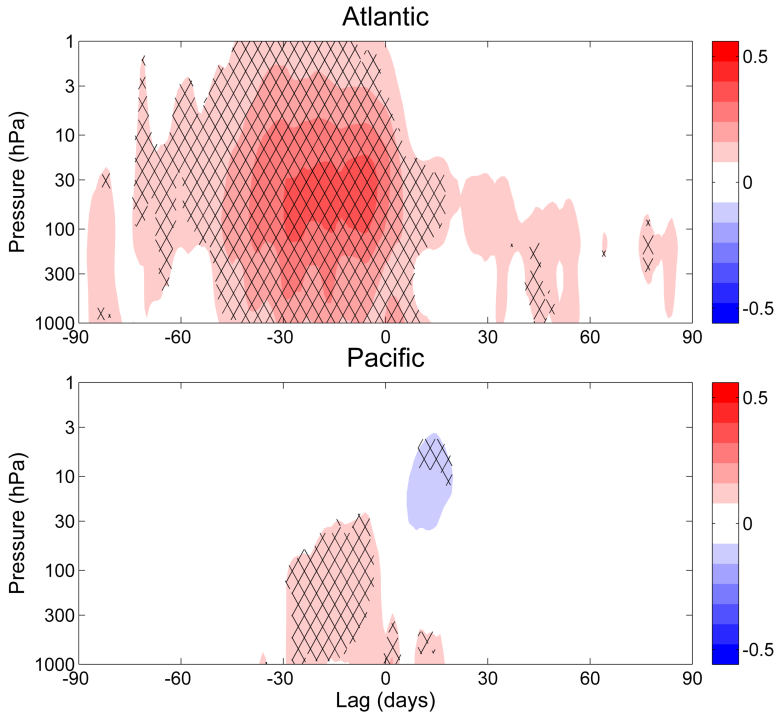

Figure 4.8: SAM composite of (top) Atlantic blocking and (bottom) Pacific summer blocking in the REF-C2 runs over 1950-2099. Hatching indicates significance ($p < 0.05$) according Wilcoxon's signed rank test

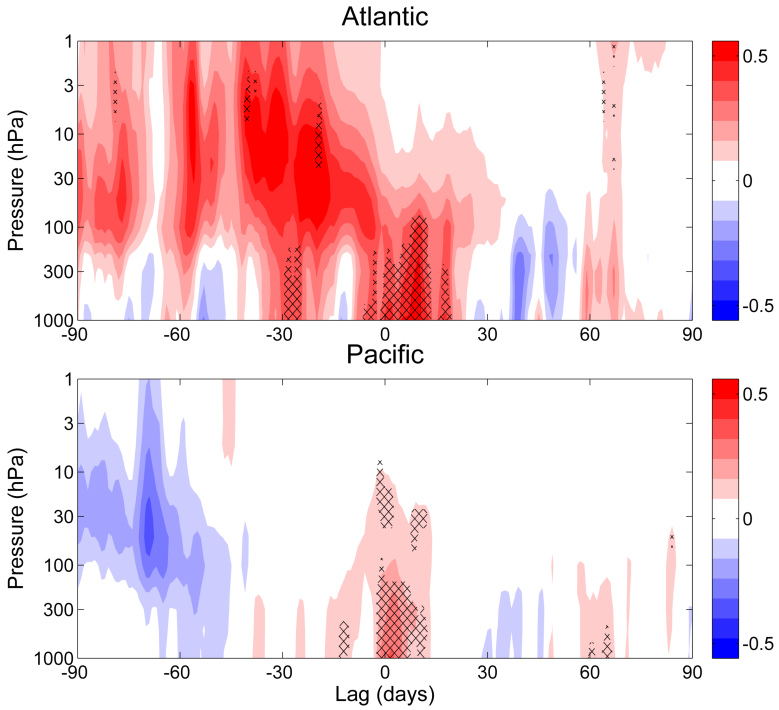

Figure 4.9: As for Figure 4.8 in the ERA-Interim reanalysis 1979-2014

an issue for the NIWA-UKCA model which exhibits a poleward bias in the position of the polar front jet (see appendix).

Figures 4.2 and 4.3 show that ozone depletion is responsible for an increase in the frequency of blocking in the South Atlantic. This change in blocking frequency will likely have consequences for the climate of South America due to the links demonstrated by Mendes et al. (2008) and Kayano (1999) (cf. section 4.2). In the NIWA-UKCA simulations, the effect of ozone forcing is larger than that of GHG forcing. In the REF-C2 ensemble, the blocking frequency increases from ∼5% during the 1960s (i.e. before the onset of the ozone hole) to ∼10% during the mid 2010s before decreasing to ∼7% towards the end of the century when GHG forcing will be the main driver of any change. Furthermore, it is also possible that the ozone-depletion driven change simulated by the model may be an underestimation of the real impact as it is shown that the rate of increase in blocking calculated from the ERA-Interim reanalysis exceeds that of the model. The ERA-Interim data cover a relatively short timespan, and given that the model simulations show considerable variability amongst ensemble mem-

bers and on interdecadal timescales, the data at our disposal is insufficient for attributing the full increase in blocking to ozone forcing. However, we find that ozone depletion likely exerts a bigger influence on blocking in the South Atlantic during austral summer than increasing GHGs.

Another aspect of this association of ozone depletion and blocking is the demonstration of a link between stratospheric processes (i.e. a SAM anomaly at 10 hPa) and blocking, a tropospheric phenomenon. Such stratosphere-to-troposphere coupling has been demonstrated earlier regarding the NAM and SAM (respectively, Baldwin and Dunkerton, 2001; Thompson et al., 2005). A number of subsequent studies have also investigated the links between the stratosphere and tropospheric blocking, most of which focus on Northern Hemisphere blocking. The mechanisms at work in such links are, however, not well understood.

In a somewhat analogous study of Northern Hemisphere blocking, Woollings et al. (2010) show that the first EOF of 10 hPa GPH (which has an annular structure), correlates with a 6-day lead with blocking in certain regions of the Northern Hemisphere. In particular, blocking over Europe was positively correlated with the phase of this EOF which described anomalously strong Arctic polar vortex conditions. However, Yao and Luo (2015) find that blocking events over Southern Europe follow the positive phase of the North Atlantic Oscillation (NAO+). This effect is explained simply as the high pressure lobe of the NAO (which normally is located over the mid-Atlantic) migrating east with the enhanced westerly wind associated with the NAO+. We find that this type of mechanism however does not apply in the case of South Atlantic blocking because Figure 4.6 does not show the same large GPH anomalies prior to the blocking event.

Martius et al. (2009) examined the occurrence of sudden stratospheric warming (SSW) events in the Northern Hemisphere relative to the occurrence of blocking events building on earlier work which identified a possible two-way interplay between these phenomena. That study showed a distinct link between planetary scale waves and atmospheric blocks. For example, in SSW split events, they reported an almost perfect co–location between the blocking maximum in the Pacific with the positive wavenumber 2 wave peak at lower levels. There was also clear evidence of constructive interference of wavenumber 1 and 2 in the upper stratosphere resulting in the vortex split events. The current analysis (see Figure 4.4) also displays clear signs of syn-

chronized wave phases during blocking in the Southern Hemisphere which would be related to constructive interference between the various planetary waves modes.

Recent work by Davini et al. (2014) also examined blocking in the Northern Hemisphere and its relationship to stratosphere-troposphere coupling. Their study analyses the influence of stratospheric extremes (SSWs and also vortex intensification (VI) events) on blocking frequency and patterns in the Northern Hemisphere. The impact of the stratosphere can be summarized as a change of the blocking frequency on the flanks of the eddy driven jet streams. Similar to the results presented in this study, Davini et al. (2014) find that there is a different sensitivity of the tropospheric blocking to the stratospheric forcing in the two ocean basins, with vortex anomalies leading tropospheric blocking in the Atlantic, but having no clear relationship in the Pacific. They also note a clear displacement of the Atlantic eddy-driven jet equatorward for SSWs and an opposite response for VI events. Davini et al. (2014) then examine one of the possible theories to explain stratosphere-troposphere coupling which involves the modulation of tropospheric synoptic waves by the lower stratospheric flow (Kunz et al., 2009). In that theory, the value of the stratospheric zonal wind vertical shear determines the evolution of the baroclinic wave life cycles between two states. Davini et al. (2014) show, in agreement with Kunz et al. (2009), that the stratospheric jets impact the zonal wind vertical shear and can enhance the occurrence of Rossby wave breaking which they note is linked to blocking (Pelly and Hoskins, 2003).

In the case of the Southern Hemisphere, various case studies (e.g., Kodera et al., 2013; Nishii and Nakamura, 2005) have shown links between the stratosphere and tropospheric blocking. They demonstrate planetary waves of tropospheric origin either being reflected (Kodera et al., 2013) or refracted (Nishii and Nakamura, 2005) in the stratosphere back towards the troposphere where they cause a blocking event. These examples are taken for SH winter when westerlies are strong such that planetary wave reflection is initiated (in the Nishii and Nakamura (2005) case study) by an increase in the strength of the westerlies. In this case, while the positive SAM anomaly is associated with increased westerlies, the strength of the westerlies during summer is not sufficient to instigate wave reflection - indeed one might expect less wave reflection due to the decreased frequency of easterlies in

the stratosphere. Therefore it seems it is not the change in zonal winds that is responsible for the change in blocking frequency here. The mechanisms identified in Nishii and Nakamura (2005) and Kodera et al. (2013) are therefore unlikely to be viable mechanisms in this case. One possible interpretation of the link between the SAM and Atlantic blocking, demonstrated in Figure 4.8, is due to the zonally asymmetric component of the SAM. While the stratospheric SAM is mostly zonally symmetric, it also features a zonal wave 1 pattern. In the positive phase it is orientated such that the trough is located over the South East Pacific (Thompson and Wallace, 2000a). Figure 4.6 shows that a trough in this location is present in the 10 days prior to Atlantic blocking events. This might suggest that it is the state of the planetary waves that influence the blocking frequency and the SAM modifies the planetary wave state in such a way that it influences only blocking in the Atlantic. A tendency toward a positive SAM (driven by ozone depletion (Arblaster and Meehl, 2006; Karpechko et al., 2010b; Morgenstern et al., 2014)) therefore drives the increase in Atlantic blocking that we find, while having little effect on blocking in the Pacific. The nature of the mechanism initiating these summer blocking events is still unclear. Further investigation of wave propagation is perhaps required but is beyond the scope of this study due to limitations on the model output available.

4.6 Appendix: Model Evaluation

This appendix provides a comparison between the NIWA-UKCA model and ERA-Interim reanalysis to identify the model characteristics and biases that may be relevant to this study. First we examine the simulated ozone depletion. Figure 4.10 shows the October mean total column ozone south of 70°S for REF-C2 (blue) and SEN-C2-fODS (red) individual model runs compared to the ERA-Interim reanalysis (black).While the REF-C2 simulation reproduces the ozone depletion trend well, it does not seem to capture the year-to-year variability (although the 2002 spike in ozone shown in ERA-Interim is due to a stratospheric sudden warming (SSW) that is not present in the model). The ozone recovery phase shows the model predicting a return to 1980 levels around the 2050s which is consistent with other chemistry-climate models (Eyring et al., 2010).

Next we examine the mean state of the zonal winds. Figure 4.11 shows

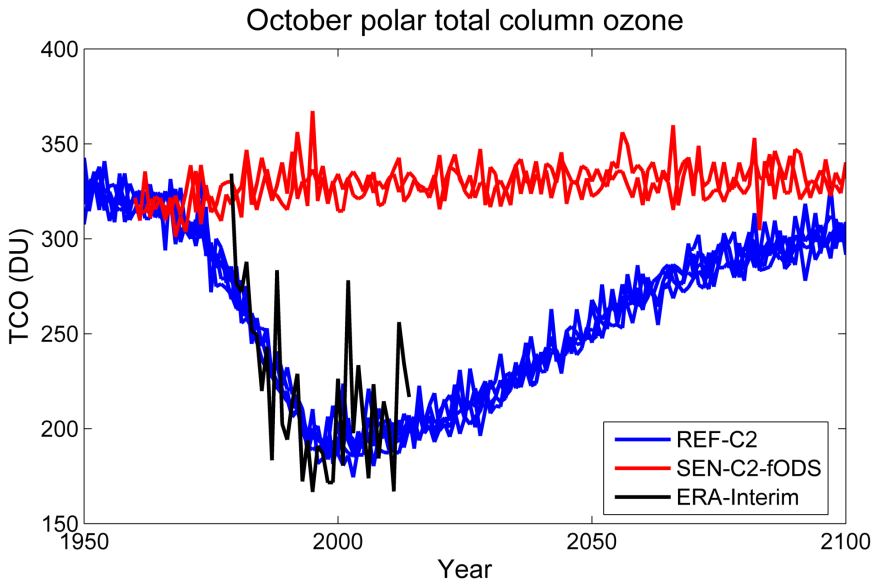

Figure 4.10: October mean total column ozone south of 70°S for REF-C2 (blue), SEN-C2-fODS (red) and ERA-Interim (black)

the difference in summer zonal mean zonal wind between the REF-C2 ensemble and ERA-Interim reanalysis over the period 1979-2014. It can be seen that the model overestimates the wind strength in the polar stratosphere. This wind strength bias is present in all seasons. However, in summer, the bias is exacerbated somewhat by the model tendency to delay the break-up of the polar vortex. It is possible that this bias in the mean state of the model may cause some bias in the simulation of blocking, as is demonstrated in Scaife et al. (2010).

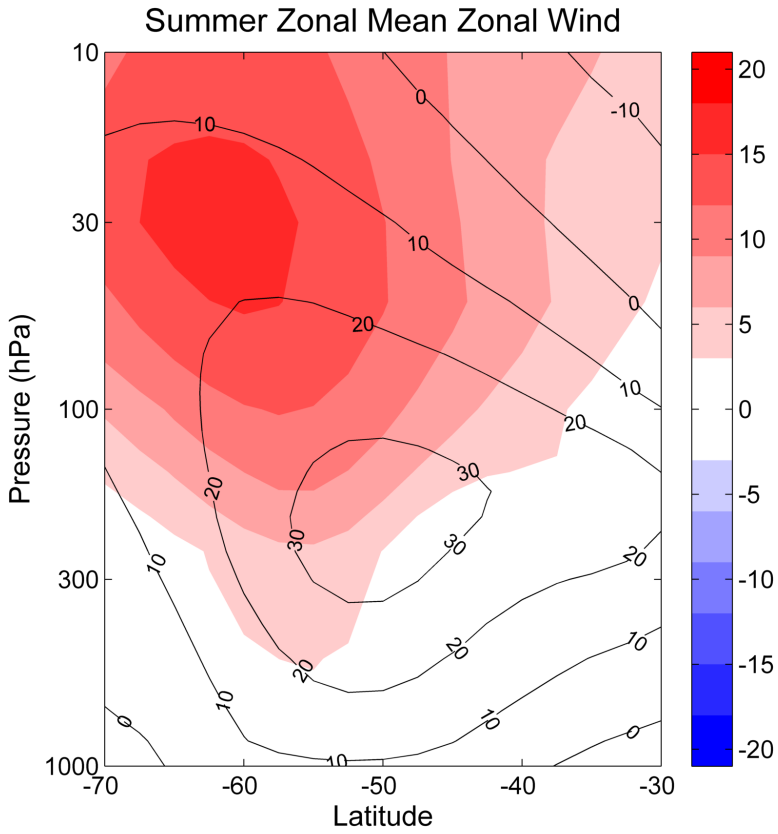

Figure 4.11: Summer zonal mean zonal wind for the REF-C2 simulations over the period 1979-2014 (contours) and the difference between REF-C2 and the ERA interim reanalysis (shading)

Chapter 5

Zonally Asymmetric Ozone

5.1 Introduction

The previous two chapters focus on the role of zonally symmetric features in driving changes in tropospheric climate initiated by stratospheric ozone forcing. In this chapter, we examine changes in the zonal asymmetry of ozone and the effect this has on climate. Until recently, most general circulation models (GCMs) have used zonally averaged ozone distributions (Randall et al., 2007; Hegerl, 2007), but a number of studies have emphasized the importance of modelling the zonal asymmetry of ozone for simulating stratosphere polar temperatures. These studies take the approach of comparing model simulations with zonally averaged ozone to those with either prescribed three dimensionally varying ozone (Crook et al., 2008) or interactively modelled ozone (Gillett et al., 2009; Waugh et al., 2009). Crook et al. (2008) found a cooling in the stratosphere and upper troposphere associated with the asymmetric ozone. This cooling was located around 150°E - the region with above average ozone - which showed that this effect is not due directly to radiative heating but instead to dynamical heating. Gillett et al. (2009) and Waugh et al. (2009) improve on the methods of Crook et al. (2008) by instead utilizing interactively modelled ozone, thus ensuring ozone is consistent with atmospheric dynamics. The findings of these studies are consistent with those of Crook et al. (2008). Additionally, Waugh et al. (2009) notes that the zonally asymmetric cooling effect is larger, when the ozone hole itself is larger, meaning that Antarctic temperature trends are underestimated as a result of zonally averaged ozone being used in climate

models.

In addition to the effect on stratospheric temperature, zonally asymmetric ozone also affects tropopause height. Evtushevsky et al. (2008) find that the tropopause height and sharpness are influenced by zonally asymmetric ozone during spring, the below average ozone regions being associated with a higher tropopause and a thicker transition layer. Thickening of the transition layer between stratosphere and troposphere increases troposphere - stratosphere exchange and mixing activity.

Ozone has also been shown to be an important factor modulating the atmospheric refractive index and thus the propagation of planetary waves (Nathan and Cordero, 2007; Gabriel et al., 2007). Gabriel et al. (2007) finds the introduction of zonally asymmetric ozone results in a change in the upward and eastward directed wave flux. Compared to the case of zonally symmetric ozone, these wave fluxes are increased in the western Northern Hemisphere stratosphere and reduced in the east. Albers and Nathan (2012), using a mechanistic model, explore the ways in which zonally asymmetric ozone, via its influence on wave propagation, affects the polar vortex. They identify two pathways in which the polar vortex is influenced. The first describes the effect of zonally asymmetric ozone on vertical energy flux and planetary wave drag, the second describes the effect on zonal-mean temperature (and hence thermal wind balance) of wave-ozone flux convergence. Both pathways are found to be important in influencing the polar vortex.

The asymmetry in ozone during winter and spring is caused by planetary wave driven displacement or distortions of the polar vortex (Waugh, 1997; Ialongo et al., 2012). The polar vortex and ozone hole are closely linked as ozone depletion affects the temperature gradient and thus the strength of the vortex, while the strength of the vortex affects the degree to which ozone depleted air is isolated from the relatively ozone rich air at mid-latitudes (Beron-Vera et al., 2012; Smith and McDonald, 2014). The distribution of ozone varies with low wavenumber patterns, primarily wavenumber 1 (Ialongo et al., 2012). In the Southern Hemisphere, the asymmetry is typically such that ozone depleted air extends further poleward in the Atlantic region.

Over the period 1979-2003, Grytsai et al. (2005) find the position of the ozone minimum at 65°S drifts eastward at a rate of 23.6±7.2° per decade, with the position of the maximum remaining constant. Grytsai et al. (2007) extended this study showing eastward trends in the ozone minimum for all

latitudes between 50 and 80°S. However, the cause of this trend was not identified.

This chapter examines the changes in the characteristics of the zonally asymmetric ozone. The metrics used to describe the ozone asymmetry are detailed in Section 5.2. Simulation of the ozone asymmetry by the NIWA-UKCA model is assessed by comparison with reanalysis output in Section 5.3.1. The evolution of ozone asymmetry in the model from 1950-2099 is examined in Section 5.3.2. This section also investigates the role of ozone and greenhouse gas (GHG) forcing on zonal asymmetries by using model simulations in which either the ozone depleting substances (ODSs) or GHGs are held fixed. Section 5.4 provides a discussion and summary of the results.

5.2 Data and Methods

The links between asymmetric ozone and tropospheric climate are examined in both the ERA-Interim reanalysis and the REF-C2, SEN-C2-fODS and SEN-C2-fGHG ensembles of the NIWA-UKCA model (see Chapter 2). The asymmetry in ozone is calculated from total column ozone (TCO) fields. The effect on the stratosphere is shown in the 50 hPa temperature and the 500 hPa geopotential height (GPH) is used as a measure of the tropospheric climate. The following two metrics are used as measures of asymmetry.

Ellipse Fit

Elliptical diagnostics have previously been shown by Waugh (1997) to be useful in examining the polar vortices. In that case, the long-lived tracer N_2O was used to fit the ellipse. Here we use an ellipse fitted to the 300 Dobson unit (DU) contour of the October mean TCO to describe the distribution of ozone. The 300 DU contour was chosen to ensure the contour would be clearly defined over the entire model simulation (1950-2100). The latitude/longitude coordinates of this contour are converted to Cartesian coordinates and an ellipse is fitted to the contour using the Taubin (1991) algorithm. The fitted ellipse is defined in terms of the parameters: angle of rotation, latitude/longitude of centre, eccentricity and area. Eccentricity is defined as

$$e = \sqrt{\frac{a^2 - b^2}{a^2}}$$

where a is the length of the major axis and b the minor axis. In analysis of the centre longitude, only data for which the centre is significantly displaced from the pole (centre latitude >-89°) is used as centres close to the pole have a larger uncertainty associated with the longitude.

Longitude of Maximum/Minimum TCO

The other measures we use are the longitude of the maximum (lon_{max}) and minimum (lon_{min}) September-November mean TCO at 65°. This is the measure used by Grytsai et al. (2005, 2007). Grytsai et al. (2007) also examines this measure at other latitudes and find that the maximum and minimum moves toward the east at higher latitudes. However, the trend in this measure over the historical period is found to be consistent across the range of latitudes.

5.3 Results

5.3.1 Reanalysis/Model Comparison

Figure 5.1 shows the climatological monthly means of the TCO for August to December over the period 1979-2014 in the ERA-Interim dataset (left column) and the model REF-C2 ensemble (middle column) as well as the difference between the two (right column). In the reanalysis, it is clear that during spring there is a wavenumber 1 asymmetry in the TCO with the ozone minimum offset from the pole toward the Weddell Sea region. The model significantly underestimates this asymmetry in ozone; during spring the ozone depletion is centred closer to the pole. As such, the model simulates more ozone over the Weddell Sea during August to October as well as the Bellingshausen Sea during August and September. During October, there is relatively less ozone over the Ross Sea region in the model. Furthermore, the vortex break-up occurs later in the model; this is illustrated in Figure 5.1 by the polar ozone depletion persisting into November and December. A delayed breakup of the vortex is a common problem among climate models (Butchart et al., 2011).

The differences in the characteristics of asymmetry can be quantified using the metrics described in Section 5.2. Figure 5.2 shows the time series for the October ellipse parameters for the reanalysis (black) and the

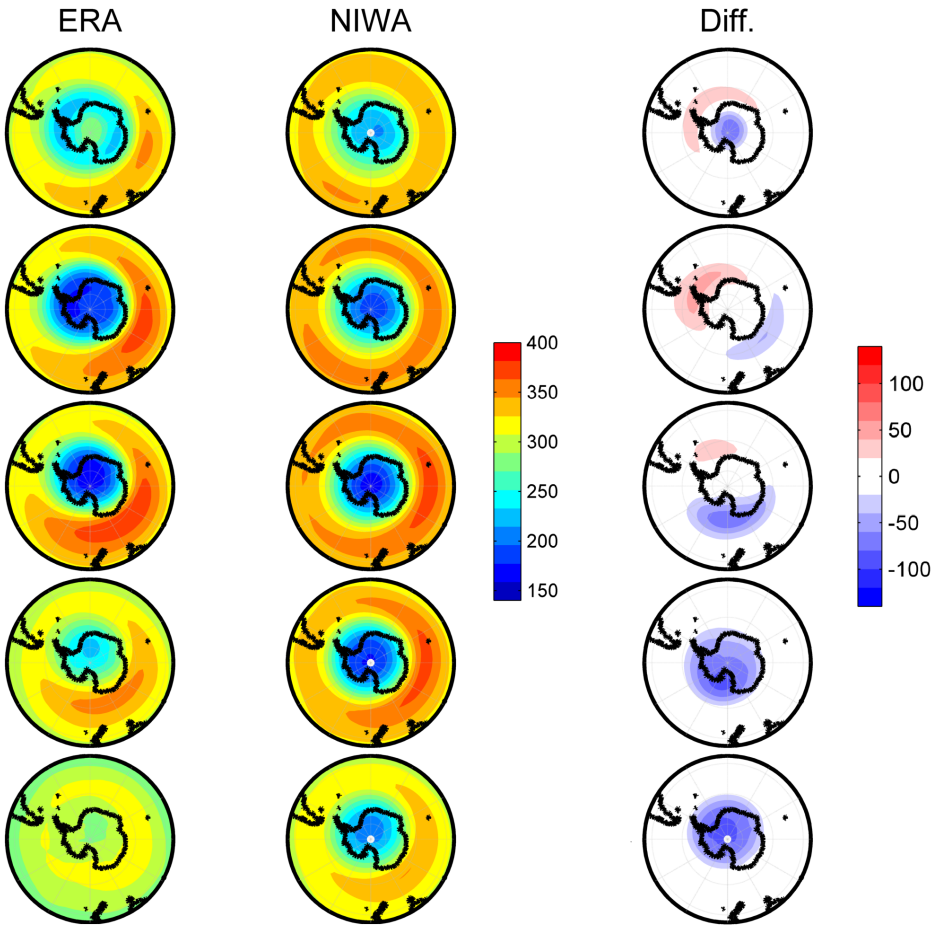

Figure 5.1: Monthly mean TCO (DU) for August to December (top to bottom) in the ERA-Interim dataset (left), NIWA-UKCA model (middle) and the difference between the two (right) over the period 1979-2014

REF-C2 ensemble (blue). The shaded region indicates plus and minus one standard deviation from the model ensemble mean. The differences between the reanalysis and model illustrated by Figure 5.1 are confirmed by these metrics. Most notably, the latitude of the ellipse centre for the model is much closer to the pole. The reanalysis averages around 80°S although exhibits considerable variability, ranging between 88°S and 73°S. The model averages approximately 87.5°S, with very little variation. The reanalysis shows an equatorward trend of 1.2°/dec (significant at the 95% level) during the period 1979-2014. However, the model shows no such trend over this period. The centre longitude is more consistent between the reanalysis and model; over the period 1979 to 2014 the mean longitude is slightly

eastward in the reanalysis compared to the REF-C2 runs (22°W compared to 37°W), although this difference is not statistically significant. The model shows a change in trend around the mid 1990s; however, this is not evident in the reanalysis. The eccentricity of the ellipse is significantly less circular in the reanalysis than the model over this period ($e = 0.48$ compared to $e = 0.38$). Figure 5.2 also illustrates the ellipse area. The modelled ellipse area matches the reanalysis reasonably well; previous chapters have shown the model to simulate the magnitude of ozone depletion well (see Figure 4.10) so this suggests that the ellipse measure provides a faithful indicator of ozone depletion. Note that the anomalously low TCO during 2002 in the reanalysis is a result of a stratospheric sudden warming (SSW). This is the only SSW recorded in the Southern Hemisphere (Baldwin et al., 2003); none are present in the model simulations. The angle of rotation of the ellipse is not shown here as this parameter exhibits a large amount of variability in the model due to the very circular nature of the ellipse.

Figure 5.3, similar to Figure 5.2, shows the times series for the longitude of the minimum (lon_{min}) and maximum (lon_{max}) TCO at 65°. For both lon_{min} and lon_{max} the model is biased 10-20° west relative to the reanalysis, although this difference is not statistically significant. In both the model and reanalysis there is a eastward trend. The trends are shown in Table 5.1 for both the 1979-2014 period, i.e. the full reanalysis period, and 1979-2005 for comparison with the Grytsai et al. (2007) results. The trend in the reanalysis agrees with the findings of Grytsai et al. (2007) (who used data from the Total Ozone Mapping Spectrometer (TOMS)) within the uncertainty bounds. The model underestimates the trend in lon_{min}, while correctly identifying no statistically significant trend in lon_{max} over the 1979-2005 period. However, analysis of the full 1979-2014 period shows the lon_{max} trend in both the reanalysis and models is larger and is statistically significant in the case of the model. On the other hand, in both the reanalysis and model lon_{min}, the trend appears to reverse during the late 2000s resulting in smaller overall trends.

5.3.2 The Effect of Ozone Depletion and Recovery

Figure 5.4 shows the October ellipse parameters for the REF-C2 (blue), SEN-C2-fODS (red) and SEN-C2-fGHG (green) ensembles over the length of the simulation. The ensemble means are smoothed with a 15 year running

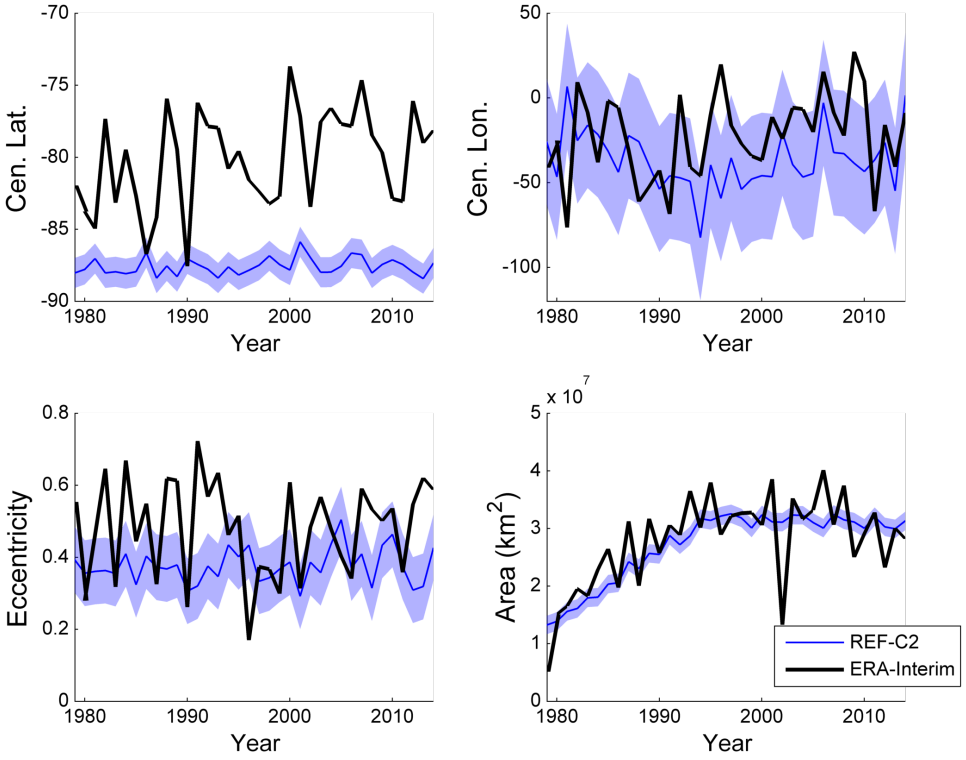

Figure 5.2: Time series of the October TCO ellipse parameters: centre longitude, centre latitude, eccentricity and area for the REF-C2 (blue) and ERA reanalysis (black). The shaded region indicates ±1 standard deviation from the ensemble mean

mean and the shaded region indicates plus and minus one standard deviation from the REF-C2 ensemble mean (the other simulations have similar levels of uncertainty but are not shown for clarity). To identify the influence of ozone depletion, the Student's t test is applied to the differences between 15 year time slices of the REF-C2 and SEN-C2-fODS ensembles. During periods for which the test shows the difference between the ensemble means is significant ($p < 0.05$) the line is solid, if the test shows no significant difference the line is dashed. Figure 5.4 shows that the centre latitude of the ellipse is similar between the ensembles, only showing intermittent differences which are likely the result of natural variability, therefore, indicating no significant influence of either ozone depletion or GHG forcing on this parameter. The central longitude, however, shows a sustained difference between the SEN-C2-fODS and both the REF-C2 and SEN-C2-fGHG ensembles. For the REF-C2 ensemble, the period that may be considered

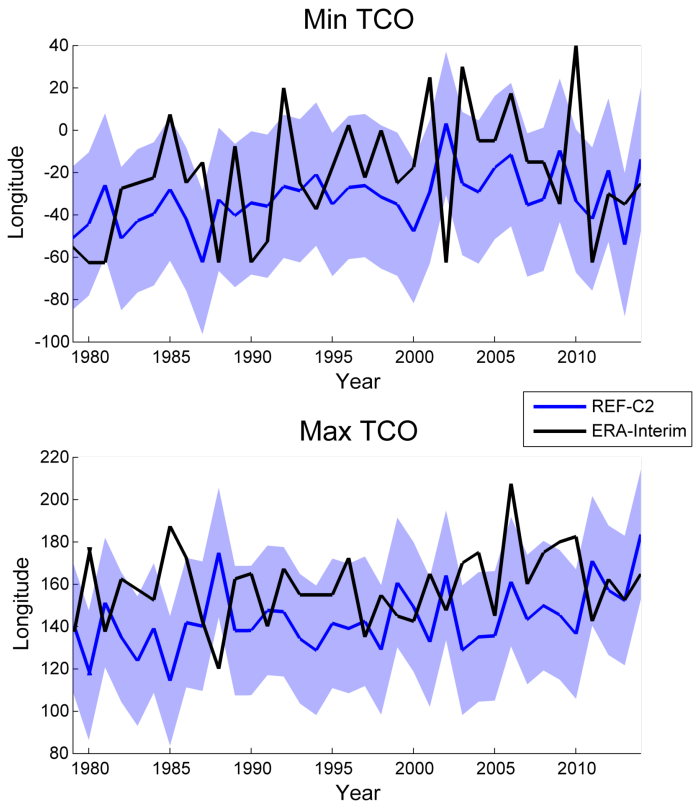

Figure 5.3: Time series of the longitude of the minimum and maximum TCO at 65° for the REF-C2 (blue) and ERA reanalysis (black). The shaded region indicates ±1 standard deviation from the REF-C2 ensemble mean

significantly different ($p < 0.05$) lasts from around 1980 to the mid 2050s, which corresponds closely to the period in which polar ozone is depleted to levels below 220DU (see Figure 3.3(a)). Over this period, the difference between the two ensembles is as much as 50°, with the central longitude in the REF-C2 and SEN-C2-fGHG ensembles displaced toward the west.

The trends in centre longitude are summarized in Table 5.2; split into the periods 1960-1999, representing the period of ozone depletion and 2000-2099, representing the period of ozone recovery. REF-C2 has a trend of -19°/dec over 1960-1999, which is similar to SEN-C2-fGHG within the bounds of uncertainty. Over this period the SEN-C2-fODS simulation displays no significant trend. This indicates that ozone depletion is the main cause of the shift during this period. Over the 2000-2099 period SEN-C2-fODS exhibits a small, but significant positive trend in the centre longitude. Also, the REF-C2 trend is somewhat larger than that of the SEN-C2-fGHG ensem-

Table 5.1: Trend in longitude of maximum and minimum TCO (°/dec). Uncertainty is indicated by the 95% confidence interval in the case of ERA-Interim and REF-C2 and 1σ in the case of the Grytsai et al. (2007) results.

	1979-2005		1979-2014	
	lon_{min}	lon_{max}	lon_{min}	lon_{max}
ERA-Interim	16.4 ± 8.9	0.0 ± 8.1	7.7 ± 8.9	3.8 ± 5.6
REF-C2	9.1 ± 5.4	2.8 ± 6.8	5.4 ± 4.0	6.6 ± 4.4
Grytsai et al. (2007)	16.4 ± 5.2	3.6 ± 4.7		

Table 5.2: Trend in the centre longitude (°/dec) for each of the model ensembles. Uncertainty is indicated by the 95% confidence interval

	1960-1999	2000-2099
REF-C2	-19.0 ± 5.1	7.6 ± 1.3
SEN-C2-fODS	-0.8 ± 8.5	2.8 ± 1.3
SEN-C2-fGHG	-16.2 ± 7.6	6.3 ± 1.9

ble. These two results suggest that increasing GHG forcing over the 21^{st} century acts in conjunction with ozone recovery to cause the eastward trend in the centre longitude.

In the case of the ellipse eccentricity parameter, the SEN-C2-fODS ensemble is relatively consistent at around 0.47; the REF-C2 and SEN-C2-fGHG ensembles also begin around this level. However, during the 1970s, the REF-C2 and SEN-C2-fGHG ellipses become increasingly circular, reaching around $e = 0.4$ and remaining at that level for the remainder of the simulation. It would seem this transition is related to ozone depletion as this change coincides with the beginning of the ozone depletion period. However, it appears eccentricity is only sensitive to ozone up to a certain limit as the REF-C2 and SEN-C2-fGHG ensemble mean trends end well in advance of peak ozone depletion.

The centre latitude and eccentricity are negatively correlated with the 10 hPa SAM index in both the reanalysis ($r = -0.69$ and $r = -0.54$, respectively) and the model ($r = -0.54$ and $r = -0.21$, respectively). Thus, a positive SAM, and hence a strong vortex, is associated with a more circular ozone hole that is more concentric with the pole. The stratospheric SAM exhibits a positive trend during the historical period associated with ozone depletion (Thompson and Wallace, 2000b; McLandress et al., 2010). This could potentially explain the negative trend in eccentricity over this early

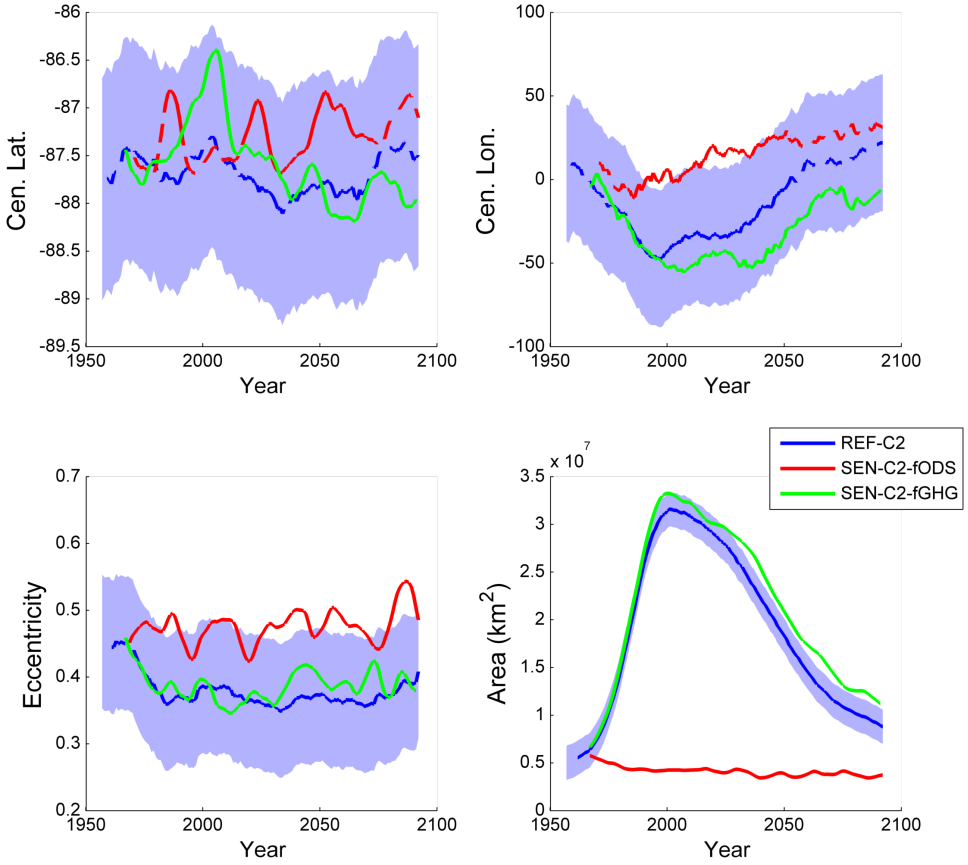

Figure 5.4: Time series of the October TCO ellipse parameters: centre longitude, centre latitude, eccentricity and area for the REF-C2 (blue), SEN-C2-fODS (red) and SEN-C2-fGHG (green). Lines show the ensemble mean smoothed with a 15 year low pass filter, the lines are dashed if the difference between the REF-C2 and SEN-C2-fODS is not statistically significant. The shaded region indicates ±1 standard deviation from the ensemble mean

period. The centre longitude shows no such correlation with the SAM.

Figure 5.4 also shows the time series of the ellipse area parameter. After peaking around 2000, both the REF-C2 and SEN-C2-fGHG ensemble recover close to pre-ozone hole levels by the end of the 21^{st} century. By 2100, REF-C2 recovers 90% of the ozone deficit relative to the peak depletion. Eyring et al. (2010) produce similar results using an ensemble of chemistry climate models. It is notable that the recovery of ozone in the SEN-C2-fGHG ensemble is somewhat slower than that of the REF-C2 ensemble. A similar result was found by Södergren et al. (2016) who show that ozone recovery was hastened by increasingly severe GHG emission scenarios. This

effect is due to GHG-induced stratospheric cooling which acts to suppress certain temperature dependant reactions involved in ozone depletion.

Figure 5.5 shows the timeseries of centre longitude for ellipses fitted to TCO contours from 220 to 300 DU using the REF-C2 ensemble. This shows that the behaviour shown in Figure 5.4 for the 300 DU is consistent for other levels, with all contours displaying similar westward trends up until approximately the year 2000 followed by a more gradual eastward trend over the 21^{st} century. However, it is notable that the centre longitude for successively smaller ellipses is located successively further to the east (similarly, Grytsai et al. (2007) show that lon_{min} is located further east at more poleward latitudes). This shows that the centre longitude displays a similar tendency if the size of the ellipse is increased by either, increasing the TCO value of the edge contour or, by increased depletion of ozone. It is therefore possible that the centre longitude is only determined by the latitudinal position of the ellipse edge (due to a change in the phase of the climatological wave the contour encounters at different latitudes, for example), rather than a change in the ozone modulated atmospheric dynamics. To test this hypothesis we can examine the variation of the centre longitude on the inter-annual timescale to ascertain if it responds similarly to changes in the size of the ellipse. We find that the centre longitude is in fact not correlated with the ellipse area on this shorter timescale. Therefore, we conclude that the cause of these trends is more likely a dynamical effect of ozone depletion and recovery.

In a similar manner to Figure 5.4, Figure 5.6 can also be used to show the influence of ozone depletion and recovery on lon_{min} and lon_{max}. The separation between the REF-C2 and SEN-C2-fODS ensemble is not as clear in this case as it was for the centre longitude. For REF-C2, lon_{min} is displaced around 20° to the east, relative to the SEN-C2-fODS ensemble, around the period of maximum ozone depletion. Over the period 1995 to 2013 the difference is statistically significant (as previously, using Student's t test on 15 year time slices, $p < 0.05$). While, lon_{max} shows no sustained difference between REF-C2 and SEN-C2-fODS ensembles.

The lon_{min} and lat_{max} trends are summarized in Table 5.3. In the REF-C2 simulation, both lon_{min} and lat_{max} exhibit eastward trends over 1960-1999 (8.4 and 3.2 °/dec, respectively) and then remain relatively constant over the 21^{st} century. For lon_{min}, the SEN-C2-fODS ensemble shows no significant trend during the 20^{st} century and an eastward trend over the

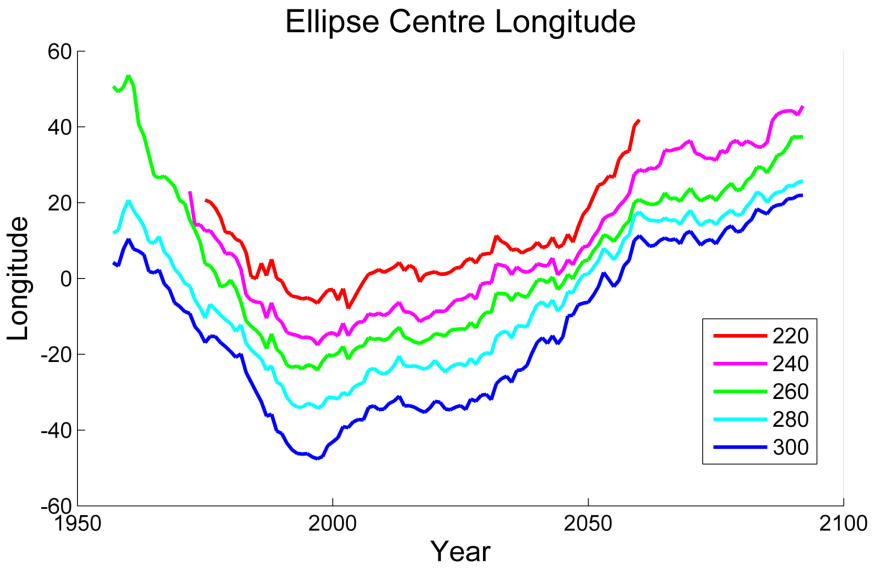

Figure 5.5: Time series of the ellipse centre longitude in the REF-C2 ensemble for different TCO contours

Table 5.3: Trend in lon_{min} and lon_{max} (°/dec) for each of the model ensembles. Uncertainty is indicated by the 95% confidence interval

	1960-1999		2000-2099	
	lon_{min}	lon_{max}	lon_{min}	lon_{max}
REF-C2	8.4 ± 3.2	3.2 ± 4.0	0.1 ± 1.2	0.6 ± 1.0
SEN-C2-fODS	1.5 ± 4.0	-1.0 ± 5.8	2.5 ± 1.9	1.0 ± 1.8
SEN-C2-fGHG	3.4 ± 4.9	5.5 ± 4.2	-0.8 ± 1.4	-0.6 ± 1.1

21^{st} century. This suggests that it is ozone depletion driving the early trend in REF-C2, followed by the opposing influences of ozone recovery and GHG forcing which result in lon_{min} remaining constant over the later period in the REF-C2 ensemble. The SEN-C2-fGHG ensemble offers only weak support for this hypothesis; although the 1960-1999 trend is positive and the 2000-2099 trend is negative (as would be expected by this hypothesis), neither trend is significant at the 95% confidence level. In the case of lon_{max}, SEN-C2-fGHG shows an eastward trend over 1960-1999 similar to REF-C2 where SEN-C2-fODS does not, thus suggesting this trend is driven by ozone depletion. However, over the 2000-2099 period none of the ensembles show a significant trend, meaning no determination as to the influence of ozone recovery or GHG forcing can be made for this period.

We now focus on the effect asymmetric ozone has on stratospheric cli-

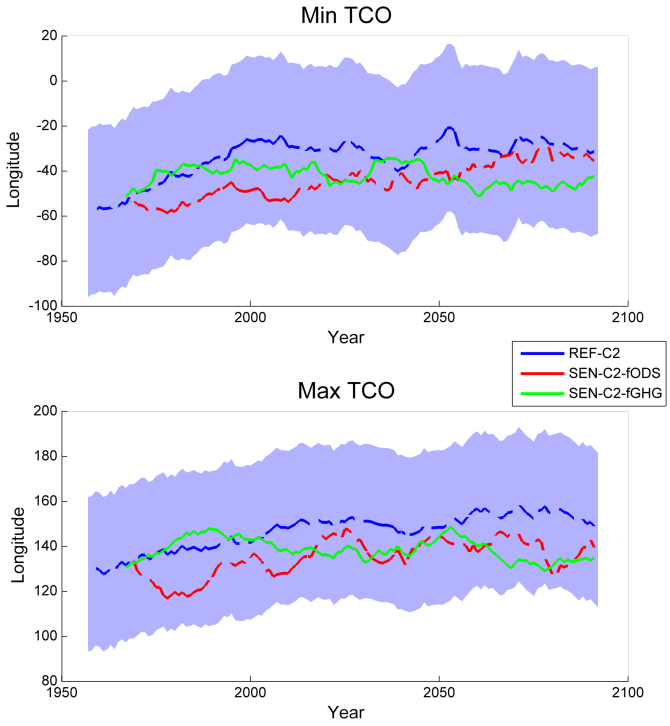

Figure 5.6: As for Figure 5.4 for longitude of the minimum and maximum TCO at 65°.

mate. We will examine the centre longitude and lon_{min} parameters as these show the clearest response to both ozone depletion and recovery. Figure 5.7 shows the correlation of the centre longitude with the October monthly mean temperature at 50 hPa (the approximate level of the ozone layer) for the reanalysis (top) and REF-C2 runs (bottom) over the period 1979-2014. Significant correlations ($p < .05$) are indicated by the green contours. For both the reanalysis and model, the correlations show a dipole with positive correlations over the south-eastern Pacific and negative over the Atlantic and Indian Oceans. This shows that a eastward(westward) shift of the ozone hole (which is typically located around 30°W) will result in positive(negative) temperature anomalies over the Pacific and negative(positive) temperature anomalies over the Atlantic/Indian region. This is consistent with a change in radiative heating caused by the shifting of the ozone hole.

Similarly, Figure 5.8 shows the correlation between lon_{min} and the 50 hPa temperature. As in the case of the centre longitude, lon_{min} produces a change in the temperature field that is consistent with a change in radia-

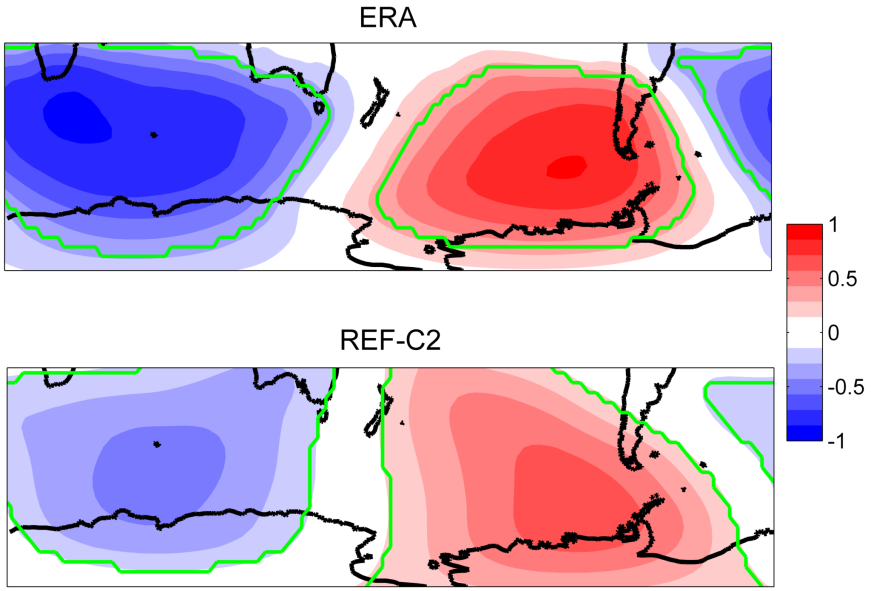

Figure 5.7: Correlation of October central longitude ellipse parameter with the 50 hPa temperature for the ERA-Interim reanalysis (top) and model (bottom)

tive heating associated with the shifted ozone distribution. An eastward shift in lon_{min} is associated with a positive temperature anomaly over the Pacific and a negative anomaly over the Atlantic and Indian regions. For both centre longitude and lon_{min} the correlations are notably stronger in the reanalysis compared to the model.

We now examine the connection between zonally asymmetric ozone and tropospheric climate. Figure 5.9 shows the equivalent of Figure 5.7 for the 500 hPa GPH. The reanalysis shows negative correlations in the Western Antarctic and, to a lesser degree, the eastern Pacific. There are also positive correlations over the Indian and south Atlantic Ocean. In the case of the model the geographic pattern shows some similarities, although the correlations are substantially lower. The figure displays boxes around regions that receive further analysis later in this section.

Figure 5.10 shows the equivalent of Figure 5.9 for lon_{min}. For the reanalysis the correlation pattern is generally similar to that of the centre longitude with negative correlations in the western Antarctic and the eastern Pacific and positive correlations over the Indian and south-western Atlantic Ocean. In this case there is also a significant positive correlation south

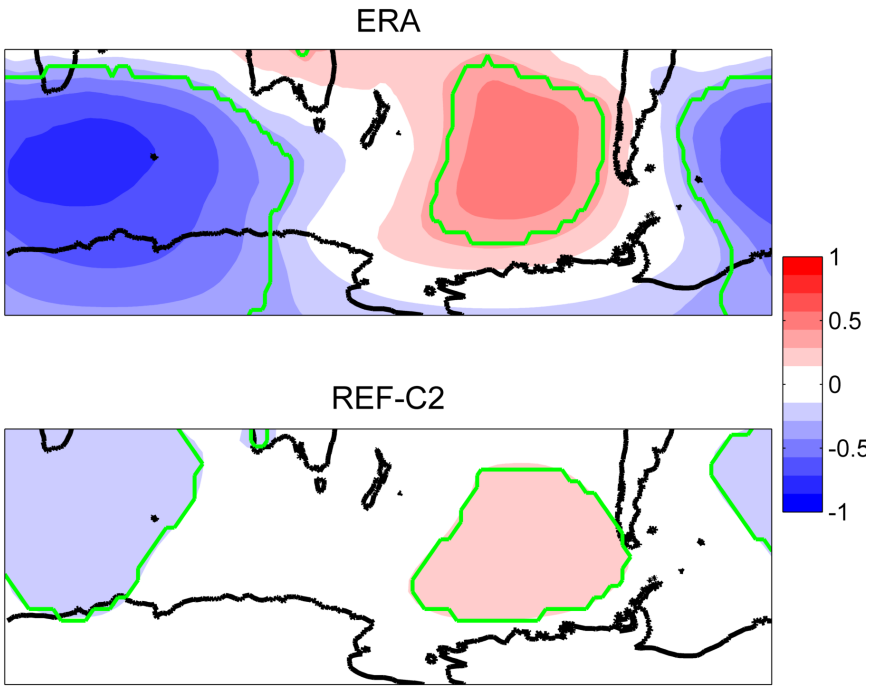

Figure 5.8: As for Figure 5.7 with lon_{min} instead of centre longitude

of New Zealand. It is evident here that the correlation pattern shows a wavenumber 3 in mid-latitudes. Also, compared to Figure 5.9, the negative correlation at high latitudes has a greater extent. This makes it somewhat reminiscent of a SAM pattern; however, lon_{min} does not show a significant correlation with the 500 hPa SAM in either the reanalysis or model. The model shows a similar, albeit much weaker, pattern in mid-latitudes and no correlation over high latitudes.

It is possible that the stratospheric ozone is influencing the troposphere or that it is the troposphere driving changes in the stratosphere. In order to investigate the direction of influence we now utilise daily data rather than monthly mean data which has been used up to this point to examine the relationship on shorter timescales. We focus on the regions shown to exhibit large correlations, marked by the pink boxes in Figure 5.9. Figure 5.11 shows the correlation of the ellipse centre longitude with the mean 500 hPa GPH in each of these regions over a range of lag times (a negative lag denotes the GPH leads the centre longitude); only significant ($p < 0.05$) correlations are shown. It is apparent that for the reanalysis the GPH anomalies in both the Atlantic Ocean and West Antarctic regions lead the shift in centre longitude;

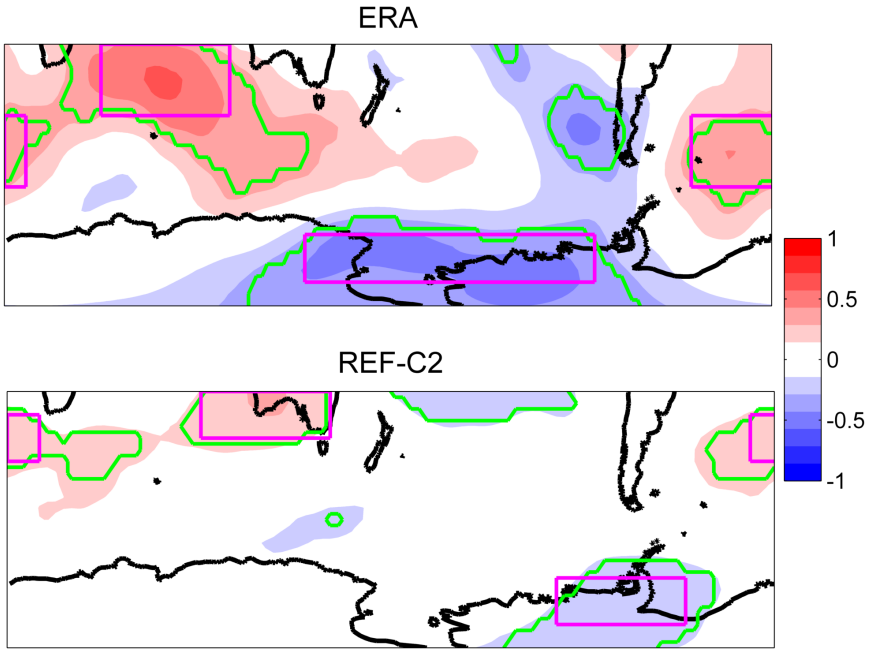

Figure 5.9: As for Figure 5.7 but with 500 hPa GPH, the boxes illustrate the regions analysed in Figure 5.11

the correlation maximizing at a lag of around -10 to -15 days. This suggests the direction of influence is from the troposphere to the stratosphere. The Indian Ocean relationship however, remains unclear as the correlation is shown to maximize at a lag of zero. The correlations in the model are too small too draw any conclusions. Similar analysis is not shown for lon_{min} as this measure has a much larger uncertainty on the daily timescale.

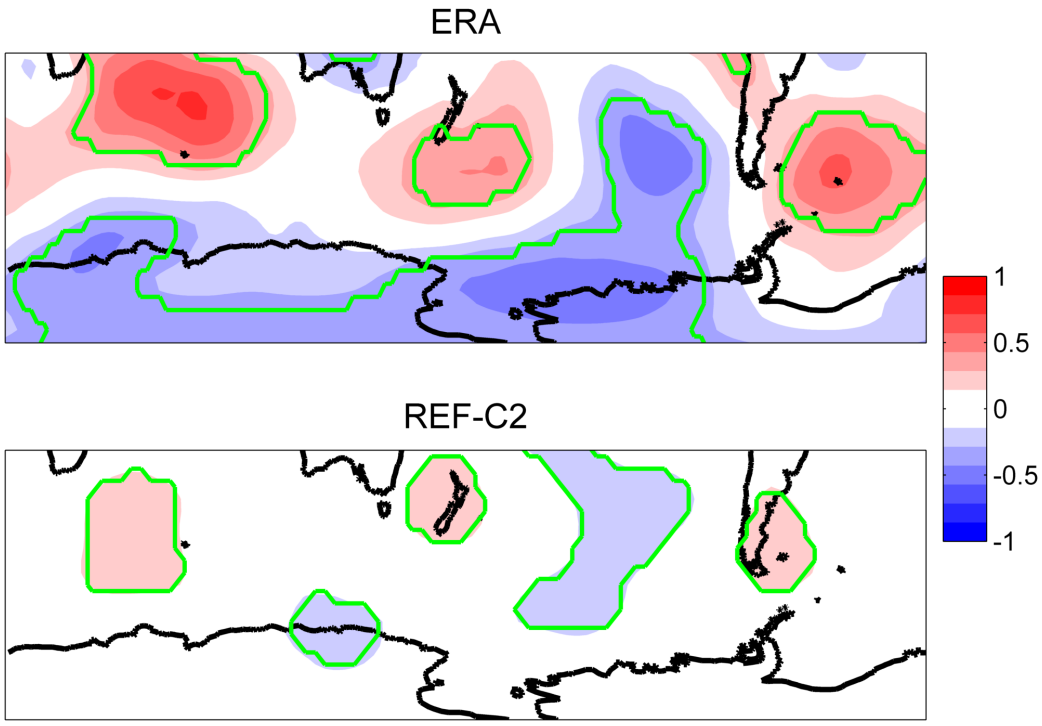

Figure 5.10: As for Figure 5.9 but with lon_{min}

5.4 Discussion and Summary

During the spring the distribution of ozone over polar regions exhibits a significant amount of zonal asymmetry. This asymmetric distribution of ozone is described by an ellipse fitted to the 300 DU contour. This ellipse metric reveals that the model underestimates this asymmetry in that it simulates a more circular ozone hole, which is centred too near the pole. However, the ellipse centre longitude is correctly simulated; both the reanalysis and model show the ozone hole displaced from the pole toward South America. The asymmetry is also quantified by identifying the longitude of the TCO minimum and maximum at 65°S (lon_{min} and lon_{max}). These metrics again show that the longitudinal orientation of the ozone hole displacement is correctly simulated by the model.

The ellipse centre longitude and lon_{min} prove to be interesting as Figure 5.4 and 5.6 show these parameters to be influenced by both ozone depletion and recovery in the model. As ozone depletion occurs the centre longitude moves west, while lon_{min} moves east, i.e the change in distribution of ozone

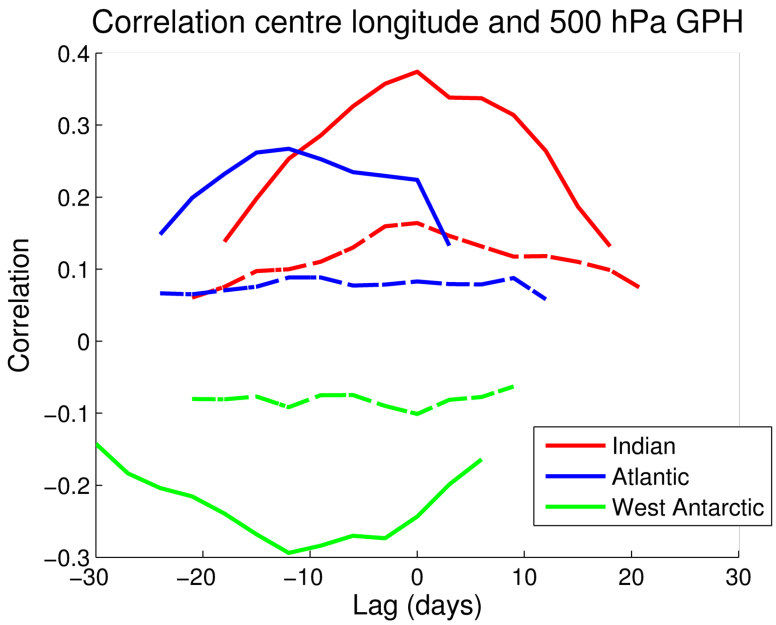

Figure 5.11: Correlation between the ellipse centre longitude and the 500 hPa GPH over a range lags in the Indian Ocean (red), Atlantic Ocean (blue) and West Antarctic region (green) for the ERA-Interim reanalysis (solid) and REF-C2 ensemble (dashed).

is not simply by a rotation about the pole but is more like a combined translation and rotation. Comparison between the REF-C2 and SEN-C2-fODS simulations demonstrates that this movement is the result of ozone depletion. This is especially clear in the case of the centre longitude which shows a shift of up to 50° attributable to ozone depletion.

As ozone recovery occurs over the 21^{st} century the centre longitude returns to its pre-ozone hole position. It appears that both ozone recovery and increasing GHG forcing contribute to the eastward trend over this period. This is a somewhat unusual result as ozone recovery (which causes a warming of the polar stratosphere) and GHG forcing (which causes a cooling of the polar stratosphere) ought to oppose each other. This is the case for lon_{min} which remains relatively constant over the 21^{st} century in the REF-C2 simulation while SEN-C2-fODS and SEN-C2-fGHG are shown to have opposing trends. Similarly opposing influences of ozone recovery and GHG forcing have been shown in other studies with regard to the timing of the vortex breakup (McLandress et al., 2010) and the SAM (McLandress et al., 2011; Morgenstern et al., 2014).

The ellipse eccentricity is also shown be influenced by ozone depletion. The behaviour of eccentricity differs slightly from that of the centre longitude and lon_{min} in that the influence appears to end around the mid 1980s, 10-15 years prior to peak ozone depletion. It is possible the effect is saturated as the ellipse approaches the limit of circularity. While e=0 denotes a perfect circle, it is possible something near e=0.25 may be close to a practical limit of circularity as this describes an ellipse for which the major axis is only 3% longer than the minor axis. The eccentricity shows no sign of returning to pre-ozone hole values for much of the 21^{st} century, with the lack of trends in either the SEN-C2-fODS or SEN-C2-fGHG indicating the lack of ozone or GHG forcing. As the effect appeared to become saturated during the 1980s, it is possible the ozone may need to recover to 1980s levels before eccentricity is noticeably impacted. In the model ozone recovers to these levels around 2060; from 2060-2099 the REF-C2 eccentricity does exhibit a small, but statistically significant, trend of 0.02/dec which offers some evidence that this may be the case.

The mechanism driving the changes in eccentricity can potentially be explained via the SAM. In both the model and reanalysis the correlation between the 10 hPa SAM and the eccentricity is negative. This is likely due to a positive SAM, and hence a strong polar vortex, inhibiting the upward propagation of planetary waves thus limiting the distortion of the vortex and the ozone depleted air it contains. The SAM, which exhibits a positive trend over the ozone depletion period can thus explain the negative trend in eccentricity. The same cannot be said for either the centre longitude or lon_{min}, both of which display no significant correlation with the stratospheric SAM. Further work is required to investigate the mechanisms driving the trends in these metrics.

The shift in the position of the ozone hole affects climate. In the stratosphere a shift in the zonally asymmetric ozone is associated with a perturbation in the zonally asymmetric temperature (see Figure 5.7 and 5.8). The perturbation is such that when the ozone hole shifts toward a region, that region experiences a decrease in temperature, which is consistent with a decrease in the radiative heating. Previous results (Gabriel et al., 2007; Crook et al., 2008; Gillett et al., 2009; Waugh et al., 2009) have shown dynamical heating can be an important factor in the response to zonally asymmetric ozone, but this is not necessary to explain the results in this case.

For both the central longitude and lon_{min}, the correlations with the 50 hPa temperature are stronger in the reanalysis compared to the model. The reanalysis features a more pronounced asymmetry in the ozone distribution and so these measures likely produce a more distinct relationship with the temperature in this case. The linear regression coefficients are also larger for the reanalysis ($\sim$0.2 K/deg) for both centre longitude and lon_{min}. At 50 hPa the October temperature is around 210 K, so a 1σ variation in centre longitude or lon_{min} is associated with an anomaly of the order of 3% in temperature in the reanalysis. In the model this figure is less than 1%.

The asymmetric ozone also has links to some regions of the troposphere. In the Indian Ocean and Atlantic Ocean regions the GPH is positively correlated with eastward shifts of the ozone hole, while the GPH in the West Antarctic region shows a negative correlation. Lagged correlations reveal that it is the tropospheric anomaly preceding the shift in the ozone hole for the Atlantic and West Antarctic regions, while correlations in the Indian Ocean region prove inconclusive in this respect. Particularly of note is the negative correlation between the ellipse centre and GPH over the South Atlantic. A link between ozone and the troposphere in this region was also discovered in Chapter 4 which showed an increase in blocking frequency in response to ozone depletion. The particulars of the link are different in the two cases, in this case the relationship occurs during October and the direction of influence is upward while, in the case of the Atlantic blocking the relationship was in summer and it was shown that changes in the stratosphere preceded the tropospheric effect. However, this suggests that the Atlantic region is particularly important in the two way coupling between the stratosphere and troposphere.

Chapter 6

Conclusions and Future Work

One of the main themes of this work is the importance of including ozone (and in general, a full representation of the stratosphere) in climate modelling endeavours. Until recently, many climate models did not feature a model top above the level of the stratopause or interactive ozone chemistry; this is true, for example, of many CMIP5 models (see Table 2.3). This study utilized the NIWA-UKCA coupled atmosphere-ocean chemistry-climate model (AOCCM) model which features a model top near the mesopause and a relatively large number of vertical model levels as well a largely explicit ozone chemistry module. Model runs in which ODSs are fixed at 1960 (i.e. pre-ozone hole) levels ("SEN-C2-fODS") were compared to runs in which ODSs varied ("REF-C2") in order to demonstrate the role of stratospheric ozone depletion and recovery. Similarly, runs in which GHGs are held fixed at 1960 levels ("SEN-C2-fGHG") are also used to demonstrate the role of GHG forcing. Changes in stratospheric ozone, and by extension, the stratospheric features it affects such as the polar jet, have been shown in this thesis to influence aspects of the near surface climate, such as the tropospheric SAM and atmospheric blocking.

Chapter 3 investigated the effect of changing ozone on the SAM. Previous studies have shown the mean state of the SAM to respond to changes in ozone, trending toward the positive polarity as polar ozone becomes increasingly depleted (Arblaster and Meehl, 2006; Karpechko et al., 2010b; McLandress et al., 2011). These studies also showed ozone recovery to exert

the reverse influence on the SAM, although this influence is offset by that of increasing GHG forcing. This work expands on these studies, showing that ozone depletion has the effect of increasing the frequency of extremes and persistence of the SAM in the stratosphere. During the period 1990-2020 the model displayed a broadening of the SAM distribution such that instances of extremes greater than ∼2 standard deviations from the mean increased in frequency by around 50% relative to the 1950-2100 average distribution. This frequency of extreme events subsequently returned to the mean state as ozone recovery progressed. Also, over the period 1987-2036 (the timespan during which October polar ozone averaged below 220DU) the persistence of the stratospheric SAM was shown to increase by as much as 30 days relative to the fixed ODS simulation in late summer. This increase in persistence also abated towards the end of the 21^{st} century as ozone recovered.

The findings relating to the stratospheric SAM extremes and persistence lead to an investigation of stratosphere-troposphere coupling. It has been shown by Thompson et al. (2005) that extreme SAM events in the stratosphere are followed by SAM anomalies in the troposphere that persist for around two months. This finding is extended in this thesis by investigating the effect of changing ozone on the strength of this coupling. It was found that over the period 1987-2036 the tropospheric SAM lagging the stratospheric anomaly by 40-60 days displayed a larger anomaly as a result of ozone depletion. As this stratosphere-troposphere coupling is important for extended range weather forecasting (Kuroda, 2008), this result demonstrates the potential importance of considering ozone depletion in these forecasting models.

A lot of previous work has been conducted on the mechanisms underlying coupling of the stratosphere and troposphere (e.g. Thompson et al., 2006; Orr et al., 2012; Kunz and Greatbatch, 2013). This thesis adds some findings to this body of work. For example, Section 3.4.4 shows that the vertical resolution of the model in the upper troposphere/lower stratosphere is important for accurately simulating the strength of the coupling. It was also found that models that featured interactive ozone chemistry tended to overestimate the strength of the coupling. However, as this set of models included only three with interactive ozone chemistry it would be useful to expand the set of models in any future work.

Stratosphere-troposphere coupling is also a consideration in Chapter 4

which investigates the relationship between changes in stratospheric ozone and blocking events in the troposphere. A significant quantity of the literature on blocking relates to the Northern Hemisphere so this thesis is useful in that it adds to the relatively smaller body of work on Southern Hemisphere blocking. Various studies of Southern Hemisphere blocking have used reanalysis data to study the historical time period (e.g. Renwick, 2005; Mendes et al., 2008; Mendes and Cavalcanti, 2014; Kayano, 1999; Berrisford et al., 2007) while, Parsons et al. (2016) examines the impact of GHG forcing on blocking over the 21^{st} century in the Southern Hemisphere. This thesis complements these studies by investigating of the influence of ozone on Southern Hemisphere blocking over both periods. It was found that summer blocking in the South Atlantic is projected to increase in response to ozone depletion and will decrease as a result of ozone recovery. During the early 21^{st} century blocking frequency in the South Atlantic was found to be twice a high as in the fixed ODS scenario. In contrast, the other region where blocking is most frequently observed, the South Pacific, does not exhibit any discernible change attributable to ozone depletion. This poses questions regarding the mechanisms that initiate blocking events and if they differ between the two regions. It was found that South Atlantic blocking events were preceded by positive SAM anomalies in both the stratosphere and troposphere, which was not the case for South Pacific blocking events. It was speculated that the zonally asymmetric component of the SAM may be responsible for modifying the planetary wave state of the stratosphere such in such a way as to favour blocking events in the South Atlantic. This connection would benefit from further investigation, perhaps by investigating the wave propagation prior to blocking events.

Chapters 3 and 4 focus on the impact of changing ozone via the SAM which is largely zonally symmetric. The springtime ozone distribution does however exhibit a notable amount of asymmetry; this is explored in Chapter 5. Grytsai et al. (2007) show that the longitude of the 65°S ozone minima has trended eastward over the period 1979-2005. This finding is extended in this thesis by considering changes in the ozone distribution over the larger time frame of the model run and ascertaining if the external forcing from either ozone or GHGs are a factor in such shifts. The model showed a similar trend to that identified by Grytsai et al. (2007) and revealed that this trend was a result of ozone depletion. This trend was also shown to

end around the year 2000, after which the longitude of the ozone minima remain relatively constant, due to the effect of ozone recovery being offset by increasing GHG forcing. It is also demonstrated that this eastward shift in ozone minima is not totally descriptive of the entire ozone distribution. Fitting an ellipse to an ozone contour allowed for the description of the mean position of ozone depletion in terms of the ellipse centre latitude and longitude. It was found, in contrast to the ozone minima result, that the ellipse centre longitude trended westward as a result of ozone depletion and eastward as a result of ozone recovery. Also, the ellipse metric showed the ozone distribution became more circular due to ozone depletion. Hence, the effect on the ozone distribution is not fully captured by a simple rotation of the ozone hole about the pole, as may have been implied by Grytsai et al. (2007).

It was also apparent that the model underestimated the amount of asymmetry in comparison to the reanalysis, simulating an ozone hole that was too circular and located too close to the pole. It would be interesting to find out if this is common among chemistry climate models and if the above results hold for models in which the zonally asymmetric ozone is more accurately simulated.

In this thesis planetary wave propagation is often invoked to explain the mechanisms linking changes in the stratosphere to changes in the troposphere. However, further analysis of wave propagation was not pursued as three dimensional model output at daily resolution was limited to a small number of model levels. Should more data become available in the future, this represents one avenue by which this work may be furthered. For example, Kodera et al. (2013) presents a case study of a blocking event showing a number of time slices of the Plumb wave activity flux (Plumb, 1985) leading up to the blocking event - a similar analysis applied to model data would be useful. This could potentially help explain the ozone-related blocking frequency changes in the South Atlantic and conversely, why blocking in the South Pacific does not seem to be similarly affected by ozone.

The majority of this thesis dealt with a single model. This suited the analysis in various ways; for example, differences in climate due to changes in ozone could be considered very robust as the change in the concentration of ODSs were the only difference when comparing references runs to fixed ODS sensitivity runs. In using an ensemble of different models it is possible

the varying characteristics of the models in the ensemble could obscure the ozone driven changes. However, using an ensemble of different models also has a number of advantages. One simply being a greater number of runs which could increase the statistical significance of some of the results. This study was limited to five REF-C2, two SEN-C2-fODS and three SEN-C2-fGHG runs. This was particularity limiting in Chapter 3, where the analysis focused on a limited set of extreme events. Utilizing a larger number of runs here would provide the most utility in improving the robustness of the results, as well as facilitating additional analysis. For example, it was apparent that increasing the threshold for stratospheric extremes resulted in a greater response in the troposphere - a larger quality of data would be beneficial in exploring this nature of this relationship. It would be useful to know if magnitude of stratospheric SAM anomalies is linearly or non-linearly related to the tropospheric SAM response or perhaps, if there is some threshold level below which the stratospheric anomaly has no impact on the troposphere. It is shown in Chapter 3 that the frequency of stratospheric SAM extremes is effected by ozone depletion and so answers to these questions would help to clarify the tropospheric impact of this finding.

Another benefit of a multi-model ensemble would be the identification of the inter-model spread of climate response to ozone changes and what model biases may contribute to differences in the response. For example, studies have shown considerable spread in the stratosphere-troposphere coupling of models (Morgenstern et al., 2010b; Gerber et al., 2010) and the effect of model biases on simulation of blocking (Scaife et al., 2010). The NIWA-UKCA model used in this study is part of the Chemistry Climate Model Intercomparison (CCMI) project so similar analysis of the other models participating in this project represents a natural extension of the this work.

Bibliography

Albers, J. R. and Nathan, T. R. (2012). Pathways for Communicating the Effects of Stratospheric Ozone to the Polar Vortex: Role of Zonally Asymmetric Ozone. *Journal of the Atmospheric Sciences*, 69:785–801.

Andrews, D. G., Holton, J. R., and Leovy, C. B. (1987). *Middle Atmosphere Dynamics*, volume 1. Academic Press.

Anstey, J. A., Davini, P., Gray, L. J., Woollings, T. J., Butchart, N., Cagnazzo, C., Christiansen, B., Hardiman, S. C., Osprey, S. M., and Yang, S. (2013). Multi-model analysis of Northern Hemisphere winter blocking: Model biases and the role of resolution. *Journal of Geophysical Research Atmospheres*, 118:3956–3971.

Arblaster, J. M. and Meehl, G. A. (2006). Contributions of external forcings to southern annular mode trends. *Journal of Climate*, 19:2896–2905.

Baldwin, M. P. and Dunkerton, T. J. (2001). Stratospheric harbingers of anomalous weather regimes. *Science*, 294:581–584.

Baldwin, M. P., Stephenson, D. B., Thompson, D. W. J., Timothy, J., Charlton, A. J., Neill, A. O., Dunkerton, T. J., Chariton, A. J., and Neitt, A. O. (2003). Stratospheric Memory and Skill of Extended-Range Weather Forecasts. *Science*, 301(5633):636–640.

Baldwin, M. P. and Thompson, D. W. J. (2009). A critical comparison of stratospheretroposphere coupling indices. *Quarterly Journal of the Royal Meteorological Society*, 135:1661–1672.

Barnes, E. A. and Hartmann, D. L. (2010). Dynamical Feedbacks of the Southern Annular Mode in Winter and Summer. *Journal of the Atmospheric Sciences*, 67:2320–2330.

Barnes, E. A., Slingo, J., and Woollings, T. (2012). A methodology for the comparison of blocking climatologies across indices, models and climate scenarios. *Climate Dynamics*, 38:2467–2481.

Barnes, E. A., Solomon, S., and Polvani, L. M. (2016). Robust wind and precipitation responses to the Mount Pinatubo eruption as simulated in the CMIP5 models. *Journal of Climate*, 29:4763–4779.

Barriopedro, D., García-Herrera, R., Lupo, A. R., and Hernández, E. (2006). A climatology of Northern Hemisphere blocking. *Journal of Climate*, 19:1042–1063.

Beron-Vera, F. J., Olascoaga, M. J., Brown, M. G., and Koçak, H. (2012). Zonal Jets as Meridional Transport Barriers in the Subtropical and Polar Lower Stratosphere. *Journal of the Atmospheric Sciences*, 69:753–767.

Berrisford, P., Hoskins, B. J., and Tyrlis, E. (2007). Blocking and Rossby Wave Breaking on the Dynamical Tropopause in the Southern Hemisphere. *Journal of the Atmospheric Sciences*, 64:2881–2898.

Bracegirdle, T. J. and Marshall, G. J. (2012). The reliability of antarctic tropospheric pressure and temperature in the latest global reanalyses. *Journal of Climate*, 25:7138–7146.

Butchart, N., Charlton-Perez, A. J., Cionni, I., Hardiman, S. C., Haynes, P. H., Krüger, K., Kushner, P. J., Newman, P. A., Osprey, S. M., Perlwitz, J., Sigmond, M., Wang, L., Akiyoshi, H., Austin, J., Bekki, S., Baumgaertner, A., Braesicke, P., Brühl, C., Chipperfield, M., Dameris, M., Dhomse, S., Eyring, V., Garcia, R., Garny, H., Jöckel, P., Lamarque, J. F., Marchand, M., Michou, M., Morgenstern, O., Nakamura, T., Pawson, S., Plummer, D., Pyle, J., Rozanov, E., Scinocca, J., Shepherd, T. G., Shibata, K., Smale, D., Teyssèdre, H., Tian, W., Waugh, D., and Yamashita, Y. (2011). Multimodel climate and variability of the stratosphere. *Journal of Geophysical Research Atmospheres*, 116:1–21.

Chapman, S. (1930). On Ozone and Atomic Oxygen in the Upper Atmosphere. *Philosopical Magazine*, 10(64):369–383.

Charney, J. G. and Drazin, P. G. (1961). Propagation of planetary-scale disturbances from the lower into the upper atmosphere. *Journal of Geophysical Research*, 66(1):83–109.

Chen, G. and Held, I. M. (2007). Phase speed spectra and the recent poleward shift of Southern Hemisphere surface westerlies. *Geophysical Research Letters*, 34:1–5.

Christensen, J., Kumar, K. K., Aldria, E., An, S.-I., Cavalcanti, I., Castro, M. D., Dong, W., Goswami, P., Hall, A., Kanyanga, J., Kitoh, A., Kossin, J., Lau, N.-C., Renwick, J., Stephenson, D., Xie, S.-P., and Zhou, T. (2013). Climate Phenomena and their Relevance for Future Regional Climate Change Supplementary Material. *Climate Change 2013: The Physical Science Basis. Contribution of Working Group I to the Fifth Assessment Report of the Intergovernmental Panel on Climate Change*, page 62.

Christiansen, B. (2001). Downward propagation of zonal mean zonal wind anomalies from the stratosphere to the troposphere: Model and reanalysis. *Journal of Geophysical Research*, 106:27307.

Christiansen, B. (2005). Downward propagation and statistical forecast of the near-surface weather. *Journal of Geophysical Research D: Atmospheres*, 110:1–10.

Cionni, I., Eyring, V., Lamarque, J. F., Randel, W. J., Stevenson, D. S., Wu, F., Bodeker, G. E., Shepherd, T. G., Shindell, D. T., and Waugh, D. W. (2011). Ozone database in support of CMIP5 simulations: Results and corresponding radiative forcing. *Atmospheric Chemistry and Physics*, 11:11267–11292.

Cohen, J. and Saito, K. (2002). A test for annular modes. *Journal of Climate*, 15:2537–2546.

Collins, M., Knutti, R., Arblaster, J., Dufresne, J.-L., Fichefet, T., Friedlingstein, P., Gao, X., Gutowski, W. J., Johns, T., Krinner, G., Shongwe, M., Tebaldi, C., Weaver, A. J., and Wehner, M. (2013). Long-term Climate Change: Projections, Commitments and Irreversibility. *Climate Change 2013: The Physical Science Basis. Contribution of Working Group I to the Fifth Assessment Report of the Intergovernmental Panel on Climate Change*, pages 1029–1136.

Cowan, T., Van Rensch, P., Purich, A., and Cai, W. (2013). The association

of tropical and extratropical climate modes to atmospheric blocking across southeastern Australia. *Journal of Climate*, 26:7555–7569.

Crook, J. A., Gillett, N. P., and Keeley, S. P. E. (2008). Sensitivity of Southern Hemisphere climate to zonal asymmetry in ozone. *Geophysical Research Letters*, 35:3–7.

Crutzen, P. J. (1974). Estimates of possible future ozone reductions from continued use of fluoro-chloro-methanes (CF2Cl2, CFCl3). *Geophysical Research Letters*, 1(5):205–208.

D'Andrea, F., Tibaldi, S., Blackburn, M., Boer, G., Déqué, M., Dix, M. R., Dugas, B., Ferranti, L., Iwasaki, T., Kitoh, a., Pope, V., Randall, D., Roeckner, E., Straus, D., Stern, W., Van Den Dool, H., and Williamson, D. (1998). Northern Hemisphere atmospheric blocking as simulated by 15 atmospheric general circulation models in the period 1979-1988. *Climate Dynamics*, 14:385–407.

Daniel, J. S., Solomon, S., and Albritton, L. (1995). On the evaluation of halocarbon radiative forcing and global warming potentials. *Journal of Geophysical Research : Atmospheres*, 100:1271–1285.

Davies, T., Cullen, M. J. P., Malcolm, A. J., Mawson, M. H., Staniforth, A., White, A. A., and Wood, N. (2005). A new dynamical core for the Met Office's global and regional modelling of the atmosphere. *Quarterly Journal of the Royal Meteorological Society*, 131:1759–1782.

Davini, P., Cagnazzo, C., and Anstey, J. A. (2014). A blocking view of the stratosphere-troposphere coupling. *Journal of Geophysical Research : Atmospheres*, 119:100–115.

Dee, D. P., Uppala, S. M., Simmons, A. J., Berrisford, P., Poli, P., Kobayashi, S., Andrae, U., Balmaseda, M. A., Balsamo, G., Bauer, P., Bechtold, P., Beljaars, A. C. M., van de Berg, L., Bidlot, J., Bormann, N., Delsol, C., Dragani, R., Fuentes, M., Geer, A. J., Haimberger, L., Healy, S. B., Hersbach, H., Hólm, E. V., Isaksen, L., Kå llberg, P., Köhler, M., Matricardi, M., Mcnally, A. P., Monge-Sanz, B. M., Morcrette, J. J., Park, B. K., Peubey, C., de Rosnay, P., Tavolato, C., Thépaut, J. N., and Vitart, F. (2011). The ERA-Interim reanalysis: Configuration and

performance of the data assimilation system. *Quarterly Journal of the Royal Meteorological Society*, 137:553–597.

Dennison, F. W., McDonald, A. J., and Morgenstern, O. (2015). The effect of ozone depletion on the Southern Annular Mode and stratosphere-troposphere coupling. *Journal of Geophysical Research: Atmospheres*, 120:6305–6312.

Dole, R. M. and Gordon, N. D. (1983). Persistent anomalies of the extratropical Northern Hemisphere wintertime circulation: Geographical Distribution and Regional Persistence Characteristics. *Monthly Weather Review*, 111:1567–1586.

Dragani, R. (2011). On the quality of the ERA-Interim ozone reanalyses: comparisons with satellite data. *Quarterly Journal of the Royal Meteorological Society*, 137:1312–1326.

Ekman, V. W. (1905). On the Influence of the Earth's Rotation on Ocean-Currents. *Arkiv för matematik, astronomi och fysik*, 2(11):1 – 52.

Evtushevsky, O. M., Grytsai, A. V., Klekociuk, A. R., and Milinevsky, G. P. (2008). Total ozone and tropopause zonal asymmetry during the Antarctic spring. *Journal of Geophysical Research Atmospheres*, 114:1–12.

Eyring, V., Arblaster, J. M., Cionni, I., Sedláček, J., Perlwitz, J., Young, P. J., Bekki, S., Bergmann, D., Cameron-Smith, P., Collins, W. J., Faluvegi, G., Gottschaldt, K. D., Horowitz, L. W., Kinnison, D. E., Lamarque, J. F., Marsh, D. R., Saint-Martin, D., Shindell, D. T., Sudo, K., Szopa, S., and Watanabe, S. (2013a). Long-term ozone changes and associated climate impacts in CMIP5 simulations. *Journal of Geophysical Research: Atmospheres*, 118:5029–5060.

Eyring, V., Cionni, I., Bodeker, G. E., Charlton-Perez, A. J., Kinnison, D. E., Scinocca, J. F., Waugh, D. W., Akiyoshi, H., Bekki, S., Chipperfield, M. P., Dameris, M., Dhomse, S., Frith, S. M., Garny, H., Gettelman, A., Kubin, A., Langematz, U., Mancini, E., Marchand, M., Nakamura, T., Oman, L. D., Pawson, S., Pitari, G., Plummer, D. A., Rozanov, E., Shepherd, T. G., Shibata, K., Tian, W., Braesicke, P., Hardiman, S. C., Lamarque, J. F., Morgenstern, O., Pyle, J. A., Smale, D., and Yamashita,

Y. (2010). Multi-model assessment of stratospheric ozone return dates and ozone recovery in CCMVal-2 models. *Atmospheric Chemistry and Physics*, 10:9451–9472.

Eyring, V., Lamarque, J.-F., Hess, P., Arfeuille, F., Bowman, K., Martyn, C., Duncan, B., Fiore, A., Gettelman, A., Giorgetta, M. A., Granier, C., Hegglin, M., Doug, K., Markus, K., Langematz, U., Luo, B., Martin, R., Matthes, K., Newman, P. A., Peter, T., Robock, A., Ryerson, T., Saiz-Lopez, A., Salawitch, R., Schultz, M., Shepherd, T. G., Shindell, D., Staehelin, J., Tegtmeier, S., Thomason, L., Tilmes, S., Vernier, J.-P., Waugh, D. W., and Young, P. J. (2013b). Overview of IGAC/SPARC Chemistry-Climate Model Initiative (CCMI) community simulations in support of upcoming ozone and climate assessments. *SPARC Newsletter*, 40(January):48–66.

Farman, J. C., Gardiner, B. G., and Shanklin, J. D. (1985). Large losses of total ozone in Antarctica reveal seasonal ClOx/NOx interaction. *Nature*, 315:207–210.

Feller, W. (1948). On the Kolmogorov-Smirnov limit theorems for empirical distributions. *The Annals of Mathematical Statistics*, 19(2):177–189.

Flato, G., Marotzke, J., Abiodun, B., Braconnot, P., Chou, S., Collins, W., Cox, P., Driouech, F., Emori, S., Eyring, V., Forest, C., Gleckler, P., Guilyardi, E., Jakob, C., Kattsov, V., Reason, C., and Rummukainen, M. (2013). Chapter 9: Evaluation of Climate Models. *Climate Change 2013: The Physical Science Basis. Contribution of Working Group I to the Fifth Assessment Report of the Intergovernmental Panel on Climate Change*, pages 741–866.

Fogt, R. L., Bromwich, D. H., and Hines, K. M. (2011). Understanding the SAM influence on the South Pacific ENSO teleconnection. *Climate Dynamics*, 36:1555–1576.

Gabriel, A., Peters, D., Kirchner, I., and Graf, H. F. (2007). Effect of zonally asymmetric ozone on stratospheric temperature and planetary wave propogation. *Geophysical Research Letters*, 34.

Garfinkel, C. I., Waugh, D. W., and Gerber, E. P. (2013). The effect of tro-

pospheric jet latitude on coupling between the stratospheric polar vortex and the troposphere. *Journal of Climate*, 26:2077–2095.

Gerber, E. P., Baldwin, M. P., Akiyoshi, H., Austin, J., Bekki, S., Braesicke, P., Butchart, N., Chipperfield, M., Dameris, M., Dhomse, S., Frith, S. M., Garcia, R. R., Garny, H., Gettelman, A., Hardiman, S. C., Karpechko, A., Marchand, M., Morgenstern, O., Nielsen, J. E., Pawson, S., Peter, T., Plummer, D. A., Pyle, J. A., Rozanov, E., Scinocca, J. F., Shepherd, T. G., and Smale, D. (2010). Stratosphere-troposphere coupling and annular mode variability in chemistry-climate models. *Journal of Geophysical Research: Atmospheres*, 115:1–15.

Gerber, E. P. and Polvani, L. M. (2009). Stratosphere-troposphere coupling in a relatively simple AGCM: The importance of stratospheric variability. *Journal of Climate*, 22:1920–1933.

Gillett, N. P. and Fyfe, J. C. (2013). Annular mode changes in the CMIP5 simulations. *Geophysical Research Letters*, 40:1189–1193.

Gillett, N. P., Kell, T. D., and Jones, P. D. (2006). Regional climate impacts of the Southern Annular Mode. *Geophysical Research Letters*, 33:1–4.

Gillett, N. P., Scinocca, J. F., Plummer, D. A., and Reader, M. C. (2009). Sensitivity of climate to dynamically-consistent zonal asymmetries in ozone. *Geophysical Research Letters*, 36:1–5.

Gong, D. and Wang, S. (1999). Definition of Antarctic Oscillation index. *Geophysical Research Letters*, 26(4):459.

Gong, T., Feldstein, S. B., and Luo, D. (2010). The Impact of ENSO on Wave Breaking and Southern Annular Mode Events. *Journal of the Atmospheric Sciences*, 67:2854–2870.

Graversen, R. G. (2003). Downward propagation from the stratosphere to the troposphere: A comparison of the two hemispheres. *Journal of Geophysical Research*, 108:1–10.

Grise, K. M., Thompson, D. W. J., and Forster, P. M. (2009). On the role of radiative processes in stratosphere-troposphere coupling. *Journal of Climate*, 22:4154–4161.

Grytsai, A., Grytsai, Z., Evtushevsky, A., and Milinevsky, G. (2005). Interannual variability of planetary waves in the ozone layer at 65 S. *International Journal of Remote Sensing*, 26:3377–3387.

Grytsai, A. V., Evtushevsky, O. M., Agapitov, O. V., Klekociuk, A. R., and Milinevsky, G. P. (2007). Structure and long-term change in the zonal asymmetry in Antarctic total ozone during spring. *Annales Geophysicae*, 25:361–374.

Haigh, J. D. and Roscoe, H. K. (2009). The final warming date of the Antarctic polar vortex and influences on its interannual variability. *Journal of Climate*, 22:5809–5819.

Hall, A. and Visbeck, M. (2002). Synchronous variability in the Southern Hemisphere atmosphere, sea ice, and ocean resulting from the annular mode. *Journal of Climate*, 15:3043–3057.

Hartmann, D. L. and Lo, F. (1998). Wave-Driven Zonal Flow Vacillation in the Southern Hemisphere. *Journal of the Atmospheric Sciences*, 55:1303–1315.

Haynes, P. H., Marks, C. J., McIntyre, M. E., Shepherd, T. G., and Shine, K. P. (1991). On the Downward Control of Extratropical Diabatic Circulations by Eddy-Induced Mean Zonal Forces. *Journal of the Atmospheric Sciences*, 48(4):651–678.

Hegerl, G. C. (2007). Understanding and Attributing Climate Change. *Climate Change 2007: The Physical Science Basis. Contribution of Working Group I to the Fourth Assessment Report of the Intergovernmental Panel on Climate Change*, pages 665–745.

Hendon, H. H., Thompson, D. W. J., and Wheeler, M. C. (2007). Australian rainfall and surface temperature variations associated with the Southern Hemisphere annular mode. *Journal of Climate*, 20:2452–2467.

Hewitt, H. T., Copsey, D., Culverwell, I. D., Harris, C. M., Hill, R. S. R., Keen, A. B., McLaren, A. J., and Hunke, E. C. (2011). Design and implementation of the infrastructure of HadGEM3: The next-generation Met Office climate modelling system. *Geoscientific Model Development*, 4:223–253.

Hines, K. M., Bromwich, D. H., and Marshall, G. J. (2000). Artificial surface pressure trends in the NCEP-NCAR reanalysis over the southern ocean and Antartica. *Journal of Climate*, 13:3940–3952.

Hoffmann, L., Hoppe, C. M., Müller, R., Dutton, G. S., Gille, J. C., Griessbach, S., Jones, A., Meyer, C. I., Spang, R., Volk, C. M., and Walker, K. A. (2014). Stratospheric lifetime ratio of CFC-11 and CFC-12 from satellite and model climatologies. *Atmospheric Chemistry and Physics*, 14:12479–12497.

Holton, J. R., Haynes, P. H., Mcintyre, M. E., Douglass, A. R., and Rood, B. (1995). Stratosphere-Troposphere Exchange. *Reviews of Geophysics*, 33(4):403–439.

Hunke, E. C., Lipscomb, W. H., Turner, A. K., Jeffery, N., and Elliott, S. (2015). CICE : the Los Alamos Sea Ice Model Documentation and Software User's Manual LA-CC-06-012. Technical report, Los Alamos National Laboratory.

Ialongo, I., Sofieva, V., Kalakoski, N., Tamminen, J., and Kyrölä, E. (2012). Ozone zonal asymmetry and planetary wave characterization during Antarctic spring. *Atmospheric Chemistry and Physics*, 12:2603–2614.

Ivy, D. J., Solomon, S., and Rieder, H. E. (2016). Radiative and Dynamical Influences on Polar Stratospheric Temperature Trends. *Journal of Climate*, 29:4927–4938.

Kang, S. M., Polvani, L. M., Fyfe, J. C., and Sigmond, M. (2011). Impact of polar ozone depletion on subtropical precipitation. *Science*, 332:951–954.

Karoly, D. J. (1990). The role of transient eddies in low-frequency zonal variations of the Southern Hemisphere circulation. *Tellus A*, 42:41–50.

Karpechko, A. Y., Gillett, N. P., Dall'Amico, M., and Gray, L. J. (2010a). Southern Hemisphere atmospheric circulation response to the El Chichón and Pinatubo eruptions in coupled climate models. *Quarterly Journal of the Royal Meteorological Society*, 136:1813–1822.

Karpechko, A. Y., Gillett, N. P., Gray, L. J., and Dall'Amico, M. (2010b). Influence of ozone recovery and greenhouse gas increases on Southern

Hemisphere circulation. *Journal of Geophysical Research: Atmospheres*, 115:1–15.

Kayano, M. (1999). Meteorology and Atmospheric Physics Southeastern Pacific Blocking Episodes and their Effects on the South American Weather. *Meteorology and Atmospheric Physics*, 155:145–155.

Kidson, J. W. (1988). Interannual Variations in the Southern Hemisphere Circulation.

Kidston, J., Renwick, J. A., and McGregor, J. (2009). Hemispheric-scale seasonality of the southern annular mode and impacts on the climate of New Zealand. *Journal of Climate*, 22:4759–4770.

Kidston, J., Scaife, A. A., Hardiman, S. C., Mitchell, D. M., Butchart, N., Baldwin, M. P., and Gray, L. J. (2015). Stratospheric influence on tropospheric jet streams, storm tracks and surface weather. *Nature Geoscience*, 8(6):433–440.

Kodera, K., Mukougawa, H., and Fujii, A. (2013). Influence of the vertical and zonal propagation of stratospheric planetary waves on tropospheric blockings. *Journal of Geophysical Research: Atmospheres*, 118:8333–8345.

Kunz, T., Fraedrich, K., and Lunkeit, F. (2009). Response of Idealized Baroclinic Wave Life Cycles to Stratospheric Flow Conditions. *Journal of the Atmospheric Sciences*, 66:2288–2302.

Kunz, T. and Greatbatch, R. J. (2013). On the Northern Annular Mode Surface Signal Associated with Stratospheric Variability. *Journal of the Atmospheric Sciences*, 70:2103–2118.

Kuroda, Y. (2008). Role of the stratosphere on the predictability of medium-range weather forecast: A case study of winter 2003-2004. *Geophysical Research Letters*, 35:1–5.

Kuroda, Y. and Kodera, K. (1999). Role of planetary waves in the stratospheretroposphere coupled variability in the northern hemisphere winter. *Geophysical Research Letters*, 26(15):2375.

Kushner, P. J. and Polvani, L. M. (2004). Stratosphere-troposphere coupling in a relatively simple AGCM: The Role of Eddies. *Journal of Climate*, 17:629:639.

Lefebvre, W., Goosse, H., Timmermann, R., and Fichefet, T. (2004). Influence of the Southern Annular Mode on the sea ice - Ocean system. *Journal of Geophysical Research C: Oceans*, 109:1–12.

Lejenäs, H. and Ø kland, H. (1983). Characteristics of northern hemisphere blocking as determined from a long time series of observational data. *Tellus A*, pages 967–979.

Lelieveld, J. and Dentener, F. J. (2000). What controls tropospheric ozone? *Journal of Geophysical Research*, 105(D3):3531–3551.

Lenton, A. and Matear, R. J. (2007). Role of the Southern Annular Mode (SAM) in Southern Ocean CO2 uptake. *Global Biogeochemical Cycles*, 21:1–17.

Lim, E. P., Hendon, H. H., and Rashid, H. (2013). Seasonal predictability of the southern annular mode due to its association with ENSO. *Journal of Climate*, 26:8037–8054.

Limpasuvan, V. and Hartmann, D. L. (1999). Eddies and the annular modes of climate variability. *Geophysical Research Letters*, 26(20):3133–3136.

Limpasuvan, V. and Hartmann, D. L. (2000). Wave-maintained annular modes of climate variability. *Journal of Climate*, 13:4414–4429.

Liu, Q. (1994). On the Definition and Persistance of Blocking. *Tellus A*, 46:286–298.

Lorenz, D. and Hartmann, D. (2001). Eddy-Zonal Flow Feedback in the Southern Hemisphere Winter and Summer. *Journal of the Atmospheric Sciences*, 58:3312–3327.

Madec, G. (2011). NEMO Ocean Engine. Technical Report 27, Institut Pierre Simon Laplace (IPSL).

Marshall, G. J. (2003). Trends in the Southern Annular Mode from observations and reanalyses. *Journal of Climate*, 16(1999):4134–4143.

Marshall, G. J. (2007). Half-century seasonal relationships between the Southern Annular Mode and Antarctic temperatures. *International Journal of Climatology*, 27:373–383.

Marshall, G. J., Orr, A., van Lipzig, N. P. M., and King, J. C. (2006). The impact of a changing Southern Hemisphere Annular Mode on Antarctic Peninsula summer temperatures. *Journal of Climate*, 19:5388–5404.

Martius, O., Polvani, L. M., and Davies, H. C. (2009). Blocking precursors to stratospheric sudden warming events. *Geophysical Research Letters*, 36:1–5.

Masui, T., Matsumoto, K., Hijioka, Y., Kinoshita, T., Nozawa, T., Ishiwatari, S., Kato, E., Shukla, P. R., Yamagata, Y., and Kainuma, M. (2011). An emission pathway for stabilization at 6 Wm-2 radiative forcing. *Climatic Change*, 109:59–76.

Matsueda, M., Mizuta, R., and Kusunoki, S. (2009). Future change in wintertime atmospheric blocking simulated using a 20-km-mesh atmospheric global circulation model. *Journal of Geophysical Research: Atmospheres*, 114:1–10.

Matsumi, Y. and Kawasaki, M. (2003). Photolysis of Atmospheric Ozone in the Ultraviolet Region. *Chemical Reviews*, 103:4767–4781.

McCormack, J. P., Nathan, T. R., and Cordero, E. C. (2011). The effect of zonally asymmetric ozone heating on the Northern Hemisphere winter polar stratosphere. *Geophysical Research Letters*, 38:1–5.

McLandress, C., Jonsson, A. I., Plummer, D. A., Reader, M. C., Scinocca, J. F., and Shepherd, T. G. (2010). Separating the dynamical effects of climate change and ozone depletion. Part I: Southern hemisphere stratosphere. *Journal of Climate*, 23:5002–5020.

McLandress, C., Shepherd, T. G., Scinocca, J. F., Plummer, D. A., Sigmond, M., Jonsson, A. I., and Reader, M. C. (2011). Separating the dynamical effects of climate change and ozone depletion. Part II: Southern Hemisphere troposphere. *Journal of Climate*, 24:1850–1868.

Meinshausen, M., Smith, S. J., Calvin, K., Daniel, J. S., Kainuma, M. L. T., Lamarque, J., Matsumoto, K., Montzka, S. A., Raper, S. C. B., Riahi, K., Thomson, A., Velders, G. J. M., and van Vuuren, D. P. P. (2011). The RCP greenhouse gas concentrations and their extensions from 1765 to 2300. *Climatic Change*, 109:213–241.

Mendes, M. C. D. a. and Cavalcanti, I. F. A. (2014). The relationship between the Antarctic oscillation and blocking events over the South Pacific and Atlantic Oceans. *International Journal of Climatology*, 34:529–544.

Mendes, M. C. D. a., Trigo, R. M., Cavalcanti, I. F. A., and DaCamara, C. C. (2008). Blocking episodes in the Southern Hemisphere: Impact on the climate of adjacent continental areas. *Pure and Applied Geophysics*, 165:1941–1962.

Meneghini, B., Simmonds, I., and Smith, I. N. (2007). Association between Australian rainfall and the Southern Annular Mode. *International Journal of Climatology*, 27:109–121.

Meredith, M. P. and Hogg, A. M. (2006). Circumpolar response of Southern Ocean eddy activity to a change in the Southern Annular Mode. *Geophysical Research Letters*, 33:2–5.

Minschwaner, K., Hoffmann, L., Brown, A., Riese, M., Müller, R., and Bernath, P. F. (2013). Stratospheric loss and atmospheric lifetimes of CFC-11 and CFC-12 derived from satellite observations. *Atmospheric Chemistry and Physics*, 13:4253–4263.

Molina, L. T. and Molina, M. J. (1986). Absolute absorption cross sections of ozone in the 185- to 350-nm wavelength range. *Journal of Geophysical Research*, 91:14501–14508.

Molina, M. J. and Rowland, F. S. (1974). Stratospheric sink for chlorofluoromethanes : chlorine atom-catalysed destruction of ozone. *Nature*, 249:810:812.

Morgenstern, O., Akiyoshi, H., Bekki, S., Braesicke, P., Butchart, N., Chipperfield, M. P., Cugnet, D., Deushi, M., Dhomse, S. S., Garcia, R. R., Gettelman, A., Gillett, N. P., Hardiman, S. C., Jumelet, J., Kinnison, D. E., Lamarque, J. F., Lott, F., Marchand, M., Michou, M., Nakamura, T., Olivi, D., Peter, T., Plummer, D., Pyle, J. A., Rozanov, E., Saint-Martin, D., Scinocca, J. F., Shibata, K., Sigmond, M., Smale, D., Teyssdre, H., Tian, W., Voldoire, A., and Yamashita, Y. (2010a). Anthropogenic forcing of the Northern Annular Mode in CCMVal-2 models. *Journal of Geophysical Research: Atmospheres*, 115:1–15.

Morgenstern, O., Braesicke, P., O'Connor, F. M., Bushell, A. C., Johnson, C. E., Osprey, S. M., and Pyle, J. A. (2009). Evaluation of the new UKCA climate-composition model Part 1 : The stratosphere. *Geoscientific Model Development*, 2:43–57.

Morgenstern, O., Giorgetta, M. A., Shibata, K., Eyring, V., Waugh, D. W., Shepherd, T. G., Akiyoshi, H., Austin, J., Baumgaertner, A. J. G., Bekki, S., Braesicke, P., Brühl, C., Chipperfield, M. P., Cugnet, D., Dameris, M., Dhomse, S., Frith, S. M., Garny, H., Gettelman, A., Hardiman, S. C., Hegglin, M. I., Jöckel, P., Kinnison, D. E., Lamarque, J. F., Mancini, E., Manzini, E., Marchand, M., Michou, M., Nakamura, T., Nielsen, J. E., Olivi, D., Pitari, G., Plummer, D. A., Rozanov, E., Scinocca, J. F., Smale, D., Teyssdre, H., Toohey, M., Tian, W., and Yamashita, Y. (2010b). Review of the formulation of present-generation stratospheric chemistry-climate models and associated external forcings. *Journal of Geophysical Research: Atmospheres*, 115:1–18.

Morgenstern, O., Hegglin, M. I., Rozanov, E., O'Connor, F. M., Abraham, N. L., Akiyoshi, H., Archibald, A. T., Bekki, S., Butchart, N., Chipperfield, M. P., Deushi, M., Dhomse, S. S., Garcia, R. R., Hardiman, S. C., Horowitz, L. W., Jöckel, P., Josse, B., Kinnison, D., Lin, M., Mancini, E., Manyin, M. E., Marchand, M., Marécal, V., Michou, M., Oman, L. D., Pitari, G., Plummer, D. a., Revell, L. E., Saint-Martin, D., Schofield, R., Stenke, A., Stone, K., Sudo, K., Tanaka, T. Y., Tilmes, S., Yamashita, Y., Yoshida, K., and Zeng, G. (2017). Review of the global models used within the Chemistry-Climate Model Initiative (CCMI). *Geoscientific Model Development*, 10:639–671.

Morgenstern, O., Zeng, G., Abraham, N. L., Telford, P. J., Braesicke, P., Pyle, J. a., Hardiman, S. C., O'connor, F. M., and Johnson, C. E. (2013). Impacts of climate change, ozone recovery, and increasing methane on surface ozone and the tropospheric oxidizing capacity. *Journal of Geophysical Research Atmospheres*, 118:1028–1041.

Morgenstern, O., Zeng, G., Dean, S. M., Joshi, M., Abraham, N. L., and Osprey, A. (2014). Direct and ozone-mediated forcing of the Southern Annular Mode by greenhouse gases. *Geophysical Research Letters*, 41:1–8.

Nathan, T. R. and Cordero, E. C. (2007). An ozone-modified refractive index for vertically propagating planetary waves. *Journal of Geophysical Research*, 112.

Newman, P. A., Daniel, J. S., Waugh, D. W., and Nash, E. R. (2007). A new formulation of equivalent effective stratospheric chlorine (EESC). *Atmos. Chem. Phys. Atmospheric Chemistry and Physics*, 7:4537–4552.

Nishii, K. and Nakamura, H. (2005). Upward and downward injection of Rossby wave activity across the tropopause: A new aspect of the tropospherestratosphere dynamical linkage. *Quarterly Journal of the Royal Meteorological Society*, 131:544–563.

North, G. R., Bell, T. L., Cahalan, R. F., and Moeng, F. J. (1982). Sampling Errors in the Estimation of Empirical Orthogonal Funtions.

Nowack, P. J., Luke Abraham, N., Maycock, A. C., Braesicke, P., Gregory, J. M., Joshi, M. M., Osprey, A., and Pyle, J. A. (2015). A large ozone-circulation feedback and its implications for global warming assessments. *Nature Climate Change*, 5:41–45.

Oberländer-Hayn, S., Gerber, E. P., Abalichin, J., Akiyoshi, H., Kerschbaumer, A., Kubin, A., Kunze, M., Langematz, U., Meul, S., Michou, M., Morgenstern, O., and Oman, L. D. (2016). Is the Brewer-Dobson circulation increasing or moving upward? *Geophysical Research Letters*, 43:1772–1779.

Oliveira, F. N. M., Carvalho, L. M. V., and Ambrizzi, T. (2014). A new climatology for Southern Hemisphere blockings in the winter and the combined effect of ENSO and SAM phases. *International Journal of Climatology*, 1692(August 2013):1676–1692.

Orr, A., Bracegirdle, T. J., Hosking, J. S., Feng, W., Roscoe, H. K., and Haigh, J. D. (2013). Strong dynamical modulation of the cooling of the polar stratosphere associated with the antarctic ozone hole. *Journal of Climate*, 26:662–668.

Orr, A., Bracegirdle, T. J., Hosking, J. S., Jung, T., Haigh, J. D., Phillips, T., and Feng, W. (2012). Possible Dynamical Mechanisms for Southern Hemisphere Climate Change due to the Ozone Hole. *Journal of the Atmospheric Sciences*, 69:2917–2932.

Orr, A., Cresswell, D., Marshall, G. J., Hunt, J. C. R., Sommeria, J., Wang, C. G., and Light, M. (2004). A low-level explanation for the recent large warming trend over the western Antarctic Peninsula involving blocked winds and changes in zonal circulation. *Geophysical Research Letters*, 31.

Palmer, T. N., Doblas-Reyes, F. J., Weisheimer, a., and Rodwell, M. J. (2008). Toward seamless prediction: Calibration of climate change projections using seasonal forecasts. *Bulletin of the American Meteorological Society*, 89(April):459–470.

Pan, L. L., Randel, W. J., Gary, B. L., Mahoney, M. J., and Hintsa, E. J. (2004). Definitions and sharpness of the extratropical tropopause: A trace gas perspective. *Journal of Geophysical Research D: Atmospheres*, 109:1–11.

Parsons, S., Renwick, J. A., and McDonald, A. J. (2016). An Assessment of Future Southern Hemisphere Blocking Using CMIP5 Projections from Four GCMs. *Journal of Climate*, 29:7599–7611.

Pelly, J. L. and Hoskins, B. J. (2003). A New Perspective on Blocking. *Journal of the Atmospheric Sciences*, 60:743–755.

Perlwitz, J. and Harnik, N. (2004). Downward coupling between the stratosphere and troposphere: The relative roles of wave and zonal mean processes. *Journal of Climate*, 17:4902–4909.

Pezza, A. B., van Rensch, P., and Cai, W. (2012). Severe heat waves in Southern Australia: Synoptic climatology and large scale connections. *Climate Dynamics*, 38:209–224.

Plumb, R. A. (1985). On the Three-Dimensional Propagation of Stationary Waves.

Polvani, L. M. and Kushner, P. J. (2002). Tropospheric response to stratospheric perturbations in a relatively simple general circulation model. *Geophysical Research Letters*, 29(7):40–43.

Polvani, L. M. and Waugh, D. W. (2004). Upward wave activity flux as a precursor to extreme stratospheric events and subsequent anomalous surface weather regimes. *Journal of Climate*, 17:3548–3554.

Polvani, L. M., Waugh, D. W., Correa, G. J. P., and Son, S.-W. (2011). Stratospheric Ozone Depletion: The Main Driver of Twentieth-Century Atmospheric Circulation Changes in the Southern Hemisphere. *Journal of Climate*, 24:795–812.

Pook, M. J., Risbey, J. S., McIntosh, P. C., Ummenhofer, C. C., Marshall, A. G., and Meyers, G. A. (2013). The Seasonal Cycle of Blocking and Associated Physical Mechanisms in the Australian Region and Relationship with Rainfall. *Monthly Weather Review*, 141:4534–4553.

Quintanar, A. I. and Mechoso, C. R. (1995). Quasi-stationary waves in the Southern Hemisphere. Part I: observational data.

Randall, D. A., Wood, R. A., Bony, S., Colman, R., Fichefet, T., Fyve, J., Kattsov, V., Pitman, A., Shukla, J., Srinivasan, J., Stouffer, R. J., Sumi, A., and Taylor, K. E. (2007). Climate Models and Their Evaluation. *Climate Change 2007: The Physical Science Basis. Contribution of Working Group I to the Fourth Assessment Report of the Intergovernmental Panel on Climate Change*, pages 591–662.

Randel, W. J. and Wu, F. (1999). Cooling of the Arctic and Antarctic polar stratospheres due to ozone depletion. *Journal of Climate*, 12:1467–1479.

Renwick, J. A. (2005). Persistent Positive Anomalies in the Southern Hemisphere Circulation. *Monthly Weather Review*, 133:977–988.

Renwick, J. A. and Thompson, D. W. J. (2006). The Southern Annular Mode and New Zealand climate. *Water and Atmosphere*, 14(2):24–25.

Rex, D. F. (1950). Blocking Action in the Middle Troposphere and its Effect upon Regional Climate. I. An Aerological Study of Blocking Action. *Tellus*, 2:196–211.

Rienecker, M. M., Suarez, M. J., Gelaro, R., Todling, R., Bacmeister, J., Liu, E., Bosilovich, M. G., Schubert, S. D., Takacs, L., Kim, G. K., Bloom, S., Chen, J., Collins, D., Conaty, A., Da Silva, A., Gu, W., Joiner, J., Koster, R. D., Lucchesi, R., Molod, A., Owens, T., Pawson, S., Pegion, P., Redder, C. R., Reichle, R., Robertson, F. R., Ruddick, A. G., Sienkiewicz, M., and Woollen, J. (2011). MERRA: NASA's modern-era retrospective analysis for research and applications. *Journal of Climate*, 24:3624–3648.

Risbey, J. S., Pook, M. J., McIntosh, P. C., Wheeler, M. C., and Hendon, H. H. (2009). On the Remote Drivers of Rainfall Variability in Australia. *Monthly Weather Review*, 137:3233–3253.

Robock, A., Adams, T., Moore, M., Oman, L., and Stenchikov, G. (2007). Southern Hemisphere atmospheric circulation effects of the 1991 Mount Pinatubo eruption. *Geophysical Research Letters*, 34:1–6.

Roscoe, H. K. and Haigh, J. D. (2007). Influences of ozone depletion, the solar cycle and the QBO on the Southern Annular Mode. *Quarterly Journal of the Royal Meteorological Society*, 133:1855–1864.

Rozema, J., van de Staaij, J., Björn, L. O., and Caldwell, M. (1997). UV-B as an environmental factor in plant life: stress and regulation. *Trends in Ecology & Evolution*, 12:22–28.

Scaife, A. A., Woollings, T., Knight, J., Martin, G., and Hinton, T. (2010). Atmospheric blocking and mean biases in climate models. *Journal of Climate*, 23:6143–6152.

Sen Gupta, A. and England, M. H. (2006). Coupled Ocean Atmosphere Ice Response to Variations in the Southern Annular Mode. *Journal of Climate*, 19:4457–4486.

Shaw, T. A., Perlwitz, J., and Harnik, N. (2010). Downward wave coupling between the stratosphere and troposphere: The importance of meridional wave guiding and comparison with zonal-mean coupling. *Journal of Climate*, 23:6365–6381.

Shaw, T. A., Perlwitz, J., Harnik, N., Newman, P. A., and Pawson, S. (2011). The impact of stratospheric ozone changes on downward wave coupling in the Southern Hemisphere. *Journal of Climate*, 24:4210–4229.

Shutts, G. J. (1983). The propagation of eddies in diffluent jetstreams: Eddy vorticity forcing of blocking flow fields. *Quarterly Journal of the Royal Meteorological Society*, 109(462):737–761.

Shutts, G. J. (1986). A Case Study of Eddy Forcing During an Atlantic Blocking Episode. *Advances in Geophysiscs*, 29:135–162.

Sigmond, M. and Fyfe, J. C. (2010). Has the ozone hole contributed to increased Antarctic sea ice extent? *Geophysical Research Letters*, 37:2–6.

Sigmond, M. and Fyfe, J. C. (2014). The antarctic sea ice response to the ozone hole in climate models. *Journal of Climate*, 27:1336–1342.

Sinclair, M. R. (1996). A Climatology of Anticyclones and Blocking for the Southern Hemisphere. *Monthly Weather Review*, 124:245–264.

Smith, M. L. and McDonald, A. J. (2014). A quantitativemeasure of polar vortex strength using the functionM. *Journal of Geophysical Research: Atmospheres*, 119:1–20.

Södergren, A. H., Bodeker, G. E., Kremser, S., Meinshausen, M., and McDonald, A. J. (2016). A probabilistic study of the return of stratospheric ozone to 1960 levels. *Geophysical Research Letters*, 43:1–9.

Solomon, S., Garcia, R. R., Rowland, F. S., and Wuebbles, D. J. (1986). On the depletion of Antarctic ozone. *Nature*, 321:755–758.

Solomon, S., Ivy, D. J., Kinnison, D., Mills, M. J., Neely III, R. R., and Schmidt, A. (2016). Antarctic ozone layer. *Science*, 353(6296):269–274.

Son, S. W., Tandon, N. F., Polvani, L. M., and Waugh, D. W. (2009). Ozone hole and Southern Hemisphere climate change. *Geophysical Research Letters*, 36:3–7.

Song, Y. and Robinson, W. A. (2004). Dynamical Mechanisms for Stratospheric Influences on the Troposphere. *Journal of the Atmospheric Sciences*, 61:1711–1725.

Sudo, K. and Akimoto, H. (2007). Global source attribution of tropospheric ozone: Long-range transport from various source regions. *Journal of Geophysical Research Atmospheres*, 112:1–21.

Taubin, G. (1991). Estimation of Planar Curves, Surfaces, and Nonplanar Space Curves Defined by Implicit Equations with Applications to Edge and Range Image Segmentation.

Taylor, K. E., Stouffer, R. J., and Meehl, G. A. (2012). An overview of CMIP5 and the experiment design. *Bulletin of the American Meteorological Society*, 93:485–498.

Thompson, D. W. J., Baldwin, M. P., and Solomon, S. (2005). StratosphereTroposphere Coupling in the Southern Hemisphere. *Journal of the Atmospheric Sciences*, 62:708–715.

Thompson, D. W. J., Furtado, J. C., and Shepherd, T. G. (2006). On the Tropospheric Response to Anomalous Stratospheric Wave Drag and Radiative Heating. *Journal of the Atmospheric Sciences*, 63:2616–2629.

Thompson, D. W. J. and Solomon, S. (2002). Interpretation of Recent Southern Hemisphere Climate Change. *Science*, 296(5569):895–899.

Thompson, D. W. J., Solomon, S., Kushner, P. J., England, M. H., Grise, K. M., and Karoly, D. J. (2011). Signatures of the Antarctic ozone hole in Southern Hemisphere surface climate change. *Nature Geoscience*, 4(11):741–749.

Thompson, D. W. J. and Wallace, J. M. (2000a). Annular Modes in the Extratropical Circulation . Part I : Month-to-Month Variability. *Journal of Climate*, 13:1000–1016.

Thompson, D. W. J. and Wallace, J. M. (2000b). Annular modes in the extratropical circulation. Part II: Trends. *Journal of Climate*, 13(689):1018–1036.

Tibaldi, S. and Molteni, F. (1990). On the operational predictability of blocking. *Tellus A*, 42A:343–365.

Trenberth, K. F. and Mo, K. C. (1985). Blocking in the Southern Hemisphere.

Ummenhofer, C. C. and England, M. H. (2007). Interannual extremes in New Zealand precipitation linked to modes of Southern Hemisphere climate variability. *Journal of Climate*, 20:5418–5440.

Ummenhofer, C. C., Sen Gupta, A., and England, M. H. (2009). Causes of late twentieth-century trends in New Zealand precipitation. *Journal of Climate*, 22:3–19.

van den Broeke, M. (2005). Strong surface melting preceded collapse of Antarctic Peninsula ice shelf. *Geophysical Research Letters*, 32:1–4.

van den Broeke, M. R. and van Lipzig, N. P. M. (2004). Changes in Antarctic temperature, wind and precipitation in response to the Antarctic Oscillation. *Annals of Glaciology*, 39:119–126.

van Vuuren, D. P., Edmonds, J., Kainuma, M., Riahi, K., Thomson, A., Hibbard, K., Hurtt, G. C., Kram, T., Krey, V., Lamarque, J. F., Masui, T., Meinshausen, M., Nakicenovic, N., Smith, S. J., and Rose, S. K. (2011). The representative concentration pathways: An overview. *Climatic Change*, 109:5–31.

Wallace, J. M. (2000). North Atlantic Oscillation / annular mode: two paradigms - one phenomenon. *Quarterly Journal of the Royal Meteorological Society*, 126:791–805.

Wallace, J. M. and Hobbs, P. V. (2006). *Atmospheric Science: An Introductory Survey*. Academic Press, 2nd edition.

Waugh, D. N. W. (1997). Elliptical diagnostics of stratospheric polar vortices. *Quarterly Journal of the Royal Meteorological Society*, 123:1725–1748.

Waugh, D. W., Oman, L., Newman, P. A., Stolarski, R. S., Pawson, S., Nielsen, J. E., and Perlwitz, J. (2009). Effect of zonal asymmetries in stratospheric ozone on simulated Southern Hemisphere climate trends. *Geophysical Research Letters*, 36:1–6.

Wiedenmann, J. M., Lupo, A. R., Mokhov, I. I., and Tikhonova, E. a. (2002). The climatology of blocking anticyclones for the Northern and Southern Hemispheres: Block intensity as a diagnostic. *Journal of Climate*, 15:3459–3473.

Wilcoxon, F. (1945). Individual Comparisons by Ranking Methods. *Biometrics Bulletin*, 1(6):80–83.

Wirth, V. (1993). Quasi-stationary planetary waves in total ozone and their correlation with lower stratospheric temperature. *Journal of Geophysical Research*, 98(D5):8873–8882.

WMO (2011). Scientific Assessment of Ozone Depletion: 2010. Technical Report 52, World Meteorological Organisation, Geneva, Switzerland.

Woollings, T., Charlton-Perez, A., Ineson, S., Marshall, A. G., and Masato, G. (2010). Associations between stratospheric variability and tropospheric blocking. *Journal of Geophysical Research: Atmospheres*, 115:1–17.

Yamazaki, A. and Itoh, H. (2009). Selective absorption mechanism for the maintenance of blocking. *Geophysical Research Letters*, 36:4–7.

Yao, Y. and Luo, D. (2015). Do European Blocking Events Precede North Atlantic Oscillation Events ? *Advances in Atmospheric Sciences*, 32:1106–1118.

Yin, J. H. (2005). A consistent poleward shift of the storm tracks in simulations of 21st century climate. *Geophysical Research Letters*, 32:1–4.